

Thesis for the Degree of Doctor of Philosophy

# Relationship between Rheology and Molecular Structure of Innovative Crystalline Elastomers

**Naveed Ahmad**



Department of Chemical Engineering

University of Naples

“Federico II”

Italy

March, 2013

# Relationship between Rheology and Molecular Structure of Innovative Crystalline Elastomers

by

**Naveed Ahmad**

Supervised by

**Prof. Nino Grizzuti, Ph.D**

Submitted to the Department of Chemical Engineering  
University of Naples, “Federico II” in partial fulfillment  
of the requirements for the degree of  
Doctor of Philosophy

Prof. Nino Grizzuti (Ph.D. Advisor) .....

Prof. Andrea D'Anna (Ph.D. Co-ordinator) .....

---

## Abstract

The study of the rheology of polyolefins based on homogenous metallocenic catalyst has been mainly devoted to the understanding of material process ability. When used at a more advanced and sophisticated level, however, rheology is a useful tool to highlight the details of the polymer microstructure, such as the chemical stereo-regularity or the degree of chain branching. Rheology is also used to study the crystallization kinetics of the polymers and it gives more precise analysis than the conventional techniques like differential scanning calorimetry (DSC) when the crystallization kinetics are slow. When cooled below thermodynamic melting temperature, crystalline polymers undergo crystallization. The early stages of this process are characterized by the gradual change in the mechanical response of the material from the liquid to the solid, which is due to the microstructure evolution of the system. This is one of the great features of the rheological technique, which distinguishes it from the traditional DSC technique.

In the present research work relationships between rheological parameters and molecular structure of syndiotactic polypropylenes (sPP) and poly-1butenes of different stereoregularity are explored by performing oscillatory shear experiments using ARES rheometer. The rheological response is found very sensitive to the degree of syndiotacticity of syndiotactic polypropylene, while in the case of poly-1butenes, it is also found dependent on the stereoregularity.

Crystallization behavior of a series of syndiotactic polypropylenes of different degrees of syndiotacticity is investigated by performing both

---

isothermal and non-isothermal crystallization tests using rheological and differential scanning calorimetric techniques. The aim is to investigate the effect of degree of syndiotacticity on the crystallization behavior of the syndiotactic polypropylene and to couple the rheological methods to more conventional techniques (such as Differential Scanning Calorimetry). Crystallization behavior is found strongly dependent on the degree of syndiotacticity of syndiotactic polypropylene. Good agreement is found between the results obtained by both the rheological and differential scanning calorimetric (DSC) methods.

The effect of extensional flow on the crystallization kinetics of sPB is examined both in the melt and crystal phase by applying different extensional rates using sentmanat extensional rheometer (SER). Extensional flow is found to enhance the rate of crystallization in the crystal phase, which is further proved by the small angle X-Ray scattering experiment (SAX).

---

*Dedicated To  
my respected parents, especially to my beloved Father for their  
never ending support and for their open-mindedness and endless  
support.*

---

## Acknowledgement

First and foremost, I would like to give my sincere thanks to ALLAH SWT, the Almighty, the source of my life and hope for giving me the strength and wisdom to complete the research.

I am most grateful to my supervisor Prof. Nino Grizzuti for giving me an opportunity to pursue a PhD degree. Many times, his patience and constant encouragement has steered me to the right direction. Again, I am most grateful to Prof. Nino Grizzuti for his support and help in my Research work. I would also like to thank my Co-supervisors Prof. Giovanni Iannibuerto, Rossana pasquino and Prof. Giovanni Talarico for his suggestions and help.

I would like to also express my gratitude to all other faculty members of the Departments of Chemical Engineering and Chemistry for their effort in helping and providing me with the all chemicals and other experimental tools that I needed for this research.

Naveed Ahmad

Naples, Italy

March, 2013

---

## List of Symbols

Symbol	Description
$\sigma$	Stress
F	Force
A	Area
$\gamma$	Deformation
$\eta$	Viscosity
$\beta_1$	Fluid viscosity
$\omega$	Frequency
$\delta$	Phase angle
$G'$	Elastic modulus
$G''$	Viscous modulus
$R^2$	end-to-end mean square radius
b	Monomer length
$N_e$	Average number of monomers
$\tau$	Relaxation time
$\omega_{co}$	Cross over frequency
$\zeta$	Chain monomer friction co-efficient
$D_c$	Chain diffusion coefficient
k	Boltzmann constant

---

$T_{\text{rep}}$	Reptation time
$G_{(t)}$	Stress relaxation modulus
$G_N^0$	Plateau modulus
$\nu$	Entanglement density
$M_e$	Molecular weight between entanglements
$N_A$	Avogadro's number
$p$	Packing length
$v_0$	Monomer volume
$N$	Number of monomer in the chain
$\rho_0$	Polymer density at a reference temperature
$\rho$	Polymer density at temperature T
$a_T$	Horizontal shift factor
$b_T$	Vertical shift factor
$\tau_0$	Relaxation time at reference temperature
$\omega_0$	Frequency at reference temperature
$R$	Universal gas constant
$E_a$	Activation energy
$T_g$	Glass transition temperature
$c_1$ and $c_2$	WLF equation parameters
$M_w/M_n$	Molecular weight distribution

---

$G^*$	Complex modulus
$t_{0.5}$	Half crystallization time
$n$	Avrami exponent
$x(t)$	Relative degree of crystallization
$T_c$	Crystallization temperature
$A$	Dimensionless parameter
$G'_0$	Initial plateau value of elastic modulus
$G'_\infty$	Final plateau value of elastic modulus
$\beta_1$	Fluid viscosity
$t$	Time
$\Delta G_q$	Free energy contribution under quiescent
$\Delta G_f$	Free energy contribution under shear flow conditions
$\gamma^{-1}$	Characteristic flow time
$T_R$	Rouse relaxation time
$T_d$	Reptation or disengagement time
$De$	Deborah number
$\Gamma$	Dimensionless free energy function
$\Theta$	Dimensionless induction time
$H_o$	Latent heat fusion

---

$T_m$	Melting temperature
$\eta^*$	Complex Viscosity
$\Omega$	Motor rotation rate
$F_E(t)$	Tensile force
$\rho_S$	Solid state density
$A(t)$	Instantaneous cross sectional area of the stretched specimen
D	Diameter
H	Plate gap
$\eta_E^+(t)$	Tensile stress growth function
$\rho_L$	Melt state density
$R_g$	Radius of Gyration
$C_\infty$	Characteristic ratio
$V_{sp}$	Pervaded volume
$\theta(t)$	Relative degree of crystallization
$t^*$	Maximum crystallization time
$t_{1/2}$	Half crystallization time
$k_0$	Pre-exponential factor
K	Rate constant of crystallization

---

# Table of Contents

<b>ABSTRACT</b> .....	<b>I</b>
<b>ACKNOWLEDGEMENT</b> .....	<b>IV</b>
<b>LIST OF SYMBOLS</b> .....	<b>V</b>
<b>FIGURE 1.3LIST OF FIGURES</b> .....	<b>XI</b>
<b>LIST OF TABLES</b> .....	<b>XIV</b>
<b>CHAPTER 1: INTRODUCTION</b> .....	<b>1</b>
1.1.    GENERAL INTRODUCTION .....	1
1.2.    RESEARCH OBJECTIVES .....	5
1.3.    LITERATURE REVIEW .....	7
1.3.1.  Synthesis .....	8
1.3.2.  Mechanical Properties.....	16
1.3.3.  Rheology.....	22
1.3.4.  Crystallization.....	49
1.3.5.  Flow induced crystallization.....	54
<b>CHAPTER 2: EXPERIMENTAL METHODS</b> .....	<b>63</b>
2.1.    LINEAR VISCOELASTICITY .....	63
2.1.1.  Dynamic time sweep test .....	68
2.1.2.  Dynamic strain sweep test .....	68
2.1.3.  Dynamic Frequency Sweep Test .....	69
2.1.4.  Dynamic Temperature ramp test.....	69
2.2.    EXTENSIONAL FLOW MEASUREMENTS.....	70
2.2.1.  Test Setup.....	72
2.2.2.  Data analysis .....	72
2.3.    DIFFERENTIAL SCANNING CALORIMETRY .....	74
2.3.1.  Working Principle.....	74
<b>CHAPTER 3: LINEAR VISCOELASTICITY OF SYNDIOTACTIC POLYPROPYLENES</b> .....	<b>76</b>
3.1.    INTRODUCTION .....	76
3.2.    EXPERIMENTAL SECTION .....	80
3.2.1.  Materials .....	80

## Table of Contents

---

3.2.2. Methodology .....	81
3.3. RESULTS AND DISCUSSION.....	83
3.3.1. Discussion .....	94
3.4. CONCLUDING REMARKS .....	99
<b>CHAPTER 4: QUISCENT CRYSTALLIZATION OF SYNDIOTACTIC POLYPROPYLENES.....</b>	<b>100</b>
4.1. INTRODUCTION .....	100
4.2. EXPERIMENTAL SECTION .....	102
4.2.1. Material .....	102
4.2.2. Methodology .....	103
4.3. RESULTS AND DISCUSSION.....	106
4.3.1. NON-ISOTHERMAL CRYSTALLIZATION .....	106
4.3.2. ISOTHERMAL CRYSTALLIZATION .....	111
4.3.2.1. RESULTS .....	111
4.3.2.2. DISCUSSION .....	113
4.4. CONCLUDING REMARKS .....	124
<b>CHAPTER 5: LINEAR VISCOELASTICITY OF ISOTACTIC, ATACTIC AND SYNDIOTACTIC POLY-1BUTENES .....</b>	<b>126</b>
5.1. INTRODUCTION .....	126
5.2. EXPERIMENTAL SECTION .....	127
5.2.1. Material .....	127
5.2.2. Methodology .....	128
5.2.2.1. Dynamic strain sweep test .....	128
5.2.2.2. Dynamic time sweep test .....	129
5.2.2.3. Dynamic Frequency Sweep Test .....	130
5.3. RESULTS AND DISCUSSION.....	132
5.4. CONCLUDING REMARKS .....	136
<b>CHAPTER 6: INFLUENCE OF EXTENSIONAL FLOWS ON THE CRYSTALLIZATION OF SYNDIOTACTIC POLY-1BUTENE.....</b>	<b>138</b>
6.1. INTRODUCTION .....	138
6.2. EXPERIMENTAL SECTION .....	138
6.2.1. Material .....	138
6.2.2. Methodology .....	139
6.3. RESULTS AND DISCUSSIONS.....	140
6.4. CONCLUSION.....	150
<b>CHAPTER 7: CONCLUSION.....</b>	<b>152</b>
<b>REFERENCES.....</b>	<b>155</b>

---

## List of Figures

<b>Figure 1.1</b>	Chain structure of syndiotactic (above) and atactic Polystyrene.....	3
<b>Figure 1.2</b>	Chain Initiation step of Ionic polymerization.....	8
	Chain Propagation step of Ionic polymerization.....	9
<b>Figure 1.3:</b>	Chain Propagation step of Ionic polymerization.....	9
<b>Figure 1.4</b>	Reaction mechanism of Cationic polymerization process.....	9
<b>Figure 1.5</b>	Chain initiation step during the Co-ordination polymerization process.....	10
<b>Figure 1.6</b>	Transition state during the Co-ordination polymerization process.....	10
<b>Figure 1.7</b>	Final step of alkene monomer insertion during the Co-ordination polymerization process.....	11
<b>Figure 1.8</b>	Ziegler Natta catalyst of $C_s$ -symmetry.....	11
<b>Figure 1.9</b>	Ziegler Natta catalyst of $C_2$ -symmetry.....	12
<b>Figure 1.10</b>	Mechanism of Chain shuttling polymerization process.	16
<b>Figure 1.11</b>	Engineering data from stress-strain tests.....	19
<b>Figure 1.12</b>	The Maxwell spring-and-dashpot mechanical analog...	25
<b>Figure 1.13</b>	Frequency response of a poly-butadiene at 27°C. Dashed lines represent the predictions of the Maxwell model.....	29
<b>Figure 1.14</b>	Snapshot of the conformations assumed by a single	

## List of Figures

---

	polymer chain due to Brownian motion.....	31
<b>Figure 1.15</b>	A schematic view of the entangled melt.....	33
<b>Figure 1.16</b>	A schematic picture of the tube of entanglements. In (A) the test chain is surrounded by other chains. Only entanglements are highlighted; in (B) entanglements are substituted by the tube; in (C) the polymer chain inside the tube is reduced to its primitive path of $N/N_e$ segments each of length $a$ .....	34
<b>Figure 1.17</b>	Picture of the chain in the melt. Black dots represent entanglements due to the presence of other chains. The red line is the real chain. The broken line is the primitive path, i.e., the shortest line connecting the chain ends without violating the topological constraints.....	35
<b>Figure 1.18</b>	Determination of the plateau modulus by the minimum $\tan \delta$ method.....	47
<b>Figure 1.19</b>	Determination of the plateau modulus by the Van Gorp-Palmen analysis.....	48
<b>Figure 1.20</b>	DSC curve of Polyethylene.....	50
<b>Figure 1.21</b>	Schematic representation of the flow induced crystallization.....	55
<b>Figure 2.1</b>	Rotational rheometer ARES.....	66
<b>Figure 2.2</b>	Parallel plates of 8 mm diameter.....	67
<b>Figure 2.3</b>	Dynamic time sweep test set-up screen.....	68
<b>Figure 2.4</b>	Dynamic strain sweep test set-up screen.....	68
<b>Figure 2.5</b>	Dynamic frequency sweep test set-up screen.....	69
<b>Figure 2.6</b>	Dynamic temperature ramp test set-up screen.....	70

## List of Figures

---

<b>Figure 2.7</b>	Schematic diagram of Sentmanat Extensional Rheometer.....	71
<b>Figure 2.8</b>	Diagram of operation DSC cell.....	75
<b>Figure 3.1</b>	Plot between changes in length of plates vs Temperature.....	82
<b>Figure 3.2</b>	Dynamic time sweep for sPP-9 at 200°C and 10 rad/s..	84
<b>Figure 3.3</b>	Dynamic time sweep for sPP-9 at 200°C and 10 rad/s. The thick line is the best fit of Eq. (3.13).....	84
<b>Figure 3.4</b>	Dynamic strain sweep test of sPP-9 at 150°C.....	85
<b>Figure 3.5</b>	Dynamic frequency sweep test of sPP-3 at 200°C.....	86
<b>Figure 3.6</b>	Isothermal time sweep for sPP-5 at different temperatures.....	87
<b>Figure 3.7</b>	Spread sheet before shifting.....	89
<b>Figure 3.8</b>	Spread sheet after shifting. The vertical shift factor calculated by the software after density correction is shown in column F.....	89
<b>Figure 3.9</b>	Master curve for sPP-3 at reference temperature of 200°C.....	90
<b>Figure 3.10</b>	Master curve of the loss modulus for sPP-3 on a linear-log scale.....	90
<b>Figure 3.11</b>	Master curve for sPP-5.....	92
<b>Figure 3.12</b>	Master curve of the loss modulus for sPP-5 on a linear-log scale.....	92
<b>Figure 3.13</b>	Master curve for sPP-15 at reference temperature of 200°C.....	94
<b>Figure 3.14</b>	The molecular weight between entanglements and the packing length as a function of the degree of tacticity.	

## List of Figures

---

	The straight line is drawn through the $M_e$ data just to guide the eye.....	98
<b>Figure 4.1</b>	sPP-9 non-isothermal crystallization from 200 °C to 50 °C at a cooling rate of 10 °C / min and at a frequency and deformation of 1 rad/s and 5 % respectively.....	106
<b>Figure 4.2</b>	DSC non-isothermal crystallization test of sPP-5. (Cooling from 200 <sup>0</sup> C to -30 <sup>0</sup> C at a cooling rate of 10 <sup>0</sup> C/min).....	107
<b>Figure 4.3</b>	sPP-5 Complex modulus as a function of temperature with 1 <sup>st</sup> order derivative during non-isothermal crystallization from 200 to 50°C at a frequency of 01 rad/s and strain of 5%.....	108
<b>Figure 4.4</b>	Comparison of non-isothermal tests of Rheology and DSC of sPP-5.....	109
<b>Figure 4.5</b>	Crystallization temperature as a function of degree of syndiotacticity of polypropylenes.....	110
<b>Figure 4.6</b>	Isothermal crystallization of sPP-5 at 133°C at a constant cooling rate of 40°C/min.....	112
<b>Figure 4.7</b>	Heat flux as a function of time at different temperatures for sPP-9.....	112
<b>Figure 4.8</b>	sPP-9 isothermal crystallization curves at different temperatures.....	114
<b>Figure 4.9</b>	sPP-5 characteristic times as a function of reciprocal of absolute temperature.....	115
<b>Figure 4.10</b>	sPP-8 characteristic times as a function of reciprocal	115

## List of Figures

---

	of absolute temperature.....	
<b>Figure 4.11</b>	sPP-9 characteristic times as a function of reciprocal of absolute temperature.....	116
<b>Figure 4.12</b>	sPP-11 characteristic times as a function of reciprocal of absolute temperature.....	116
<b>Figure 4.13</b>	sPP-12 characteristic times as a function of reciprocal of absolute temperature.....	117
<b>Figure 4.14</b>	sPP-5 plot of $1/T$ as a function of $1/t^*$ for the calculation of the thermodynamic crystallization temperature.....	118
<b>Figure 4.15</b>	Avrami parameters ( $n$ and $t_{1/2}$ ) as a function of temperature ( $T_{\text{cry}}$ ). The lines through the Avrami exponent and half crystallization time is for the guidance of the eye.....	120
<b>Figure 4.16</b>	Linear regression of the plot between $\frac{1}{n} \ln(k)$ and $1/T$ for sPP-9.....	122
<b>Figure 4.17</b>	Activation energy of crystallization as a function of tacticity.....	123
<b>Figure 4.18</b>	Relationship between thermodynamic crystallization temperature and degree of syndiotacticity.....	124
<b>Figure 4.19</b>	Relative crystallinity as a function of time at different temperatures for sPP-9.....	124
<b>Figure 5.1</b>	Structure of the poly-1Butene repeating unit.....	128
<b>Figure 5.2</b>	Dynamic strain sweep test set-up screen.....	128
<b>Figure 5.3</b>	Dynamic strain sweep test of sPB at $100^{\circ}\text{C}$ .....	129
<b>Figure 5.4</b>	Dynamic time sweep test set-up screen.....	129
<b>Figure 5.5</b>	Dynamic time sweep test of sPB at $150^{\circ}\text{C}$ .....	131

## List of Figures

---

<b>Figure 5.6</b>	Dynamic frequency sweep test set-up screen.....	131
<b>Figure 5.7</b>	sPB frequency response master curve at 25°C.....	132
<b>Figure 5.8</b>	aPB frequency response master curve at 25°C.....	133
<b>Figure 5.9</b>	iPB frequency response master curve at 25°C.....	134
<b>Figure 5.10</b>	The horizontal shift factor as a function of temperature for all PBs investigated. The reference temperature is 25°C. The solid line is the best fit of the WLF equation.....	135
<b>Figure 6.1</b>	Oscillatory time sweep of sPB at 25°C.....	140
<b>Figure 6.2</b>	DSC of sPB immediately after sample preparation and after one week at room temperature. The heating rate is 10°C/min.....	141
<b>Figure 6.3</b>	Extensional viscosity growth functions for sPB at 40°C. The linear viscoelasticity line is also reported for reference.....	143
<b>Figure 6.4</b>	Extensional viscosity growth functions for sPB at 25°C. The linear viscoelasticity line is also reported for reference. The legend also shows the Weissenberg (based on the cross-over relaxation time) corresponding to each applied stretching rate.....	144
<b>Figure 6.5</b>	The extensional viscosity growth function for a Low Density branched Polyethylene (LDPE) at 150°C for different values of the stretching rate HDPE).....	147
<b>Figure 6.6</b>	SAXS of sPB before (left) and after (right) a sudden stretch at 25°C. The total Hencky deformation is 2. Top: SAXS image. Bottom: Equatorial intensity profiles.....	147

## List of Figures

---

<b>Figure 6.7</b>	Dimensionless induction time as a function of the Weissenberg number for sPB 5°C.....	148
<b>Figure 6.8</b>	The Hencky strain at the onset of crystallization as a function of the stretching rate for sPB 5°C.....	149
<b>Figure 6.9</b>	The specific work at the onset of crystallization as a function of the stretching rate for sPB 5°C.....	150

---

## List of Tables

<b>Table 3.1</b>	List of materials used and its properties.....	81
<b>Table 3.2</b>	List of selected temperatures for time temperature superposition principle.....	88
<b>Table 3.3</b>	The plateau modulus of the different sPP samples.....	94
<b>Table 3.4</b>	List of values of packing length and mean square end to end distance of all samples.....	96
<b>Table 4.1</b>	List of materials used and its properties.....	103
<b>Table 4.2</b>	Peak temperatures of syndiotactic polypropylenes by Rheological and DSC techniques.....	110
<b>Table 4.3</b>	List of final temperatures of isothermal crystallization for all the samples (Rheological Technique).....	111
<b>Table 4.4</b>	List of thermodynamic crystallization temperature and activation energy.....	119
<b>Table 4.5</b>	List of Avrami exponent (n) and crystallization rate constant (k).....	121
<b>Table 5.1</b>	List of materials with some properties.....	127
<b>Table 5.2</b>	List of selected temperatures for time temperature superposition principle.....	131
<b>Table 5.3</b>	Plateau modulus, entanglement molecular weight and packing length for the three PB samples.....	136
<b>Table 6.1</b>	Properties of the syndiotactic poly-1Butene.....	138

### 1.1. General Introduction

An elastomer can be defined as a viscoelastic polymeric material, which has generally noticeable low Young modulus and high yield strain compared with other plastic materials. An elastomer can also be defined as "a macromolecular material (such as rubber or a synthetic material having similar properties) that returns rapidly to approximately the initial dimensions and shape after substantial deformation by a weak stress and release of the stress" [1].

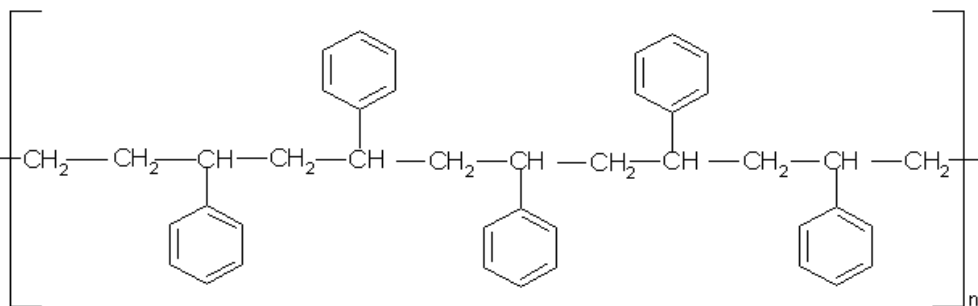
Elastomers are usually thermosets, which requires vulcanization, but can also be thermoplastics. Thermoplastics, which are also known as thermo softening plastic, are polymers that turn to a liquid when heated and freezes to a glassy state when sufficiently cooled. In other words a thermoplastic material will become a liquid at its melting temperature and will become a solid when cooled below its melting temperature. This process can be repeated over and over. A good analogy is an ice cube. When heat is supplied, it becomes liquid. And when cooled, it turns to a solid. As a consequence, thermoplastics can be reshaped by heating after repeated cycles of freezing/melting. This is the fact which makes thermoplastics recyclable. Plastics used in the soda bottle are a common example of recoverable plastic. Thermoplastic polymers differ from thermosetting polymers (such as Bakelite or epoxy polymers) in that they can be re-melted and re-moulded. Thermosets behave differently. When a sufficient amount of heat is supplied, a chemical reaction takes place and a permanent change in the material

## Chapter 1

---

occurs. The reaction is called crosslinking. After crosslinking thermoset will not melt. At higher temperatures thermosets degrade. A thermoset can never be melted after curing, which means that it is not recyclable. Thermoset materials are generally stronger than thermoplastic materials and are better suited to high temperature applications up to the degradation temperature [3].

Besides the above classification, elastomers can also be categorized into two main groups, i.e., amorphous and crystalline elastomers. In the latter case monomers are arranged in a regular order and pattern, while in amorphous elastomers there is no order and proper arrangement of monomers. The crystallinity of elastomers depends upon on its structure, as they will pack more easily into crystals if their molecular structure is regular and well ordered. For example, in the case of polystyrene, syndiotactic polystyrene is very crystalline, while atactic polystyrene is very amorphous. Crystallinity of the syndiotactic polystyrene is due to a very regular chemical structure with the phenyl groups falling on alternating sides of the chain. Such an order makes it possible for chains to be easily packed into crystals. On the other hand, atactic polystyrene has no such order. The phenyl groups come on any side of the chain in a random fashion. With no order, the chains cannot pack easily. That is why atactic polystyrene is very amorphous. The chain structure of both polymers is shown in Figure 1.



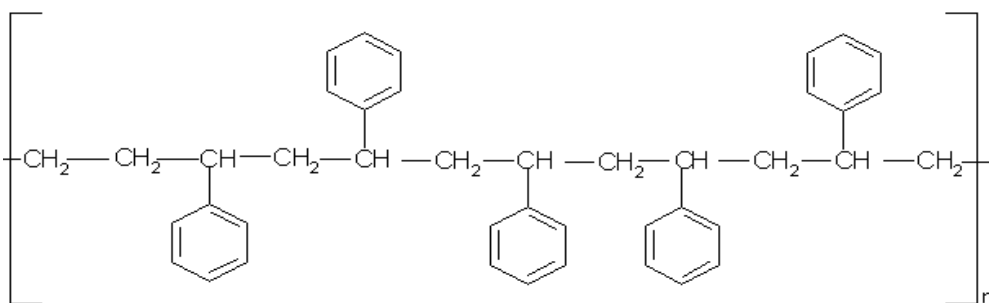


Figure 1.1: Chain structure of syndiotactic (above) and atactic Polystyrene.

Crystallinity makes a material hard, but it also makes it brittle. The amorphous regions give polymer toughness, that is, the ability to bend without breaking. However both crystalline and amorphous elastomers are important and have numerous applications. For examples in the case of making fibers, we like our polymers to be as crystalline as possible [4, 5].

The development of new, well-defined structure, homogeneous catalysts based on Group 4 metals (metallocenes and post-metallocenes) has allowed in recent years the formulation of new classes of polyolefins [6]. New copolymers with special properties have been synthesized including innovative elastomeric materials. In particular polyolefin based materials, such as syndiotactic polypropylene, have shown interesting and unexpected elastic properties [6,7]. Based on these new developments a particular class of new elastomeric materials has been developed, characterized by non-negligible degree of crystallinity and high melting temperature [8]. In these crystalline elastomers, usually formed by olefin co-polymers, the typical mechanical properties of crystalline materials (high rigidity and high stress to break) are associated with those of an elastomer (high deformability and high ductility).

For these reasons, crystalline elastomers constitute a class of very promising innovative materials for applications in different technological areas.

In the study of crystalline elastomers, a relevant area of research is certainly that of the relationships between molecular architecture and macroscopic properties. As it has been already pointed out, the use of very selective catalysts allow for the synthesis of "tailored" polyolefins where molecular characteristics such as stereoregularity, regioregularity, distribution of defects, molecular mass and distribution of molecular masses can be accurately. This, in turn, opens the way to the production of materials whose ultimate and processing physical properties can be selectively targeted.

In this area of research, the role of rheology can assume a crucial relevance. Rheology has been always used as a qualitative and quantitative tool in polymer science and engineering for many years. Areas such as polymer processing and quality control have enjoyed the use of rheological methodologies to determine the flow properties of polymer melts and more complex polymer-based systems (e.g., blends, suspensions). More recently, rheological techniques have been increasingly used as a tool to relate the behavior of polymer systems under deformation and/or flow to the local microstructure of the system at different length scales. In particular, the development of rheological models on a molecular basis [70] has led to the determination of relations (often quantitative) between the macroscopic rheological properties and the molecular characteristics of the polymeric chain (such as, for example, molecular weight, degree of branching, entanglement density). For all these reasons, rheology can be seen as a promising, successful instrument to help in a better understanding of the

molecular architecture of crystalline elastomers and of the relations between such architecture and the other macroscopic properties of these materials.

Based on the above, it can be said that rheology is expected to play a role in achieving the rational design of materials based on tailored polyolefins. Rheological techniques, in fact, are often more sensitive to certain aspects of the molecular structure and easier to use than other more conventional analytical techniques. The general aim of the present research work is to explore the relationships between the rheological response and the molecular structure of the class of innovative crystalline elastomers. Research objectives of this research work are depicted below in detail.

### 1.2. Research Objectives

1. To explore the rheological behavior of selected poly-olefin based crystalline elastomers in the melt state and to relate the rheological response to the local architecture of the polymer chain.
2. To study the quiescent crystallization behavior of selected crystalline elastomers by coupling rheological methods to more conventional techniques (such as Differential Scanning Calorimetry) and to relate the crystallization behavior to the stereo-regularity of the polymer chain.
3. To explore the role of extensional flow on the crystallization of selected polyolefins and to relate such an effect to the molecular order of the polymer chain.

**First objective:** We want to determine the rheological parameters of olefin based crystalline elastomers in the melt state, in order to relate them to the molecular architecture. For this we will need to choose and conduct suitable rheological experiments. We will carry out all the rheological experiments using linear, small amplitude shear oscillatory flow experiments. A general

advantage of this method is that a single instrument can cover a wide range of frequencies. The typical frequency range of the available rheometers is 0.001 to 500 rad/s. Different methods, such as the Time Temperature Superposition (TTS) principle will be applied to explore the rheological behavior of elastomer samples in order to uncover the higher frequency range. As a second step, the relationship between melt rheological response and molecular structure of the selected polymers will be explored. In fact, the melt rheological properties are very sensitive to the molecular structure. For example, the zero shear viscosity is used to detect the long chain branching. Moreover, melt rheological data are very sensitive to Molecular Weight (MW) and to Molecular Weight Distribution (MWD) [13]. In our case the best candidate rheological quantity to be explored is the so-called “plateau modulus”, to be obtained from linear viscoelastic data. This is an important characteristic constant of each polymer, as it can be related to other microstructure parameters using the classical reptation theories of polymer chain dynamics [70]. Our aim will be to relate the plateau modulus to the local degree of stereo-regularity of the polymer chain.

**Second objective:** In order to examine the quiescent crystallization behavior of polyolefins of different stereoregularity by rheological technique two different experimental techniques will be used (isothermal and non-isothermal crystallization). Isothermal crystallization will be conducted by fast cooling of a polymer melt from above its melting point temperature to the crystallization temperature,  $T_C$  and holding it at that temperature until crystallization is completed. While in non-isothermal crystallization the polymer melt will be cooled to the temperature below melting point by slow cooling rates. The results obtained from rheological technique will be compared with the differential scanning calorimetric (DSC) analysis.

**Third objective:** In the extensional flow study the first objective is to examine the crystallization kinetics by the application of extensional rate at a temperature above the melting point. The first step is to heat the sample above the melting point in order to break down all the crystals. After annealing for shorter time, the sample will be cooled to a temperature slightly above the melting point. The effect of extensional flow on crystallization kinetics will be estimated on the basis of change in the induction time due to extensional flow. The results will be verified by some X-Ray analysis of the stretched samples.

After successfully achieving the first objective, effect of extensional flow on the crystallization process will be examined by applying the extensional rate at a temperature below melting point and above crystallization temperature. The selection of temperature will be made by taking care of the following two points. The temperature should not be in the range where quiescent crystallization kinetics is faster. Because in this case it will not be possible to see the effect of extensional rate on the kinetics of crystallization. The temperature should also not be high to the extent that there is no effect of extensional rate on the crystallization kinetics. The selected temperature at which extensional rate will be applied should be in optimum region, where one is able to analyze the effect of extensional rate on the kinetics of crystallization.

### **1.3. Literature Review**

The literature review section has been divided into five sections i.e., synthesis, mechanical properties, rheology, crystallization and flow induced crystallization.

### 1.3.1. Synthesis

Crystalline elastomers such as polypropylene, poly-1butene, syndiotactic polystyrene and their co-polymers, are synthesized by the process of polymerization. Polymerization is the process of combining many small molecules known as monomers into a covalently bonded chain [14]. Different methods have been reported in literature [15-55]. Polymer samples which will be used in this work are olefin based crystalline elastomers synthesized by Co-ordination polymerization (Ziegler Natta catalysis and Metallocene methods). Therefore the main focus of this section will be on co-ordination methods used for the synthesis of the olefin based crystalline elastomers. Synthesis methods used so far for these polymers can be categorized into four methods: ionic polymerization, cationic polymerization, free radical polymerization and co-ordination polymerization.

Ionic polymerization occurs by the formation of the carbanion ion. Formation of the carbanion ion occurs by the attack of a nucleophilic reagent at one end of the double bond [16-18]. This first step, formation of the carbanion ion is called the initiation step. For example, in the case of ethylene.

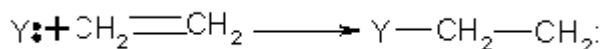


Figure 1.2: Chain Initiation step of Ionic polymerization.

Attacking of carbanion ion on another alkene molecule would give a four carbon-carbon anion and subsequent additions to further alkene molecules would lead to a higher molecular weight chain. This second step is called the chain propagation step.



Figure 1.3: Chain Propagation step of Ionic polymerization.

The third and last step during the anionic polymerization is the chain terminating step. The termination of polymerization will occur by terminating the carbanion ion. The ion can be terminated by the addition of the proton. The shortcoming and drawback of this process is that, in this process, large number of powerful electron attracting groups are required to speed up the nucleophilic attack.

In cationic polymerization, formation of the carbonium carbon occurs. This occurs by the addition of the proton to alkene from acid (suitable acid). Then, in the absence of strong nucleophilic reagents, another alkene molecule donates an electron pair and forms a longer chain cation [19].

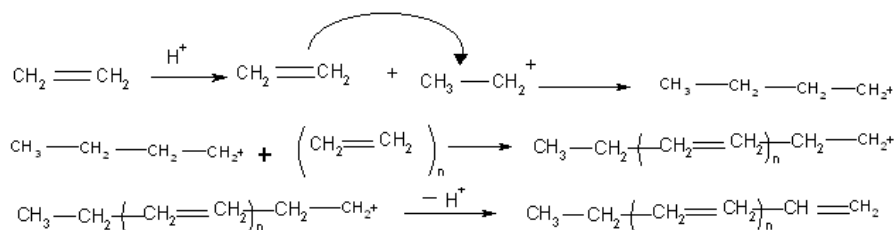


Figure 1.4: Reaction mechanism of Cationic polymerization process.

In free radical polymerization, formation of free radicals occurs (initiation). Then subsequent addition of radicals to the alkene molecules occurs (propagation). The chain termination step may occur by any reaction resulting in combination or disproportionation of free radicals [19].

In all the above different methods, special nucleophilic reagents and other reaction conditions are required. All the above methods have been

## Chapter 1

---

replaced by the Ziegler Natta catalysis, metallocene and post metallocene methods, generally known as co-ordination polymerization methods [20-55]. Co-ordination polymerization is the process of polymerization in the presence of a catalyst. Ziegler introduced a new type of catalyst in 1940 (alkane solvent containing a suspension of the insoluble reaction product from triethylealuminium and titanium tetrachloride). The Ziegler process can produce an efficient and high molecular weight with remarkable physical properties. The usual characteristics of these reactions indicate that no simple anion, cation or free radical mechanisms are involved [20-55].

Generally this type of polymerization occurs in the three steps: (i) Initiation (ii) Propagation and (iii) Termination. The mechanism of this type of chemical reaction has been explained very well by the Cossee model [22]. According to this model during the initiation step co-ordination occurs, where co-ordination occurs between the metal and the alkene monomer.

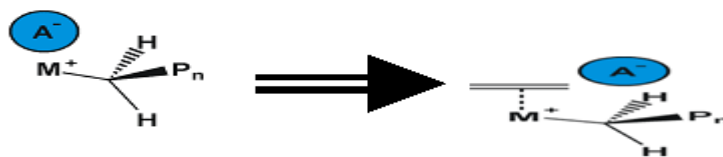


Figure 1.5: Chain initiation step during the Co-ordination polymerization process.

In the second step the co-ordination proceeds to another state called transition state..

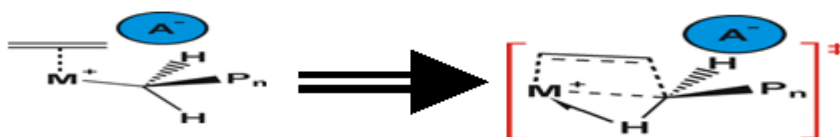


Figure 1.6: Transition state during the Co-ordination polymerization process.

The third step is the insertion of alkene monomer.

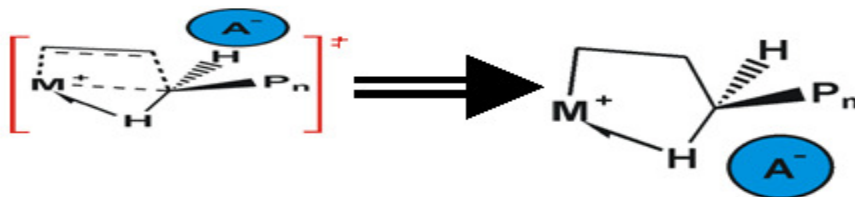


Figure 1.7: Final step of alkene monomer insertion during the Co-ordination polymerization process.

Where  $P_n$  is the growing polymer chain.

This insertion repeats several times, thus determining the propagation of the polymerization process. The last step is the termination or end of polymerization, which can be done by the deactivation of the catalyst. In general Ziegler Natta catalysts are very region-regular in nature but polymers with high stereo-regularity can also be produced by this method. Regio-regularity is the phenomenon in which macromolecules are formed by the successive insertions of the same monomer independent of the choice of configuration. Conversely in stereo-regularity there is regularity in the succession of configurations of the tertiary carbon atoms.

Ziegler Natta catalysts can be classified into two main groups.

- (a) One type of catalysts that produce stereo-regular polymers is known as  $C_s$ -symmetry catalysts. The general geometry of the  $C_s$ -symmetry catalyst is shown in Figure 1.8.

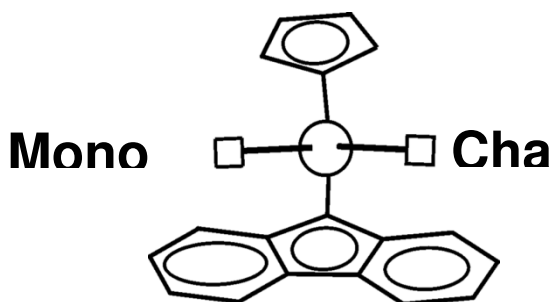


Figure 1.8: Ziegler Natta catalyst of  $C_s$ -symmetry.

According to Ewen and Razavi the syndio-specificity arises from propylene insertions occurring from alternating (enantiotopic) sides of the metallocene wedge with the propylene methyl group directed away from the larger fluorenyl ligand [51,52]. The syndio-specific  $C_s$ -symmetric catalysts are those for which the two available co-ordination positions are enantiomorphous.

It has been reported in the literature that the catalytic system based on the  $C_s$ -symmetric  $H_2Si-(2,3,4,5-Me_4C_p)(C_p)$  ligand should be substantially non enantio-selective due to the repulsion interaction between the methyl groups of the propene and the methyl groups of  $(Me_4C_p)$  ligand. This is an agreement with the low syndio-tacticity and activity experimentally observed for the catalyst based on the ligand [44-48].

(b)The other type of catalysts that produce region-regular polymers are known as  $C_2$ -symmetry catalysts.  $C_2$ -symmetry catalysts have been shown in chart 2.

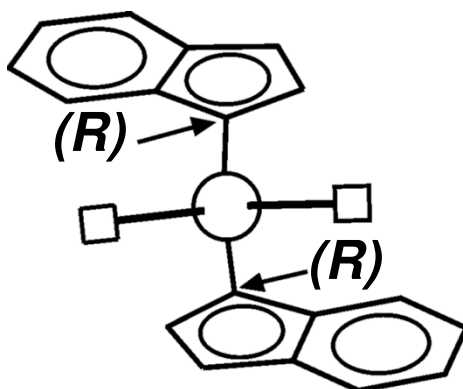


Figure 1.9: Ziegler Natta catalyst of  $C_2$ -symmetry.

The discovery of the single site metallocene catalysts has revolutionized the polyolefin technology scenario and has produced excellent control of the stereochemistry and molecular weight of polypropylene without sacrificing the narrow molecular weight distribution [9, 10, 11]. Metallocene is an

organo metallic compound consists of two cyclopentadienyl anions ( $C_5H_5^-$ ) bound to a metal center in the oxidation state resulting in the general formula  $(C_5H_5)_2M$ . M is a metal like titanium, vanadium, iron etc. Some metallocenes and its derivatives like titanium chloride or vanadium chloride exhibit catalytic properties [41, 44, 45, 49].

Literature review shows that transition metals like titanium and zirconium exhibit better catalytic properties because their electronic configuration is able to induce polymerization [41, 44, 45, 48, 49, 53]. Metallocene catalysts are homogeneous single-site systems, indicating that there is a single, uniform type of catalyst present in the system. This is in contrast to the Ziegler-Natta catalysts which are heterogeneous system and contain a wide range of catalytic sites. The catalytic properties of single-site catalysts can be varied by modification of the structure of the catalyst. A large number of studies have been conducted by academia and industry to construct high-performance metallocene catalysts based on new concepts. The first metallocene and the first catalyst in general able to produce highly syndio-tactic polypropylene (sPP) was the  $C_s$ -symmetry  $Me_2C(C_p)(9-Flu)-ZrCl_2$ .

Another type of catalysts for the polymerization process is that of post metallocene catalysts. Post-metallocene belongs to the generation of catalysts following Kaminsky catalysts, which are metallocene catalysts discovered in 1980 by Walter Kaminsky, and have been predominant in the olefin polymerization catalyst area for nearly the last twenty five years [43]. The first post-metallocene catalysts appeared in the late 1990s. Most post-metallocene catalysts are homogeneous single-site systems. This means that their catalytic properties can be controlled by modification of the structure of the catalyst. Most post-metallocene catalysts have been synthesized by using

early transition metals. However, late transition metal complexes such as nickel, palladium, and iron complexes have also been reported as good catalysts for olefin polymerization. These different techniques of the coordination polymerization have been explored by many researchers [26, 27, 28, 37, 40].

Eckstein et al. [86] have followed out research on the synthesis and rheological properties of polypropylene melts. Atactic polypropylene was synthesized using methylalumoxane (MAO) at 283 K in a mixture of liquid propene and toluene. Polymerization was executed in a 1.6 L Buechi glass autoclave reactor equipped with a torsion valve. During the polymerization process, the temperature was kept constant at 283 K by a combination of inner and outer cooling.

One way of improving or changing the properties of the polymers is to use co-monomer. A co-monomer is used in commercial polymers to alter the properties of a base polymer, for example to change its glass transition temperature, degree of crystallinity or swelling behavior, or to make it more compatible with a plasticizer or dye or to enhance its stability. The process which is used for its synthesis is called co-polymerization. When polymerization occurs in a mixture of monomers, there will be some competition between the different kinds of monomers to add to the growing chain and produce the polymer chain. The rates of incorporation of various monomers into the growing free radical chains have been studied in considerable detail. These rates depend markedly on the nature of the monomer being added and of the character of the radical at the end of the chain. The co-polymerization processes can be classified into the three types depending on the values of the monomer reactivity ratios [55, 56].

1. When the product of the two monomer reactivity ratios is unity.

2. When the product of the two monomer reactivity ratios is less than unity.
3. When the product of the two monomer reactivity ratios is greater than unity.

Ideal co-polymerization occurs in a case when both the propagating species show the same preference.

Co-polymers can be synthesized by the chain shuttling polymerization process. Chain shuttling polymerization is the process in which two catalysts and a chain shuttling agent are used. By this method co-polymers of alternating tacticity are synthesized. During this process catalyst 1 generates a polyolefin of a desired tacticity while catalyst 2 generates another chain of a different tacticity. The two chains are allowed to co-propagate in a single reactor. To alternate the tacticity a chain shuttling agent will transfer the polymer chain from its respective catalyst. The chain shuttling agent can then cling to catalyst 2 and attach the chain coming from catalyst 1 to catalyst 2. When the chain attaches to catalyst 2, the polymerization of that chain continues, except it now propagates with tacticity dictated by catalyst 2 and no longer by catalyst 1. The general result is that the chain will fluctuate between two different tacticities. As the two actions occur, the polymer chain is shuttled back and forth between the two catalysts and a block co-polymer is formed. Mechanism of the process has been explained below in a clearer way.

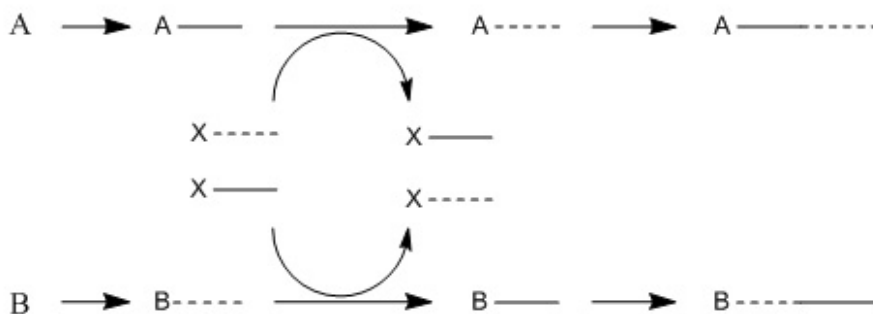


Figure 1.10: Mechanism of Chain shuttling polymerization process.

Where A, B and X are catalyst 1, catalyst 2 and chain shuttling agent respectively. — and ----- are chain 1 and chain 2 respectively.

### 1.3.2. Mechanical Properties

Several research works have been reported in the literature not only on the synthesis, but also on the mechanical and rheological properties of polyolefin polymers and co-polymers. As a way of example, Wang et al. [10], have examined the synthesis, dynamic mechanical and rheological properties of the long chain branched ethylene/propylene co-polymers. The novel series of long chain branched ethylene/propylene copolymers were synthesized with a constrained geometry catalyst (CGC),  $[\text{C}_5\text{Me}_4(\text{SiMe}_2\text{N}^t\text{Bu})]\text{TiMe}_2$ , and had various propylene molar fractions of 0.01-0.11 and long chain branch frequencies (LCBF) of 0.05-0.22. The linear ethylene/propylene co-polymers were synthesized with an ansa-zirconocene catalyst,  $\text{rac-Et}(\text{Ind})_2\text{ZrCl}_2$  (EBI), and contained similar levels of propylene incorporation as the CGC copolymers, but no long chain branched. Wang et al. showed that catalyst system, reaction conditions and synthesis technique affect the mechanical, thermal and rheological properties of the polymer

synthesized. In this section, attention will be given to the mechanical properties of crystalline elastomers.

Characteristics of polymers like stereoregularity, molecular mass and polydispersity depend upon on the catalyst system and reaction conditions of the polymerization process. These characteristics are the main structural factors, which affect the physical and mechanical properties. Mechanical properties of polyolefins are largely related to the crystal structure and morphology, which in turn depend on the chain microstructure generated by the catalyst system used [58, 59].

The mechanical properties of the crystalline polymers strongly depend upon on the stereo-regularity and initial morphology of the samples [59-64]. Unoriented samples of high stereo-regularity and crystalline syndiotactic polypropylene behave as a typical crystalline thermoplastic material showing plastic deformation via necking during stretching with high values of Young's modulus [57-60]. The samples experience a partial elastic recovery after breaking or upon releasing the tension after deformation [59-65]. On the other hand oriented fibers of syndiotactic polypropylene exhibit a perfect elastic behavior upon successive stretching and relaxation cycles [60-65].

Strength and toughness are the two main mechanical properties of the polymers. Strength is a mechanical property, which gives us information that how much a material is strong [66]. In the other words strength can also be defined as the stress needed to break the sample. In stress-strain experiments, a polymer sample is subjected to a constant elongation rate, and stress is measured as a function of time. Generally the polymer sample, which may be in the form of circular in cross-section or rectangular, is molded. It is clamped at both ends and pulled at one of the clamped ends (normally in downward direction) at constant elongation. The shape of the test sample is

designed to encourage failure at the thinner middle portion. The load or stress is determined at the fixed end by means of a load transducer as a function of the elongation, which is measured by means of mechanical, optical or electronic strain gauges. The experimental data are generally noted as engineering (nominal) stress ( $\sigma$ ) vs. engineering (nominal) strain. The engineering stress is defined as:

$$\sigma = F/A \quad (1.1)$$

Where  $\sigma$  = stress, F= Force and A= area.

When a material is subjected to stress, there are two possibilities. It will deform and will come back to its initial shape and dimensions after the removal of the stress or it will deform permanently. This ability of deformed material to recover to its original dimensions is known as elastic behavior. Beyond the limit of elastic behavior (elastic limit), a material will experience a permanent change or deformation even when the load is removed. Such a material is known to have undergone plastic deformation. For most materials, Hooke's law is obeyed within the elastic limit, that is stress proportional to strain. However proportionality between stress and strain does not always hold when a material shows elastic behavior. A typical example is rubber, which is elastic but does not exhibit Hookean behavior over the entire elastic region.

Figure 1.11 dictates mechanical properties that are obtainable from stress-strain experiments. The slope of the initial linear portion of the curve, within which Hooke's law is obeyed, gives the elastic or Young's modulus. The determination of the elastic limit is tough and is dependent on the sensitivity of the strain-measuring devices employed. Consequently, it is common practice to replace it with the proportional limit, which defines the point where the non-linear response is noted on the stress-strain curve. The

maximum on the curve denotes the yield strength. For engineering purposes, this marks the limit of usable elastic behavior or the onset of plastic deformation. The stress at which fracture occurs (material breaks apart) is referred to as the ultimate tensile strength or, simply, tensile strength. The strains associated with the yield point or the fracture point is referred to as the elongation at yield and elongation at break respectively.

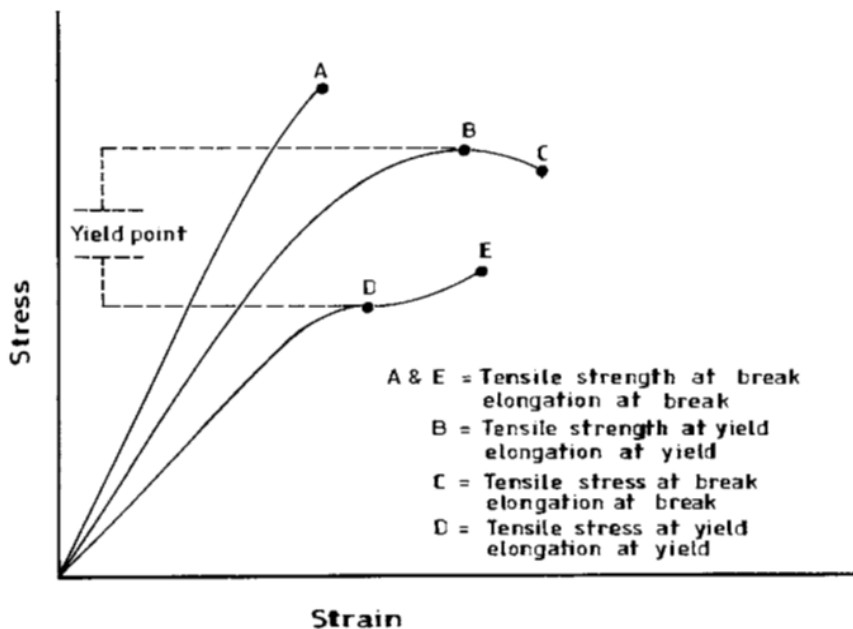


Figure 1.11: Engineering data from stress-strain tests [66].

The reaction of material to the applied stress may be described as ductile or brittle depending on the extent to which the material undergoes plastic deformation before fracture. Ductile materials have got the ability to undergo plastic deformation. On the other hand, brittle materials fail with little or no plastic deformation. Brittle materials have no capability for local yielding; hence local stresses build up around inherent flaws, reaching a critical level at which abrupt failure occurs. In case of brittle materials, a lot of force is required to break the sample, but not much energy is required. In the words

brittle materials have high strength and low toughness. Toughness of materials tells us that how much energy is required to break the sample. Therefore it is not necessary that a material will be strong as well as tough. While in the case of ductile materials, toughness is higher than the strength. Because in case of ductile material, it deforms a lot before breaking. Deformation allows a sample to dissipate energy. If a sample cannot deform, the energy would not be dissipated and will cause the sample to break.

Moving to the class of materials of specific interest for the present work, several studies have been considered the solid mechanical behavior of polyolefin crystalline elastomer and their relations with the stereo-regularity of their molecular architecture. Auriemma et al. conducted research on the mechanical properties and structure of syndiotactic polypropylene samples in order to clarify the origin of its elastic behavior [67]. They analyzed the mechanical properties of syndiotactic polypropylene samples having different degrees of tacticity. They found that the elastic properties of the syndiotactic polypropylene mainly originate from a reversible crystal-crystal phase transition, which occurs during the stretching and when the tension is removed. They found that conformational crystal-crystal transitions are responsible for the elastic behavior of the syndiotactic polypropylene. They also found that, in the less stereo-regular samples, there is a plastic and permanent deformation and elastic properties are suppressed. The reason of this behavior is the absence of crystal-crystal transition in poorly syndiotactic polypropylene samples. They also examined the mechanical properties (Young's modulus, stress and strain at break, tension and elastic recovery at a given elongation) of the samples. In their analysis they used two types of syndiotactic polypropylene samples i.e., unoriented compression molded samples and strained and stress relaxed syndiotactic polypropylene samples

(oriented samples). The latter were obtained by keeping syndiotactic polypropylene fiber samples under tension for two days and then removing the stress, thus allowing for fiber relaxation. Syndiotactic polypropylene samples were compressed and stretched up to a given strain of 400% and 600%. They concluded that the elastic properties of the unoriented samples are poor since they undergo a plastic deformation by stretching and do not present any recovery of the initial dimensions upon release of the tension. Similar behavior was observed for the less stereo-regular syndiotactic polypropylene samples. Conversely, the mechanical properties of the oriented stress relaxed fibers were found similar to the mechanical properties of true elastomers. For these samples of syndiotactic polypropylene the stress-strain curve were found to be almost linear.

In another work De Rosa et al., found almost the same mechanical properties during their investigation on the isotactic polypropylene samples. They found that poor stereo-regular samples showed remarkable strain hardening due to the low plastic resistance of crystals and by straightening of the entangled network. They also concluded that the different mechanical behavior is due to the structural transformations that occur during stretching [59].

More recently Auriemma et al. [68] confirmed the observed behavior for different types of stereo-block polypropylenes. In particular, unoriented samples have a stress-strain curve typical of thermoplastic material with a partial but significant recovery of the initial dimensions measured after breaking and after releasing the tension from different degrees of deformation. On the other hand, stress relaxed fibers were found to show tensile properties typical of thermoplastic elastomers with high values of

elongation before breaking, tensile strength and Young's modulus and showed strong strain hardening at high values of deformation [68].

In conclusion, it can be said that the mechanical properties of polyolefin based crystalline polymers are affected by the stereo- and region-regularity of the polymer chain. These properties determine both the formation and the type of the crystalline phase, which is also strongly affected by the mechanical history. In turn, all these phenomena are found to have a profound influence on the mechanical properties of the solid materials.

### **1.3.3. Rheology**

Rheology has a key role in polymer research being an important link to the chain of knowledge. Polymers such as elastomers are viscoelastic in the melt, which means that they possess both a viscous and an elastic component [69-85]. In this section we will focus only on aspects of the rheological behavior that are of interest for this work. In particular, attention will be given to the so-called linear viscoelasticity.

One of the central objectives of rheology is the determination of the so-called constitutive equation of the material. A constitutive equation is a mathematical relation that links the tensional state (the stress tensor) to the deformation history applied to the material. The study of the rheological behavior of viscoelastic materials and in particular of polymer melts has been typically conducted along two different lines. On the one hand the "continuum mechanics" approach starts from the phenomenological observation of the material response under deformation and/or flow. From there, a mechanical description of the material as mathematical "continuum" is derived without making assumptions on the particular microscopic structure of the system. Constitutive equations are then obtained that are consistent with the observed behavior, while satisfying at the same some

more general constraints (such as thermodynamic consistency). One positive aspect of the continuum mechanics approach is that the (often semi-empirical) constitutive equations possess a relative level of mathematical flexibility, thus allowing for successive refinements of the model in order to improve the agreement between theory and experimental observations.

Another, completely different approach is the so-called “molecular” or “micro-rheology” modeling. In this case constitutive equations are built on the basis of a microscopic description of the material microstructure. In the case of polymer melts, in particular, a physical model for the single polymer chain and for entangled chain network is required. Polymer chains are Brownian objects. Therefore the material macroscopic behavior can be derived only by introducing the mathematical description of the polymer chain into the classical equation of statistical thermodynamics. Following these lines, rheological constitutive equations can be derived. The main difficulty of this approach is in its generally very complex mathematical formulation. On the other hand, micro-rheology modeling allows establishing direct relations between the local details of the molecular structure and the observable rheological properties.

In the following, some basic information on constitutive equations and on micro-rheological models, which will be relevant for the subsequent development of this work will be given. [2].

### **1.3.3.1. Continuum mechanics linear viscoelasticity**

As it was said before, in continuum mechanics, constitutive equations are developed on the basis of the observed phenomenological behavior of the material. When considering viscoelastic fluids, that are materials that exhibit both a viscous and elastic materials, it is useful to start from the so-called linear viscoelasticity hypothesis. Linear viscoelasticity implies that the

response (e.g. strain) of the fluid at any time is directly proportional to the value of the initiating signal (e.g. stress). So for example, doubling the stress will double the strain. Starting from this hypothesis it is possible to develop linear constitutive equations that relate the state of stress in the fluid to the corresponding deformation history. By referring for simplicity to a single component of the stress tensor (e.g., the shear stress) and to the corresponding deformation (the shear deformation), a general differential constitutive equation for the linear viscoelasticity can be written as follows:

$$\left(1 + \alpha_1 \frac{\partial}{\partial t} + \alpha_2 \frac{\partial^2}{\partial t^2} + \dots + \alpha_n \frac{\partial^n}{\partial t^n}\right) \sigma = \left(\beta_0 + \beta_1 \frac{\partial}{\partial t} + \beta_2 \frac{\partial^2}{\partial t^2} + \dots + \beta_m \frac{\partial^m}{\partial t^m}\right) \gamma \quad (1.2)$$

Where  $\sigma$  is the stress,  $\gamma$  is the deformation and  $\alpha_i$  and  $\beta_i$  are the linear material parameters of the fluid. In Eq (1.2)  $n=m$  or  $n=m-1$ . Eq (1.2) can be generalized to a tensorial constitutive equation, but this is beyond the scopes of this work.

It is useful to study the simplest special cases of equation (1.2) will be discussed.

Case (1): If  $\beta_0$  is the only non-zero parameter then eq(1.2) becomes :

$$\sigma = \beta_0 \gamma = G \gamma \quad (1.3)$$

Eq (1.3) is the well-known equation of Hookean elasticity and  $\beta_0$  is the (shear) rigidity or (shear) elastic modulus. In this form therefore Eq. (1.2) is able to describe the linear elastic behavior which is typical of most solids at sufficiently small (linear) deformations.

Case (2): If  $\beta_1$  is the only non-zero parameter then we have

$$\sigma = \beta_1 \frac{d\gamma}{dt} = \eta \dot{\gamma} \quad (1.4)$$

Eq(1.4) is the Newton law of viscosity. Here  $\beta_1$  is the fluid viscosity. Eqs (1.3) and (1.4) are particularly relevant as they define the simplest types of linear behavior corresponding to the linear elastic solid and to the linear viscous (Newtonian liquid). A material that exhibits both characteristics will be indeed viscoelastic.

Case (3): If  $\beta_0$  and  $\beta_1$  are the only non-zero parameters, then we have

$$\sigma = \beta_1 \frac{d\gamma}{dt} + \beta_0 = \eta \dot{\gamma} + G\gamma \quad (1.5)$$

$$\sigma = G\gamma + \eta \dot{\gamma} \quad (1.6)$$

This is one of the simplest models of viscoelasticity, which is known as Kelvin-Voigt model. The Kelvin model describes sufficiently well the viscoelastic behavior of a solid material. In fact, under steady state conditions, the material obeys the linear elasticity law.

Case (4): If  $\alpha_1$  and  $\beta_1$  are the only non-zero parameters then we have:

$$\sigma + \tau \frac{d\sigma}{dt} = \eta \dot{\gamma} \quad (1.7)$$

Eq (1.7) is universally known as the Maxwell model. Here  $\alpha_1 = \tau$  is the so-called relaxation time. Eq (1.7) is the simplest constitutive continuum mechanics equation for a viscoelastic liquid. It can be easily shown that the Maxwell model can be described in terms of a simple mechanical analogy as a spring connected in series with a dashpot as shown in Figure 1.12.

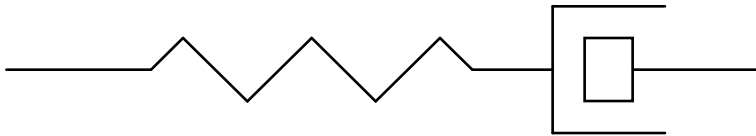


Figure 1.12: The Maxwell spring-and-dashpot mechanical analog.

If a stress is applied to both ends of this mechanical object the resulting deformation will be the sum of the deformation of the spring and of the dashpot:

$$\gamma = \gamma_E + \gamma_V \quad (1.8)$$

Differentiation of (1.8) with respect to time yields:

$$\dot{\gamma} = \frac{d\gamma_E}{dt} + \frac{d\gamma_V}{dt} \quad (1.9)$$

By assuming linear elastic behavior of the spring (with elastic modulus  $G$ ) and Newtonian behavior of the dashpot (with viscosity  $\eta$ ) Eq(1.9) can also be rearranged as :

$$\sigma + \tau \frac{d\sigma}{dt} = \eta \dot{\gamma} \quad (1.10)$$

Where the relaxation time is given by:

$$\tau = \frac{\eta}{G} \quad (1.11)$$

Eq. (1.6) is able to describe the basic features of the fluid linear viscoelastic response. In particular under steady shear flow Eq (1.6) gives:

$$\sigma = \eta \dot{\gamma} \quad (1.12)$$

That is the Newtonian liquid behavior. In the so-called step-strain test, where the fluid is instantaneously deformed by a deformation  $\gamma_0$ , the subsequent decay of stress in time is given by:

$$\sigma = G\gamma_0 \exp\left(-\frac{t}{\tau}\right) \quad (1.13)$$

Where it is clear the meaning of the relaxation time of the material.

Of particular interest is the response of a Maxwell viscoelastic fluid to periodic oscillatory shear flow. It can be easily shown that if the fluid is subjected to a sinusoidal deformation of amplitude  $\gamma_0$  and frequency  $\omega$ :

$$\gamma = \gamma_0 \sin(\omega t) \quad (1.14)$$

Under linear condition the resulting stress response will be:

$$\sigma = \sigma_0 \sin(\omega t + \delta) \quad (1.15)$$

The phase angle (or delay)  $\delta$  gives a direct indication of the viscoelastic nature of the fluid. If  $\delta=0^\circ$ , the stress is in phase with the deformation, and the behavior is that of an elastic solid. If  $\delta=90^\circ$  the stress will be in phase with the deformation rate:

$$\dot{\gamma} = \gamma_0 \omega \cos(\omega t) \quad (1.16)$$

and the observed behavior will that of a purely Newtonian fluid. When  $0^\circ < \delta < 90^\circ$ , both elastic and viscous components will be present.

The linear oscillatory viscoelastic response of the Maxwell fluid can be recast in the following form:

$$\frac{\sigma}{\gamma_0} = G' \sin \omega t + G'' \cos \omega t \quad (1.17)$$

where  $G'$  and  $G''$  are the so-called elastic (or conservative) and viscous (dissipative) moduli, as they are a measure of the two different component of the material viscoelastic response. For the Maxwell model one has:

$$\begin{aligned}G'(\omega) &= G \frac{(\tau\omega)^2}{1+(\tau\omega)^2} \\ G''(\omega) &= G \frac{\tau\omega}{1+(\tau\omega)^2}\end{aligned}\tag{1.18}$$

Eq. (1.18) shows the basic features of  $G'$  and  $G''$ . When  $\omega \ll \tau$ , the dissipative modulus is always larger than elastic modulus (both going to zero for vanishingly frequencies) and they obey the following scaling laws:

$$\begin{aligned}G' &\propto \omega^2 \\ G'' &\propto \omega\end{aligned}\tag{1.19}$$

When  $\omega \ll \tau$ ,  $G''$  goes to zero, where as  $G'$  goes to a plateau which correspond to the elastic modulus ( $G'$ ) of the Maxwell model. It will be shown later that the plateau modulus of a polymer is a fundamental parameter to describe the chain molecular structure. For  $\omega = 1/\tau$  the  $G''$  reaches a maximum which correspond also to the value where the two moduli cross-over. For this reason  $1/\tau$  is also called the cross-over frequency,  $\omega_{co}$ . A typical plot of the frequency response of the two moduli for a polymer obeying the Maxwell model (at least for not too high frequencies) is given in Figure 1.13.

As said before, the Maxwell model gives a qualitative good description of the linear viscoelastic behavior, in particular as far as the frequency response is concerned. Quantitative agreement however requires more complex models. One simple extension of the Maxwell model, which allows for good quantitative predictions of the frequency response of polymer melts is to allow for the presence of more than one relaxation time. This multi-mode Maxwell model is represented by the following equations:

$$\sigma_i + \tau_i \frac{d\sigma}{dt} = \eta_i \dot{\gamma}$$

$$\sigma = \sum_{i=1}^N \sigma_i \quad (1.20)$$

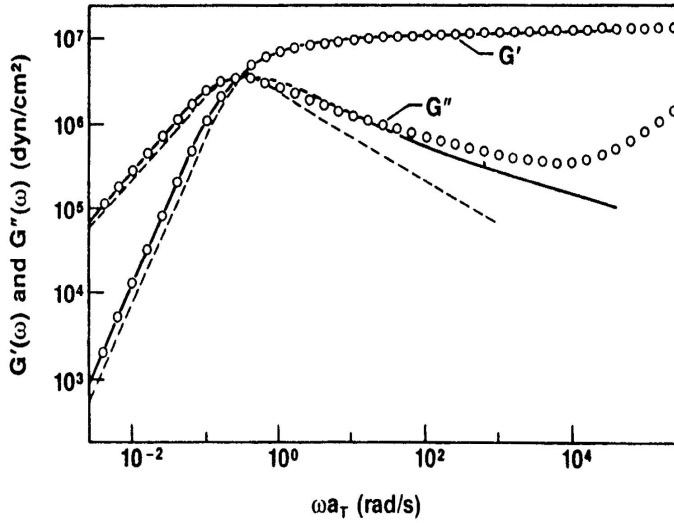


Figure 1.13: Frequency response of a poly-butadiene at 27°C. Dashed lines represent the predictions of the Maxwell model.

In Eq. (1.20) a set of  $N$  relaxation times and viscosities is introduced. It is easy to show that, in the case of a linear oscillatory flow, the viscoelastic moduli are given by:

$$G'(\omega) = \sum_{i=1}^N G_i \frac{(\tau_i \omega)^2}{1 + (\tau_i \omega)^2}$$

$$G''(\omega) = \sum_{i=1}^N G_i \frac{\tau_i \omega}{1 + (\tau_i \omega)^2} \quad (1.21)$$

Use of Eq. (1.21) to predict the linear viscoelastic behavior of polymer melts generally results in an excellent quantitative agreement with the experimental results.

### 1.3.3.2. Micro-rheological modes

The continuum mechanics approach does not consider the microscopic nature of the fluid. It only defines relations between stress and deformation history on the basis of a purely phenomenological macroscopic approach. Micro-rheology and molecular dynamics on the contrary are based on a description of the fluid microstructure. Here we refer to the situation of melts composed of linear polymer chains as it is the case for the polyolefins that are the subject of the present study.

The starting point of a micro-rheological description of polymer melts must recognize that the most important factor determining the dynamic behavior of a polymer chain is its very large length compared to its lateral dimension. Furthermore due to the very large number of internal degrees of freedom, polymer chains are able to assume many different conformations. As a consequence a single chain can be seen somewhat as a “thread”. Alternatively, the chain can be seen as a broken line composed of  $N$  monomers, each one of length  $b$ . In both cases, the shape and size of the chain continuously change due to thermal agitation. Brownian motion, in other words is able to incessantly alter the “conformation” of the chain, which will explore different configurations. An example of possible conformations assumed by a polymer chain with time is given in Figure 1.14.

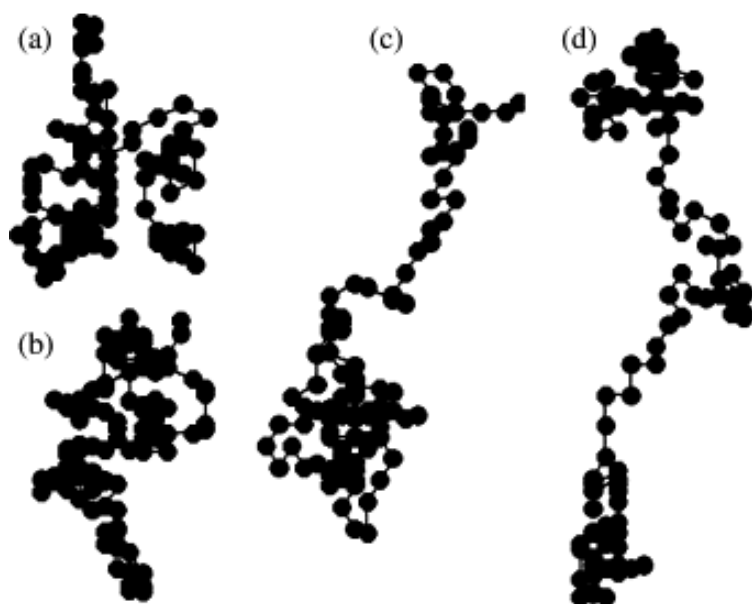


Figure 1.14: Snapshot of the conformations assumed by a single polymer chain due to Brownian motion.

Another “ingredient” in the description of the chain dynamics is that in a macroscopic sample an enormous number of chains are found. This means that if macroscopic properties are needed to calculate, this can be done only by performing appropriate averages over the large numbers of chains present.

One possibility to relatively simplify this already very complex picture is to reason as follows. Let us assume for example that we want to compute the portion of space occupied by a polymer chain, that is its size. It is apparent from Figure 1.14 that at a given time, different chains will be characterized by a different size depending on their conformation. This means that only a “mean” size can be determined by calculating the average over all chains. It can be shown that the same result can be reached by considering a single chain and calculating the average over all possible conformation that the chain can assume during time. This equivalence between space-average and

time-average is the so-called “ergodic principle”, which is at the basis of statistical thermodynamics. In particular, it can be shown that under quiescent conditions (that is in the absence of flow that can perturb the chain conformation distribution) the average chain size is represented by the square root of the so-called end-to-end mean square radius:

$$R^2 = Nb^2 \quad (1.22)$$

$R$ , as indicated by its name represents an average value of distance separating the beginning and the end of the polymer chain. Since the number of segments in the chain is directly proportional to its molecular weight. Eq (1.22) informs that the average chain size scales with the square root of the molecular weight.

The large number of conformations that can be assumed by a polymer chain is also responsible for its elastic component. Let us assume to pick the two ends of the chain and pull them in opposite directions, thus applying a force (tension) along the chain. Under the action of the force, the chain will uncoil, assuming an elongated conformation. When the force is released, Brownian motion will induce a retraction of the chain, in the sense that, all conformations becoming again available, the average size of the chain will tend to the unperturbed, equilibrium value given by Eq. (1.22). It is clear that thermal agitation plays the equivalent role of a spring-like restoring force. This “entropic elasticity” (that is, an elasticity that is related to the degree of conformational order of the chain) is at the basis of the elastic behavior of polymeric liquids.

The situation depicted above becomes much more complex when a polymer melt is considered. Here, many chains are present and interact with each other. The main additional ingredient in this picture is that the motion

of the chains (and therefore their conformational changes) is strongly restricted by the presence of the other chains (see Figure 1.15).

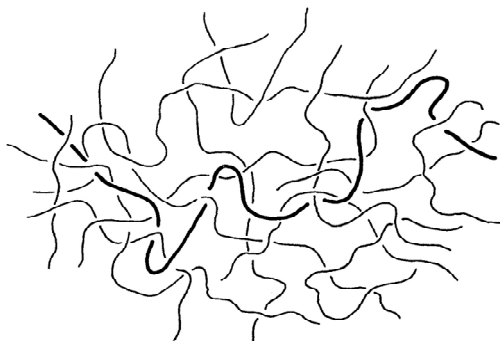


Figure 1.15: A schematic view of the entangled melt.

Chains in fact cannot physically cross each other. The steric hindrance between one chain and the others is universally known with the term “entanglement”. The network of entangled chains determines an additional elastic component on top of the entropic elasticity of the single chain.

Numerous research works have been reported in the literature on the dynamics of chains in polymer melts [60-73]. Here, specific attention will be given to one molecular or micro-rheological model, which is called the reptation model. It will be shown that from this model we can extract relations between rheological properties such as moduli, relaxation times, and microstructural properties such as molecular weight, molecular weight between entanglements and ultimately the chain molecular architecture.

According to the reptation model, the topological resistances imposed by the neighboring chains on a given polymer chain restrict its motion to a tube like region called the confining tube. A schematic view of this conceptual idea is given in Figure 1.16.

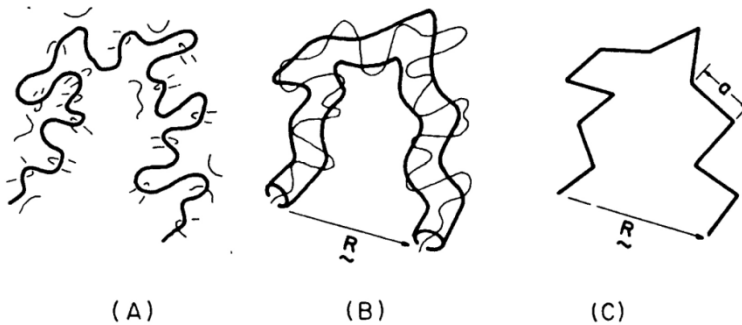


Figure 1.16: a schematic picture of the tube of entanglements. In (A) the test chain is surrounded by other chains. Only entanglements are highlighted; in (B) entanglements are substituted by the tube; in (C) the polymer chain inside the tube is reduced to its primitive path of  $N/N_e$  segments each of length  $a$ .

Rheological models, which consider chain motion as being restricted to a tube like are referred as tube models. The first and simplest tube model was proposed by De Gennes in 1971 for the motion of linear entangled polymers [92]. De Gennes utilized the Edward's idea of a single chain motion confined to a tube of surrounding chains. According to the De Gennes tube model, an entangled chain diffuses along its confining tube in a way analogous to the motion of the snake or worm. The motion of the chain consists in the diffusion of small loops along the contour of the primitive path (see Figure 1.17). The primitive path is the shortest line connecting the chain ends without violating the topological constraints and can be represented by a broken line of curvilinear length  $L$  composed by strands of individual length  $a$ . The latter therefore is a measure of the average distance between two subsequent entanglements along the chain. In this picture the real chain is composed of  $N$  monomers each of length  $b$ . If  $N_e$  is the average number of monomers contained in each tube strand, the following relations hold:

$$L = \frac{N}{N_e} a \quad (1.23)$$

$$Nb^2 = \frac{N}{N_e} a^2 \rightarrow a^2 = N_e b^2 \quad (1.24)$$

$$L = \frac{Nb^2}{a} \quad (1.25)$$

In particular, Eq. (1.23) is the definition of the primitive path length. Eq. (1.24) follows from the observation that the primitive chain ( $N/N_e$  strands of length  $a$ ) and the real chain ( $N$  monomers of length  $b$ ) share the same end-to-end mean radius, which can be derived by using Eq. (1.22). Eq. (1.25) is just a combination of Eqs (1.23) and (1.24).

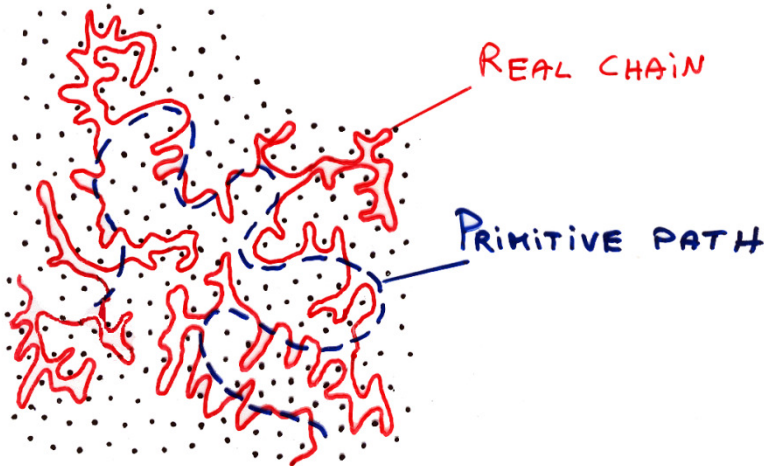


Figure 1.17: Picture of the chain in the melt. Black dots represent entanglements due to the presence of other chains. The red line is the real chain. The broken line is the primitive path, i.e., the shortest line connecting the chain ends without violating the topological constraints.

The motion of the chain along its tube satisfies the topological constraints imposed by surrounding chains and is characterized by a Rouse

friction coefficient  $N\zeta$ , where  $\zeta$  is the monomer friction coefficient. The chain diffusion coefficient  $D_c$  which describes the Brownian motion of the chain along its tube is simply the Rouse diffusion coefficient of the chain. According to the Einstein's relation it is given by:

$$D_c = \frac{kT}{N\zeta} \quad (1.26)$$

where  $k$  is the Boltzmann constant and  $T$  the absolute temperature. Due to the presence of the entanglements, the only way for the chain to “escape” from the tube of constraints is to diffuse along its backbone in reptation-like style. This means that the time taken by the chain to diffuse out of the original tube of length  $L$  will be given by:

$$T_{rep} = \frac{L^2}{D_c} = \frac{\zeta b^2 N^3}{kTN_e} = \frac{\zeta b^2 N^2}{kT} \left( \frac{N}{N_e} \right)^3 \quad (1.27)$$

To derive Eq.(1.27) use has been made of Eqs (1.22)-(1.25).  $T_{rep}$  is called for obvious reasons, the reptation time and represents the overall relaxation time of the entangled chain.  $T_{rep}$  is the longest relaxation time of the system and is related to the relaxation of the entangled network.

Eq. (1.27) has several relevant consequences. The leading term in the last equality of (1.27) is the relaxation time between entanglements,  $T_e$ .  $T_e$  corresponds to time necessary for the part of chain between two entanglements (characterized by a friction coefficient  $N_e\zeta$ ) to diffuse by a distance  $a$  (the length of a tube segment). In fact such a time is given by:

$$T_e = a^2 \frac{1}{D_R} = a^2 \frac{N_e \zeta}{kT} = \frac{N_e^2 b^2 \zeta}{kT} \quad (1.28)$$

Where Eq. (1.24), relating the two lengths  $a$  and  $b$ , has been used. The entanglement relaxation time is the characteristic time necessary for the relaxation of just a sub-section of the chain. Combining Eqs (1.27) and (1.28) one has:

$$\frac{T_{rep}}{T_e} = \left( \frac{N}{N_e} \right)^3 \propto M^3 \quad (1.29)$$

A second relevant consequence of Eq. (1.27) is that the characteristic diffusion coefficient for reptation can now be calculated. In fact when reptating through the tube of entanglements by a linear distance  $L$ , the chain will perform a three-dimensional motion over a distance equal to its end-to-end distance. It then follows that the chain diffusion coefficient is:

$$D_{rep} = \frac{R^2}{T_{rep}} = \frac{Nb^2}{\frac{\zeta b^2 N^3}{kTN_e}} = \frac{kTN_e}{\zeta N^2} \quad (1.30)$$

Eq. (1.31) shows that the three-dimensional diffusion of a polymer chain is strongly hindered by the presence of the entanglement. If entanglements were not present, the chain would diffuse in a three-dimensional fashion according to the so-called Rouse relaxation time:

$$T_R = \frac{R^2}{D_R} = \frac{\zeta Nb^2}{kT} \quad (1.31)$$

which gives:

$$\frac{T_{rep}}{T_R} = \frac{N}{N_e} \propto M \quad (1.32)$$

The reptation model described so far accounts for the dynamics of a polymer melt around equilibrium conditions. The model can be immediately

extended to the case of a melt that is suddenly deformed and then let relax in time. The simple picture is the following. Immediately after deformation the tube containing the chain is deformed, that is the orientation of tube segments (which was random at equilibrium) is now biased by application of the deformation. The chain inside the tube is oriented as well. Chain is also stretched and both orientation and stretch determine the buildup of a corresponding stress. Such a stress, which is due to the entropic elasticity of chain (Rouse motions) and to the network of entanglements eventually relaxes with time after cessation of deformation.

The relaxation roughly takes place in two steps. In a first step, whose characteristic time is the  $T_R$ , relaxation involves the stretched chain segments, which go back to their unperturbed length. For well entangled chains ( $N \gg N_e$ , see Eq. (1.32)) this process is very fast. On a much longer time scale, which corresponds to the reptation time, the chain relaxes its orientation by reptation. This large portion of the relaxation process, therefore takes place because as the time goes on, sections of the original tube are abandoned when the chain ends leave them. It is easily shown that the stress relaxation modulus, that is the ratio between the time varying stress and the applied deformation is proportional to the fraction of original tube remaining at time  $t$ . Determining such a fraction is called a first passage time problem and is performed by solving a diffusion-like equation for the probability function for the surviving tube segments. The stress relaxation modulus  $G(t)$ , for the reptation model was calculated by Doi and Edward in 1978 by solving the first passage problem for the diffusion of a chain in a tube [70]:

$$G(t) = \frac{8G_N^0}{\pi^2} \sum_{p \text{ odd}} \frac{1}{p^2} \exp\left(-\frac{t}{T_d} p^2\right) \quad (1.33)$$

In Eq. (1.33)  $G_N^0$  is the so-called "plateau modulus". The plateau modulus is relevant parameters in all micro-rheological theories, as it is strictly related to the elasticity of the entanglement network. It can be shown that:

$$G_N^0 = \frac{4}{5} \nu kT \quad (1.34)$$

where  $\nu$  is the entanglement density, that is the number of entanglements per unit volume. Eq.(1.34) can be rewritten in terms of macroscopic measurable quantities by expressing the entanglement density as:

$$\nu = \frac{\rho}{M_e} N_A \quad (1.35)$$

where  $\rho$  is the polymer bulk density,  $M_e$  is the molecular weight between entanglements and  $N_A$  is the the Avogadro's number. Finally, Eq. (1.34) becomes:

$$G_N^0 = \frac{4}{5} \frac{\rho N_A kT}{M_e} \quad (1.36)$$

Eq. (1.36) is a central equation as it relates a molecular parameter, the molecular weight between entanglements to macroscopic variables. In particular as it will be shown below, the plateau modulus can be obtained from linear viscoelastic measurements of the polymer melt. Obviously, the polymer density can be also obtained from independent measurements.

As reported in [148] the magnitude of  $M_e$  can be estimated as the minimum molecular weight a chain would need so that the volume of space "pervaded" by the chain is twice that occupied by the chain itself, leaving enough room in the pervaded volume for just one other such chain. This argument suggests that "slender" polymer molecules (such as for example polyethylene), which pervade space without themselves taking up much volume should have lower values of  $M_e$  than do "bulkier" chains (such as for example polypropylene, poly-1butene or polystyrene). This suggestion proves indeed to be the case. Fetters et al. [71] have shown that values of  $M_e$  can accurately be predicted from the so-called "packing length",  $p$ , that is related to the bulkiness of the molecule:

$$p = \frac{v_0}{b^2} = \frac{M}{Nb^2 \rho N_A} \quad (1.37)$$

In Eq. (1.37)  $v_0$  is the monomer volume. Since  $N$  (the number of monomer in the chain) is proportional to the molecular weight,  $p$  is independent on molecular weight itself. It can be also shown [148] that the plateau modulus is inversely proportional to the cube of the packing length. More specifically, Fetters et al. [71] found that the following quantitative relationships hold at a temperature of 140°C for a large number of polymers (including several polyolefins) of different molecular composition:

$$G_N^0 \approx 225.8 p^{-3} \quad (1.38)$$

$$M_e \approx 12.16 p^3 \rho \quad (1.39)$$

The numerical factor in Eq. (1.38) has units  $\text{cm}^3 \text{Å}^{-3} \text{mol}^{-1}$  and that in Eq. (1.39)  $\text{MPa Å}^3$ .

In its original formulation, the Doi-Edwards model was able to predict correctly many of the rheological properties of viscoelastic melts. In

particular, their prediction for the step strain behavior even in the non-linear regime (that is at high deformations) was in excellent agreement with the experimental parameters without the necessity of any adjustable parameters. Other rheological properties however were predicted only qualitatively. One example is the zero shear rate viscosity of the melt. The original Doi-Edwards model gave:

$$\eta = G_N^0 T_{rep} \propto M^3 \quad (1.40)$$

Eq.(1.40) shows that the viscosity of the polymer is predicted to be proportional to the cube of molar mass. This result is not in agreement with the experimental data which show a larger exponent (3.4) for the molecular weight dependence. This and other discrepancies promoted several modifications of the original theory to account for other phenomena such as contour length fluctuation [93] or the constraint release effect coming from the cooperative motion of the entangled network [94-97].

Moving to the more specific area of the rheology of crystalline elastomers, several studies have been devoted to the relation between the stereo-regularity and composition of the polymer chain and the rheological properties. Eckstein et al [86] measured the viscoelastic properties of different polypropylene melts by means of oscillatory rheometry. Samples of high molecular weight and narrow molecular weight distribution were synthesized by metallocene catalysts. The plateau moduli were determined and found to be dependent on stereo-regularity. The derived Molecular weight between entanglements (see Eq.(1.36) were found to be 6900 g/mol, 7050 g/mol and 2170 g/mol for isotactic, atactic and syndiotactic polypropylenes respectively [86].

A dramatic difference in the melt viscoelastic response between syndiotactic polypropylene (sPP) and the corresponding isotactic (iPP) and atactic (aPP) polymers was also found [86, 99]. Such a difference, which has been attributed to a different conformation in the liquid state is not yet fully understood. More recently, Fetters et al [99] have shown that it is possible to link quantitatively the viscoelastic response of polyolefine-based copolymers with molecular parameters such as the molar mass of the repetitive unit and the co-monomer composition. They explored the influence of sPP units on the rheological parameters of poly (ethylene-propylene) copolymers. Samples were synthesized in the presence of bis(salicyladimate) titanium activated by methylaluminumoxane. The value of the plateau modulus and unperturbed chain dimension in the case of sPP were found to be higher than those obtained with the atactic and isotactic units. The co-polymers with syndiotactic polypropylene segments were found to yield larger entanglement densities. Based on these findings it was concluded that ethylene/propylene co-polymers can be prepared so as to provide a high performance elastomeric amorphous polyolefin with a low glass transition temperature.

Auriemma et al., [67] studied the elastic behavior of syndiotactic polypropylene. They carried out a detailed analysis of the mechanical properties and structural study of samples of sPP samples of different stereoregularity. It was shown that the elastic properties of the syndiotactic polypropylene originate mainly from a reversible crystal-crystal phase transition, which occurs during the stretching and when the transition is removed [67].

### **1.3.3.3. Time temperature superposition principle**

Rheological methods to determine the properties described in the previous section are often quite complex. In particular, the determination of the plateau modulus requires particular care. The first requirement is the possibility to access a sufficiently large window of oscillatory frequencies. In particular, as it will become apparent in the next sections and in the subsequent chapters, the high frequency range must be accessed in order to obtain consistent and robust values of the plateau modulus. Many factors can limit the actual feasibility of the rheological experiments. In particular, laboratory rheometers are mechanically limited to a frequency range between approximately 0.01 and 100 rad/s. Access to higher frequencies, however, can be obtained by making use of the so-called Time Temperature Superposition (or TTS) principle, which will be discussed in the present section.

TTS is a valuable technique for describing the viscoelastic behavior of linear polymers over a broad range of times or frequencies by shifting data obtained at several temperatures to a common reference temperature. This technique involves the use of temperature dependent shift factors for the magnitudes of measured stresses (vertical shift factor) and for time or frequency (horizontal shift factor) to be applied to log-log plots of the storage and loss moduli as a function of frequency [3]. When the TTS principle is obeyed, the use of the shift factors will determine a master curve showing viscoelastic behavior over a much larger range of frequencies than could be studied using a single temperature. A material to which this technique is applicable is called a thermo-rheologically simple material. Thermo-rheological simplicity is obtained when all contributing retardation or relaxation mechanisms of the material have the same temperature

dependence and when stress magnitudes at all times or frequencies have the same temperature dependence. It means that data at various temperatures can be shifted horizontally by a constant distance identified as  $\log(a_T)$  and vertically by another constant distance identified as  $b_T$  to obtain a single master curve bringing together all the data. Details on the principles and implementation of the TTS principle, which are not reported here for brevity can be found elsewhere [69].

The vertical shift factor can be expressed mathematically as:

$$b_T = \frac{T_0 \rho_0}{T \rho} \quad (1.41)$$

where  $\rho_0$  is the polymer density at a reference temperature  $T_0$  and  $\rho$  the density at temperature  $T$ . The vertical shift factor is used to shift the values of the viscoelastic moduli to a single curve at the reference temperature for data obtained at a temperature different from the reference temperature. In this case the correction is:

$$G(T_0) = G(T) b_T \quad (1.42)$$

Where  $G$  is either the elastic or the loss modulus.

The horizontal shift factor can be expressed mathematically as:

$$a_T = \frac{\omega_0 \tau_0}{\omega \tau} \quad (1.43)$$

Where  $\tau$  and  $\tau_0$  are the relaxation times at temperature  $T$  and  $T_0$  and  $\omega$  and  $\omega_0$  are the frequencies where the same value of the moduli are measured at the two different temperatures. The vertical shift factor is used to shift the frequencies where viscoelastic moduli are measured to a single curve at the reference. In this case the correction is:

$$\omega = \frac{1}{a_T} \frac{\omega_0 \tau_0}{\tau} \quad (1.44)$$

In the present work use has been made of both the vertical and the horizontal shift factors to correct viscoelastic data obtained at different temperatures. Details about this method will be given in the Results and Discussion Section of this thesis.

While the vertical shift is related to dependence of the moduli upon density and temperature, the horizontal shift factor is based on the temperature dependence of the polymer relaxation times. Usually two equations, the Arrhenius and Williams-Landel-Ferry (WLF) equations are used to evaluate the temperature dependence of the horizontal shift factors [86].

The Arrhenius equation gives:

$$\log a_T = E_a / 2.303R(1/T - 1/T_0) \quad (1.45)$$

where R is the universal gas constant and  $E_a$  is activation energy. The Arrhenius equation is an empirical equation and is generally valid only well above the glass transition region (typically for  $T > T_g + 100\text{K}$ , where  $T_g$  is the glass transition temperature).

Unlike the Arrhenius equation, the WLF equation is based on a more consistent physical picture. It is a more general equation and is typically used to describe the time/temperature behavior of amorphous polymers both around and well above the glass transition temperature. The equation is based on the assumption that above the glass transition temperature the fractional free volume increases linearly with temperature. The resulting equation is:

$$\log a_T = -c_1(T-T_0)/[c_2+(T-T_0)] \quad (1.46)$$

where  $c_1$  and  $c_2$  are the WLF parameters and  $T_0$  is a reference temperature.

#### 1.3.3.4. *Determination of the plateau modulus from linear viscoelastic data*

As it has been outlined before, one of the most important rheological parameters related to the molecular architecture is the plateau modulus. The determination of the plateau modulus is not a trivial task and different methods based on more rigorous theories or on more empirical approaches are present in the literature. A critical review of the existing literature shows that different techniques are used for determining the plateau modulus as explained in more details in the following.

1. **Integration of the  $G''(w)$**  : In this method the plateau modulus is obtained by integrating the loss modulus ( $G''$ ) in the terminal zone [69].

$$G_N^0 = (2/\pi) \int_{-\infty}^{\infty} G''(w) d \ln(w) \quad (1.47)$$

Where  $G_N^0$  is the plateau modulus and  $G''$  is the loss modulus in the terminal zone

In the case of polydisperse polymers, it is more difficult to completely separate the terminal zone from the high frequency Rouse relaxation because the terminal relaxations of the low molecular weight components overlap with the high frequency Rouse modes. This method is generally used where there are not sufficient experimental data at high frequencies, but requires at least that the maximum in the  $G''$  vs. frequency curve can be detected.

2. **Minimum method:** In this method plateau modulus is determined by equating  $G_N^0$  to the value of the storage modulus, where the tangent of the phase angle is at its minimum [86]:

$$G_N^0 = (G')_{\tan \delta \rightarrow \min} \quad (1.48)$$

This concept has been depicted graphically in Fig.1.18. This method is based on theoretical considerations and generally is the most accurate method for the determination of the plateau modulus. It obviously requires that the minimum of  $\tan \delta$  is present in the data set

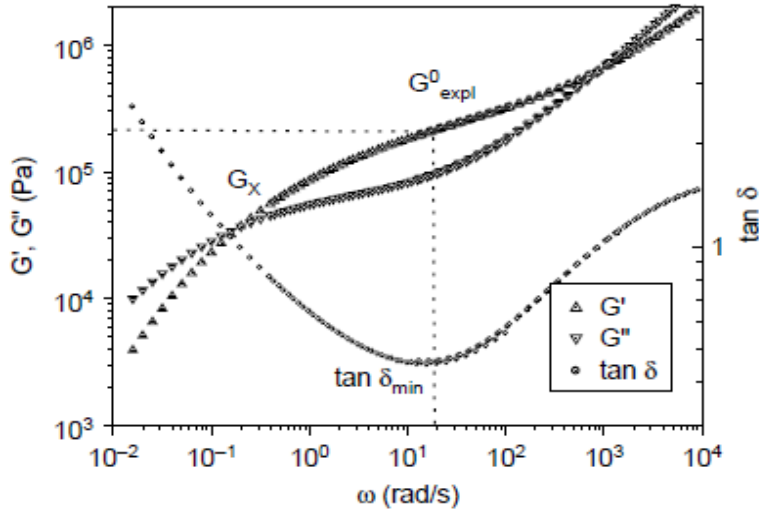


Figure.1.18: Determination of the plateau modulus by the minimum  $\tan \delta$  method [86].

3. **Max method or Empirical method:** In this method plateau modulus is calculated using an empirical approach in which plateau modulus is related to the storage modulus via a constant [89]. This relation is valid for materials which have nearly monodisperse molecular weight distributions.

$$G_N^0 = 3.45 * G''_{(\max)} \quad (1.49)$$

4. **Crossover Modulus Method:** In this technique the plateau modulus is calculated from the Wu's relation [90] and is based on the observation that the cross over parameters in the terminal zone are correlated to the sample molecular weight distribution in terms of  $M_w/M_n$ . The correlation is generally well obeyed when  $M_w/M_n \leq 3$ . The correlation is

$$\text{Log}(G_N^0 / G_{cop}) = 0.38 + [2.63 * \log(M_w / M_n) / 1 + 2.45(M_w / M_n)] \quad (1.50)$$

The accuracy of this method was improved by Nobile and Cocchini by adding  $M_z/M_n$  [101].

5. **Van Gorp-Palmen Analysis:** In this method the plateau modulus is calculated by plotting the phase angle against the absolute value of the complex modulus ( $G^*_{(w)}$ ) [91]. The minimum in the plot defines the plateau modulus. This concept has been depicted graphically in Fig.1.19 [91].

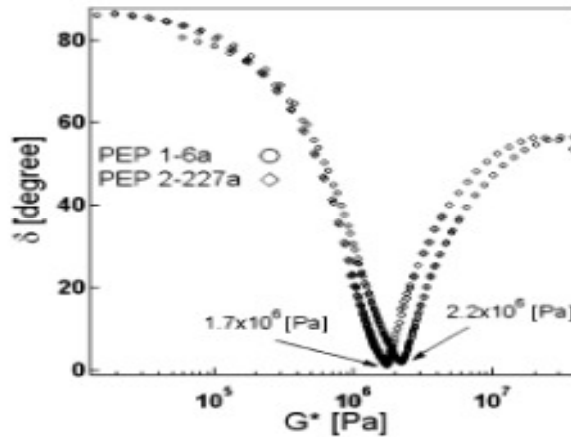


Figure.1.19: Determination of the plateau modulus by the Van Gorp-Palmen analysis [91].

### 1.3.4. Crystallization

When crystalline elastomers are cooled below the thermodynamic melting temperature, they undergo crystallization. In this section crystallization and different techniques used for the analysis of polymer crystallization are discussed and compared. Crystallization is a phase transition process driven by the excess of thermodynamic free energy in the system. This generates transport of molecules from the disordered liquid phase (liquid or melt phase) to the ordered solid phase. In the case of polymers crystallization is a process associated with the partial alignment of the molecular chains. Typically, chains fold together and form ordered regions called lamellae, which compose larger spheroidal structures named spherulites. Polymers can be crystallized by cooling from the melt, by mechanical stretching or by solvent evaporation. The first step in polymer crystallization is the formation of nuclei, which are small units of crystalline material. The formation of this primary nuclei is called primary crystallization. It is followed by the induction of more and more polymer on the growing surface, which is called secondary crystallization or growth.

During the early stages of crystallization, the mechanical response of the material changes from liquid like to solid like. Crystallinity makes a material useful. It makes a material strong but it has also demerits. Advantages and disadvantages of the crystalline material have been discussed in the first section of this chapter. Different methods (e.g., X-ray scattering, DSC) have been reported in literature for measuring the crystallinity of polymers. Rheological methods can also be used as a measure of the crystallization process. One big advantage of the rheological method is its sensitivity at low crystallization kinetics, where the more standard DSC technique can fail.

## Chapter 1

---

DSC (Differential Scanning Calorimetry) is a technique used for studying the changes occurring in polymers upon heating or cooling. In DSC the heat flux released or adsorbed by the polymer is measured as a function of temperature. This technique is used to determine the melting point, the glass transition temperature and crystallinity of the polymers. Here my focus will be on the method of determining crystallinity using this technique. Above the glass transition and below the melting point temperatures, polymers possess some mobility.

During a cooling process, at a given temperature conditions are reached that allow to attain an ordered arrangement that is crystals. When polymers fall into these arrangements, they give off heat. That is why crystallization is an exothermic reaction. Due to the exothermic transition, there is a drop in the heat flow as shown in the Fig.1.20, where the heat flux in a DSC experiments is plotted as a function of the temperature. The drop in the heat flow during crystallization is clear from the big dip in the plot. The dip provides several pieces of information. The temperature at the lowest point of the dip is usually considered to be the polymer crystallization temperature or  $T_C$ . The latent heat of energy of crystallization can be obtained by measuring the area of the dip [87].

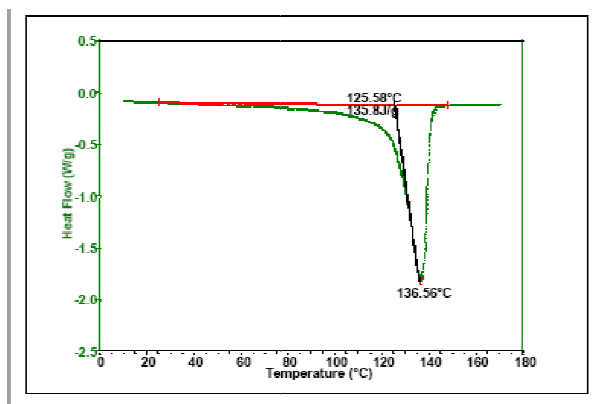


Fig.1.20: DSC curve of Polyethylene [87].

The crystallization kinetics, that is the rate at which crystallization occurs is often studied on the basis of the Avrami model [98,108]. In this model the isothermal crystallization kinetics is described by the following equation:

$$X(t) = 1 - \exp[-\ln(2) \cdot (t/t_{0.5})^n] \quad (1.51)$$

where  $X(t)$  is the relative degree of crystallization (the fraction of polymer crystallized at time  $t$  with respect to the total time),  $t_{0.5}$  is the half crystallization time and  $n$  is the Avrami exponent. The Avrami exponent ( $n$ ) can be related to the mechanism of nucleation and form of crystal growth. It can be obtained from the slope of the linear regression when  $\log[-\ln(1-x(t))]$  is plotted against  $\log(t)$ . As said before,  $t_{0.5}$  is the time needed to reach a relative crystallinity of 50%.  $t_{0.5}$  has been also reported in the literature as an increasing function of crystallization temperature.

$$t_{0.5}(T_c) = \exp(A - E_a / RT_c) \quad (1.52)$$

where  $A$  is a dimensionless parameter and  $E_a$  is the activation energy.  $T_c$  is crystallization temperature.  $R$  is the universal gas constant.

In some cases, rheological methods can provide a more sensitive and accurate measure of the crystallization kinetics. This happens when the crystallization rates are very low, as it is the case when the crystallization temperature is close to the thermodynamic limit. In these cases, the heat flux (which is a measure of the amount of heat released per unit time) can fall below the sensitivity limits of the calorimetric apparatus. On the contrary, the rheological measurement monitors the time evolution of the viscoelastic moduli. These a cumulative measurement and the sensitivity issue do not apply.

When the polymer is cooled below its melting point, crystallinity starts to develop and the material transforms into a semi crystalline material and the viscoelastic properties of the system such as elastic modulus and viscous

modulus change. Rheological parameters can be used to evaluate the relative crystallinity. Khanna et al. [88], for example suggested a linear relationship between elastic modulus and crystallinity and used this technique to study the crystallization kinetics of different polymers [88].

$$x(t) = \frac{G' - G'_0}{G'_\infty - G'_0} \quad (1.53)$$

where  $x(t)$  = crystallinity,  $G'_0$  = Initial plateau value of elastic modulus,  $G'_\infty$  = Final plateau value of elastic modulus and  $G'$  = Elastic modulus at time  $t$ .

Numerous research works have been reported in literature on the crystallization behavior of crystalline elastomers [147-149]. In the present report an attempt has been made to collect specifically the literature about the effect of molecular structure on the crystallization process.

Effect of molecular structure such as tacticity and molecular weight on the crystallization and melting behavior of polypropylene was examined by Ritva et al., [147]. They prepared polypropylenes of different degree of syndiotacticity and molecular weights by different heterogeneous catalyst systems. Crystallization and melting experiments were performed using DSC. For tacticity measurements FT-IR spectroscopy was applied. Crystallization and thermal properties were found dependent on the tacticity of the polypropylenes. A linear relationship between tacticity and thermal properties was noted. No effect of molecular weight in the range of 22000-97000 was found on the thermal properties of polypropylenes.

In another work crystallization of the syndiotactic polypropylene was examined as a function of syndiotacticity [148]. In this work the formation of the trans-planar mesomorphic form at 0°C is followed as a function of the permanence times at 0°C by using X-Ray diffraction and FT-IR spectroscopy. The mesomorphic form of syndiotactic polypropylene (sPP) was obtained by quenching the melt at 0°C and keeping the samples at 0°C

for a long time. Samples kept at 0°C for a short time rapidly crystallize into helical form 1 at room temperature, whereas longer permeance time at 0°C increases the stability of the trans-planar mesomorphic form, which remains stable and inhibits the normal crystallization of the sample into the helical form at room temperature. It was found that higher the degree of stereoregularity of the sample, the shorter the permeance time at 0°C needed to stabilize the trans-planar mesomorphic form.

More recently, an investigation on the crystallization from the melt and of the polymorphic behavior of isotactic poly (1-butene) (iPB) prepared with metallocene catalysts was carried out. Samples of isotactic polybutene of different of stereoregularity, containing different concentrations of stereodeflects (rr triads defects) and regiodeflects have been prepared with different C<sub>2</sub>- and C<sub>1</sub>-symmetric metallocene catalysts. The concentration of defects and the molecular mass are controlled by the choice of the catalyst structure and conditions of polymerization. Highly isotactic samples with concentration of rr stereodeflects lower than 2 mol %, crystallize from the melt in the metastable form II. This is a common polymorphic behavior observed in iPB samples prepared with Ziegler-Natta catalysts and extensively reported in the literature. More stereodeflective iPB samples, containing concentration of stereodeflects higher than 2 mol % crystallize from the melt as mixtures of form II and form I, the fraction of crystals of form I increases with increasing concentration of defects and decreasing cooling rate from the melt and samples with concentration of rr defects of 3-4 mol% crystallize from the melt in the pure form I at low cooling rates. The results presented in this paper give the first experimental observation of the crystallization of the stable trigonal form I of iPB from the melt at atmospheric pressure [149].

In conclusion, it can be said that the crystallization process of polyolefin based crystalline polymers are affected by the stereo- and region-regularity of the polymer chain. In nut shell all these phenomena are found to have a profound influence on the crystallization process and consequently on the mechanical properties of the solid materials.

### **1.3.5. Flow induced crystallization**

The enhancement in the rate of polymer crystallization due to the application of shear or extensional flow is known as flow induced crystallization. In the other word flow induced crystallization can be defined as the process in which the rate of polymer crystallization is accelerated by the action of flow. This phenomenon alters both processing and material final properties. The physics behind flow induced crystallization is simple. When a polymer is subjected to an extensional or shear flow, the polymer chains are oriented and stretched. This results in a decrease of the entropy or equivalent increase in free energy. This increase in free energy acts as a driving force and thus accelerates the polymer crystallization process by accelerating the rate of nucleation.

As it was said before, the process of crystallization occurs in two steps. In the first step formation of nuclei (stable nuclei) occurs, while in the second step the subsequent growth of crystallites occurs. The flow has an effect on the first step of crystallization (nucleation stage) [114]. Furthermore, while quiescent crystallization leads to the formation of spherical, non-oriented structures (spherulites) flow can also determine oriented crystalline structures, such as fibers. The mechanism of flow induced crystallization is well documented in the literature [115].

The process can be explained as stretching of long chains to form fibrous crystals. During the stretching process, the distortion of chains from their

most probable conformation results and hence a decrease in the conformational entropy occurs. If this deformation is maintained in this lower conformational entropy state then less conformational entropy needs to be sacrificed by transforming to a crystalline state. The decrease in total entropy allows the crystallization to occur at high temperatures, where the process will not take place (or will take place at a lower rate) under quiescent conditions.

Normally the formation of such fibrous morphology is accompanied by formation of an epitaxial layer over and around the inner fiber giving rise to the so called shish-kebab morphology [116]. This mechanism is explained schematically in Fig.1.21.

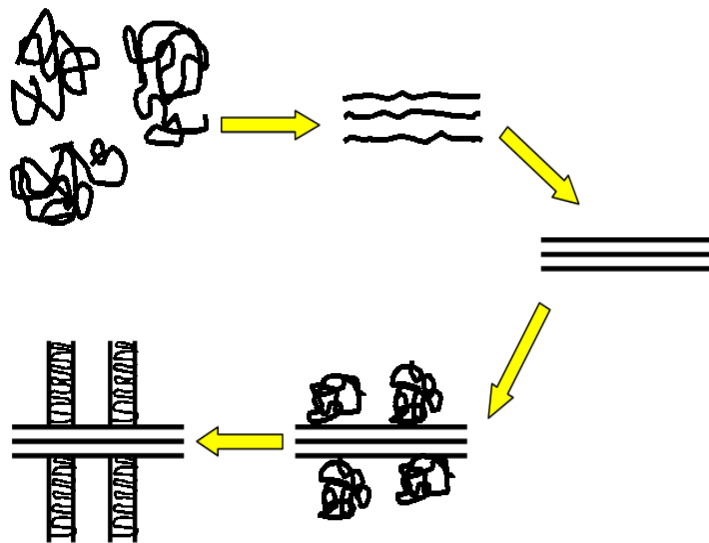


Figure.1.21: Schematic representation of the flow induced crystallization [116].

The outside kebab-like regions are essentially folded chain regions formed by chains that do not crystallize during the orientation process [115-124]. While the inner shish region form first, the formation of folded chain

discs occurs due to nucleation events taking place on the surface of the extended chains fibrils.

Numerous research works has been reported in literature about the nucleation kinetics [119,120]. According to the Lauritzen and Hoffman theory isothermal nucleation kinetics is expressed as [119]:

$$N = CkT\Delta G \exp\left(\frac{Ea}{kT}\right) \exp\left[-\frac{K}{T(\Delta G)n}\right] \quad (1.54)$$

Where  $N$  = Rate of nucleation,  $k$  = Boltzmann's constant,  $T$  = Absolute temperature,  $\Delta G = G_L - G_S$  = Volumetric free energy difference between liquid and crystalline phase,  $K$  = Constant contains geometrical and energetic factors of nucleus and  $n$  is an exponent related to the type of nucleation.

It is generally accepted that flow contributes to the free energy difference appearing in eq (1.53).

$$\Delta G = \Delta \dot{G}f + \Delta Gq \quad (1.55)$$

Here  $\Delta Gq$  and  $\Delta \dot{G}f$  refer to the free energy contribution under quiescent and shear flow conditions respectively.

In order to investigate the influence of flow on crystallization, a characteristic time for the onset of crystallization is measured. Such a quantity is usually called induction time. Induction time and nucleation rate are roughly inversely proportional. For this reason, the ratio between the induction time under quiescent and flow conditions can be defined as:

$$\Theta \equiv \frac{\dot{N}_q}{\dot{N}_f} = \frac{1}{1 + \frac{\Delta G_f}{\Delta G_q}} \exp\left[\frac{K}{T(\Delta G_q)^n} \left\{ \frac{1}{\left(1 + \frac{\Delta G_f}{\Delta G_q}\right)^n} - 1 \right\}\right] \quad (1.56)$$

Where subscript q and f refer to quiescent and flow conditions respectively. The dimensionless induction time is unity under quiescent conditions, while it is less than 1 when the shear flow is applied.

In the case of polymer melts the ability of the shear flow to produce conformation and morphological changes with respect to equilibrium and isotropic state come results from the coupling between the shear flow intensity and relaxation behavior of the chain. According to the theory of reptation [70], chain segment conformation or orientation occurs only when the characteristic flow time ( $\gamma^{-1}$ ) is smaller than the reptation or disengagement time  $T_d$  [70]. Moreover, chain stretching occurs only when  $\gamma^{-1} < T_R < T_d$ , where  $T_R$  is the Rouse relaxation time. The effect of flow on chain orientation and consequently on the flow induced crystallization can be explained in terms of a dimensional form by defining the Deborah number for the system as:

$$De = \dot{\gamma}T_d \quad (1.57)$$

The above discussion clearly depicts that for  $De < 1$ , there will be no effect on the crystallization kinetics, where a faster crystallization kinetics should be observed only in case of  $De > 1$ . Within the framework of the original Doi-Edwards theory, it can be shown that the additional jump in free energy can be written as:

$$\Delta G_f = 3ckT\Gamma(De) \quad (1.58)$$

$\Gamma$  is a dimensionless free energy function, which is a function of  $De$ . As a consequence, calculating  $\Delta G_f$  for assigned flow conditions (e.g., shear or extensional flow) can be done by using Eq. (1.57). Inserting this value in eq. (1.55) allows prediction for the dimensionless induction time.

In order to evaluate  $\Theta$  for a given polymer under isothermal flow conditions several material properties are needed. The quiescent free energy

requires the knowledge of the thermodynamic melting temperature ( $T_m$ ) and latent heat of fusion ( $H_0$ ), because:

$$\Delta G_q = H_0 \left(1 - \frac{T}{T_m}\right) \quad (1.59)$$

Values of the quiescent crystallization constant ( $K$ ) and exponent ( $n$ ) are also needed. Besides this the reptation time  $T_d$  must also be evaluated, for example from linear viscoelasticity measurements.

A critical review of the existing literature shows that the molecular structure (molecular weight, molecular weight distribution or polydispersity and tacticity) are important structural properties in quantitatively determining the shear flow induced crystallization rate [121-122]. In the case of monodisperse polymers, for example, longer polymer chains will be more oriented than shorter one under the same flow conditions, as high molecular weight chains have longer relaxation times. The same applies on polydisperse polymers. The presence of a long tail of molecular weight chains enhances the flow induced nucleation rate.

Jay et al., (1999) and Dulpay et al. [122] conducted fiber pulling experiments on long series of isotactic polypropylenes of different molecular weight. They found that the overall crystallization kinetics exponentially increased upon increasing the polymer molecular weight at a fixed shear rate [123]. The same general trend of increase in rate of flow induced crystallization with increase in the molecular weight and molecular weight distribution was found by Vlieshouwers and Meijer [123]. They conducted rheological flow induced crystallization experiments on isotactic polypropylene samples of different molecular weight and molecular weight distribution. They found an increase in the rate of crystallization by increasing molecular weight of the samples at constant shear rate.

Furthermore they found that after a combined thermo mechanical treatment that mainly caused a degradation of the high molecular weight tail, the effect of the shear rate on the crystallization rate was strongly reduced.

Monasse and his coworkers have examined the influence of molecular structure of polypropylene on the crystallization, both quiescent and shear induced [121,122]. They showed that in quiescent conditions the higher degree of isotacticity and the decrease in chain defects weakly enhanced the growth rate of crystalline structures, whereas the molecular weight ( $M_w$ ) and molecular weight distribution (MWD) were found to be less relevant parameters. The independence of the kinetics on  $M_w$  was explained taking into account that during the growth mechanism only a small portion of chain (order of 100 monomers) is involved in the deposit of crystalline segment at the growth front. This amount is negligible in comparison to the high degree of polymerization [128]. On the contrary, during shear the growth rate was governed by molecular weight. A critical molecular weight value, related to the critical mass between entanglements, below which the polymer is insensitive to shear flow, was obtained by Haudin *et al.* [130].

The influence of the molecular weight on flow induced crystallization has been also investigated by Bove and Nobile [131,132]. They used rheological measurements to investigate the evolution of crystallization in quiescent conditions as well as after the application of a shear flow. Strong enhancement in crystallization kinetics was observed when the step shear flow was applied on poly(1-butene) samples (PB) with different  $M_w$  and on a polypropylene sample (PP). They also found that a critical shear rate (at a constant strain) coupled to a critical shear strain (at a constant shear rate) are necessary to obtain the enhancement of the overall-crystallization rate.

Moreover, a relevant molecular weight effect was noted in the step shear flow crystallization, while in quiescent conditions no evidence was found.

Recently, Acierno *et al.* [133] have explained the combined effects of shear flow and polymer molecular weight introducing the dimensionless Weissenberg number,  $W_i$ , i.e. the product of the relaxation time inherent to the material and the deformation rate for the flow process. They analyzed the influence of shear flow on the crystallization of a sequence of Polybutenes with different Mw, and found that the application of a shear flow significantly accelerates the crystallization kinetics, as reflected by a faster light intensity dynamics in turbidity measurements. By the definition of a dimensionless crystallization time, obtained normalizing the crystallization time after shear with the same time in static conditions, it was shown that the kinetic deviation from quiescent state occurs at lower shear rates as the molecular weight increases. They also showed that the dimensionless crystallization times of different molecular weight PB falls on the same master curve if they are plotted against the Weissenberg number ( $W_i$ ).

More recently, Fenguan *et al.* [125] obtained the same results by investigating the process using differential scanning calorimetry (DSC), rheological techniques, polarized optical microscope and X-ray diffraction techniques. They performed experiments on both linear and branched chain polypropylene. Long chain branched polypropylene showed accelerated crystallization kinetics in comparison with that of low branched chains. The crystallization of long chain branched polypropylene was found more sensitive to shear flow than that of linear polypropylene during the induced period at low shear rates, which indicates that the longer relaxation time of the polymer chains plays an important role in the nucleation of polypropylene under shear flow fields.

As mentioned earlier the application of flow to increase the rate of crystallization can be shear or extensional. Extensional flow means a type of deformation which involves the elongation or stretching of a viscous material [127]. Extensional flow is expected to produce more relevant effects than shear in flow-induced crystallization [134]. Extensional flow is more sensitive to the molecular structure of the polymer than the shear flow. For example, at the same level of, it generates a much higher degree of molecular orientation and stretching than the simple shear. The strain requirement for the flow induced crystallization is less in extension than in the shear.

Another difference of extensional flow with respect to simple shear is the absence of slip issue. Slip is a relevant problem in simple shear because it reduces the applied shear deformation, making it very difficult to remove the effects of slip from the physical response of the material to deformation [135].

Both extensional and shear flows produce alignment, which enhance the crystallization process. Literature data suggest that flow induced crystallization can reduce the induction time of crystallization by several orders of magnitude, when compared to quiescent crystallization [135, 136]. As in the case of shear flow, the effect of extensional flow depends upon on the strength of flow, which can be characterized by the Weissenberg number.

Hadinata et al. [141] studied and compared both the extensional flow and shear flow induced crystallization of a high molecular weight isotactic poly-1-butene. They used an extensional viscosity fixture on a rotational rheometer to apply an extensional flow to the melts. They found that the flow induced crystallization occurring in the extensional flow is much stronger than that observed under shear. They also found that beyond a critical

extension rate, the onset of crystallization time decreased roughly with the inverse of the extension rate.

Sentmanat et al. [142] used the Sentmanat extensional viscosity fixture on a rotational rheometer, which is similar to extensional viscosity fixture used by Hadinata et al. [138]. They handled the problem of sample sagging in the rheometer by quenching the samples with water after the application of extensional flow. Their findings indicate that a higher degree of crystallization can be achieved by the application of extensional flow near the melting temperature.

More recently, Chellamuthu et al. [143] conducted extensional flow induced crystallization measurements of isotactic poly-1-butene using a filament stretching rheometer. They found that extensional flow is effective in enhancing the polymer crystallization process. They conducted DSC and small angle X-ray scattering measurements for the estimation of the degree of crystallinity and found an increase in the degree of crystallinity from 45 to 62% with an increase in the extension rate from  $0.01\text{s}^{-1}$  to  $50\text{s}^{-1}$  for a fixed imposed strain. Moreover, they found that below a threshold extension rate no flow induced crystallization occurs. Conversely, a decrease in flow induced crystallization above a second critical threshold was also found.

## Chapter 2

---

# Experimental Methods

In the present work linear viscoelasticity, quiescent crystallization and extensional flow induced crystallization of polypropylene and poly-1Butene were investigated. To this end, different experimental apparatuses were used. Linear viscoelasticity in shear oscillatory flow was performed by means of an Advanced Rheometric Expansion System (ARES, TA Instruments Ltd) strain controlled rotational rheometer. The ARES rheometer was also used for extensional measurements. In this case it was equipped by the using the Sentamanat Extensional Rheometer (SER, Xpansion Company) fixture. Differential Scanning Calorimetry was performed by means of a Shimadzu 60 calorimeter (Shimadzu Corporation).

### 2.1. Linear Viscoelasticity

Numerous experimental techniques have been reported in the literature for the measurement of viscoelasticity of elastomers. But the recommended one and the most used experimental technique is the dynamic oscillatory method. A general advantage of this method is that a single instrument can cover a wide range of frequency. Viscoelastic measurements of elastomers can be carried out by dynamic method successfully either by applying a constant strain or stress.

Oscillatory shear is the most popular and common because it is easier to measure the storage and loss moduli using the oscillatory shear experiments than to generate the step strains or stresses and measure the resulting stress or strain. In oscillatory shear experiments, the sample is subjected to a

homogenous deformation at a sinusoidally varying strain or shear stress. In a controlled strain experiment, one generates a strain that is as close as possible to a sine wave [13].

$$\gamma = \gamma_0 \sin(\omega t) \quad (2.1)$$

If the strain amplitude is sufficiently small, so that the response is linear, the resulting stress is also sinusoidal and can be written in terms of the stress amplitude ( $\sigma_0$ ) and the phase angle also called loss angle ( $\delta$ ).

$$\sigma(t) = \sigma_0 \sin(\omega t + \delta) \quad (2.2)$$

Viscoelastic experiments are performed in the frequency domain rather than in the time domain. Since in an oscillatory experiment with a sine wave input, the resulting stress wave form is fitted to a sinusoidal function at each frequency and this fitting process acts as a filter that rejects noise which is non-sinusoidal or is at a frequency other than imposed. This noise rejection technique improves with increasing number of measuring cycles.

In the case of a linear system in the frequency domain, the results can be expressed in terms of the amplitude ratio  $G_d = \sigma_0/\gamma_0$  and a phase angle ( $\delta$ ) which are functions of frequency. The dynamic test results are usually reported in terms of the storage and loss moduli ( $G'$  and  $G''$ ) as a function of frequency.

$$\sigma(t) = \gamma_0 [G'(\omega) \sin(\omega t) + G''(\omega) \cos(\omega t)] \quad (2.3)$$

It is sometimes useful to express the dynamic data in terms of the loss and storage moduli by considering it the imaginary and real parts of the complex modulus ( $G^*$ ).

$$G^* = G'(\omega) + iG''(\omega) \quad (2.4)$$

It follows that the magnitude of the complex modulus is given by:

$$|G^*| = \sqrt{(G')^2 + (G'')^2} \quad (2.5)$$

The dynamic data can be expressed alternatively in terms of a complex viscosity ( $\eta^*$ ):

$$\eta^* = \frac{G^*}{i\omega} = \frac{1}{\omega} (G'' - iG'(\omega)) = \eta' - i\eta'' \quad (2.6)$$

$$|\eta^*| = \frac{|G^*|}{\omega} = \frac{\sqrt{(G')^2 + (G'')^2}}{\omega} \quad (2.7)$$

The complex viscosity is a particular useful quantity when the viscous behavior of viscoelastic polymer melts is to be studied. In the limit of zero shear rate, continuum mechanics imposes that [69]:

$$\eta'(\omega) \Big|_{\omega \rightarrow 0} = \frac{G''(\omega)}{\omega} \Big|_{\omega \rightarrow 0} = \eta(\dot{\gamma}) \Big|_{\dot{\gamma} \rightarrow 0} \quad (2.8)$$

In the case of viscoelastic fluids, the elastic component to  $\eta'$  disappears in the low frequency limit, and one has:

$$|\eta^*(\omega) \Big|_{\omega \rightarrow 0} = \eta(\dot{\gamma}) \Big|_{\dot{\gamma} \rightarrow 0} = \eta_0 \quad (2.9)$$

Where  $\eta_0$  is the zero-shear rate viscosity. For most linear polymer melts, as it is the case for the crystalline elastomers investigated in the present work, the empirical Cox-Merz rule often applies [69]:

$$\eta^*(\omega) \cong \eta(\dot{\gamma}) \quad (2.10)$$

Even in the case of non-vanishing frequencies and shear rate. The consequence of Eq. (2.10) is that the steady-shear viscosity curve as a function of shear rate can be obtained by performing a linear viscoelastic frequency response measurement of the polymer melt. All quantities described above have been measured in the present work by using an ARES strain controlled rotational rheometer (TA Instruments). Data acquisition and

## Chapter 2

---

analysis was performed by means of the rheometer software TA Orchestrator. The ARES is shown in Fig.2.1.



Figure.2.1: Rotational rheometer ARES.

The Advanced Rheometric Expansion System (ARES) is a mechanical spectrometer that is capable of subjecting a sample to either a dynamic (sinusoidal) or steady shear strain deformation and then measuring the resultant torque exerted on the sample in response to this shear strain [102]. The shear strain is applied by CC, direct-drive motor that moves the lower tool. The resulting torque is measured on the upper tool by a Force Rebalance Transducer (FRT), which guarantees very sensitive, stable torque. In the present work all experiments were performed in parallel plate geometry. A plate of 8 mm diameter was used to minimize the sample quantity needed for the experiments. The parallel plate tools are shown in Fig.2.2.

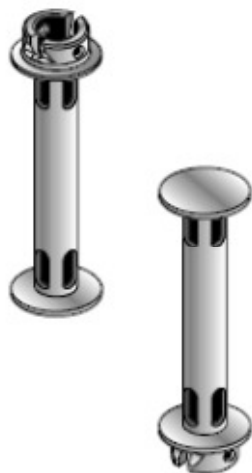


Figure.2.2: Parallel plates of 8 mm diameter.

Temperature control was guaranteed by a convective oven (an open view of the oven can be seen in Figure 2.1). The oven consists of two resistive heater guns mounted on the left side that are used to produce heat. The heat is transferred from the heaters to the plates by the forced convection process using a carrier gas (air or nitrogen). The temperature of the oven is monitored by three platinum thermo-resistances (PRT), which are installed inside the oven. Two of them are used to monitor the air temperature, while the third one monitors the temperature of the lower sample tool in use. A PID controller is used to control both the oven and tool temperature. The oven can be used to control temperature both above or below the ambient temperature. In the latter case, a liquid nitrogen Dewar was used as a gas supply system. Cold nitrogen coming from the Dewar was heated by the heating guns to the desired temperature.

When in the parallel plate configuration, the ARES rheometer was used to perform different types of tests, which are described in the following. Figures are screen shots of the TA Orchestrator software illustrating the set-up parameters of each type of test.

### 2.1.1. Dynamic time sweep test

A time sweep test takes successive measurements at constant temperature; frequency and strain for a selected interval of time (see Fig.2.3). The time required to make a measurement is frequency dependent. At frequencies less than 2 rad/sec, it is equal to the time required to complete approximately 1.5 cycles of oscillation. At high frequency the limit is approximately 2 seconds per measurement.

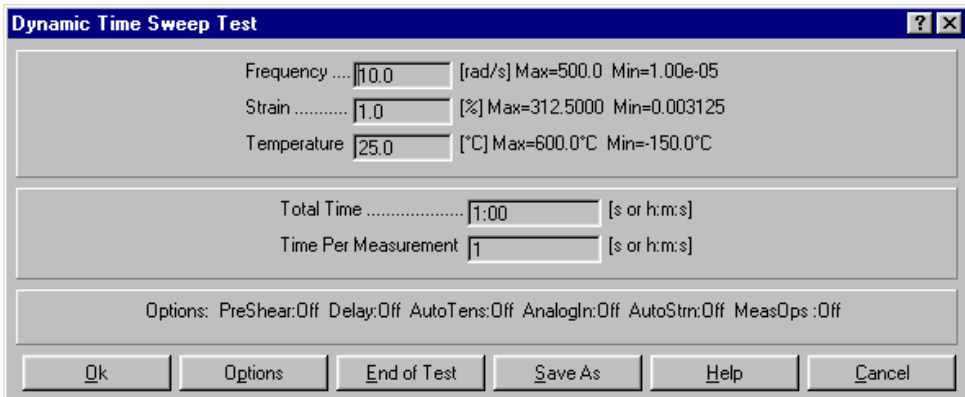


Fig.2.3: Dynamic time sweep test set-up screen.

### 2.1.2. Dynamic strain sweep test

The dynamic strain sweep test is usually performed to check the linearity limits of the sample. The test (see Fig.2.4) performs a strain sweep within a defined strain window while keeping frequency and temperature fixed.

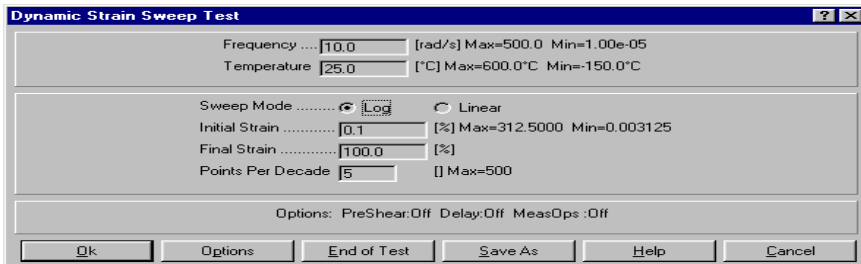


Fig.2.4: Dynamic strain sweep test set-up screen.

### 2.1.3. Dynamic Frequency Sweep Test

The frequency sweep test (Fig.2.5) is used to build the frequency linear viscoelastic response of the sample. It takes successive measurements at selectable frequencies while holding the temperature and strain constant. The time it takes to complete the test is highly dependent on the lower end of frequency selected. Lower values of the minimum frequency will increase the test time. Typically, dynamic frequency sweep tests were conducted at different temperatures in the frequency range of 0.1 to 100 rad/sec at a strain smaller than the linear viscoelastic limit.

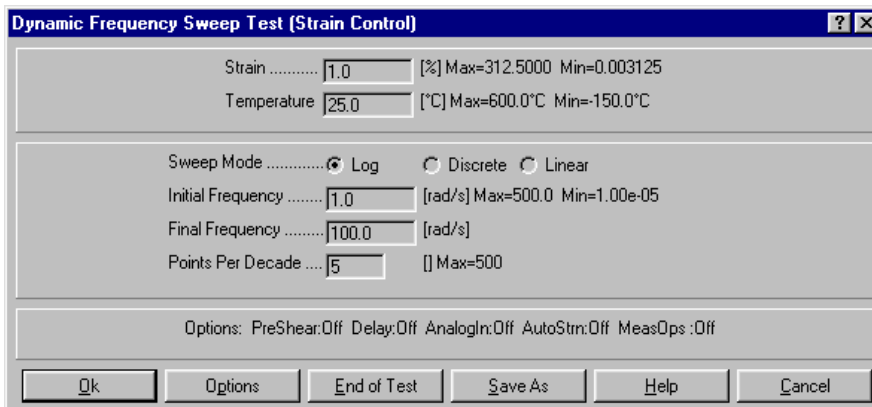


Fig.2.5: Dynamic frequency sweep test set-up screen.

### 2.1.4. Dynamic Temperature ramp test

In this test a constant cooling or heating rate is imposed at constant frequency and strain. This test is used for different purposes like to quickly analyze the behavior of the material as a function of temperature or to determine the crystallization or melting kinetics under non isothermal conditions. In this test (Fig.2.6) the temperature is automatically increased or decreased at a given rate within the upper and lower imposed.

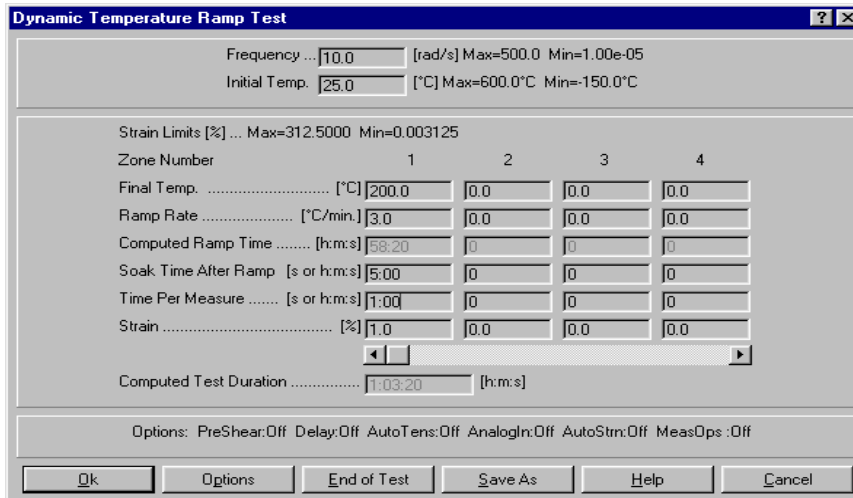


Fig.2.6: Dynamic temperature ramp test set-up screen.

## 2.2. Extensional flow Measurements

In order to perform extensional viscosity measurements, the Sentmanat Extensional Rheometer (SER) is attached to the ARES rotational rheometer. A schematic diagram of Sentmaant Extensional Rheometer (SER) is shown in Fig.2.7. The sample ends are clamped to two rotating cylinders. The inner cylinder is directly connected to the force transducer and the outer cylinder to the driving motor by means of two intermeshing gears to the motor. The outer cylinder rotates around the inner one, while rotating on its own axis. By this way an uniaxial extension is applied to the sample. The torque measured by the FR Transducer can be then translated into an elongational force.

Using the TA Orchestrator software, which the proper SER operation is simulated by imposing a parallel plate geometry with a diameter  $D=0.812$  mm and a plate gap  $h=0.501$  mm. In parallel plate geometry, the ARES software calculates the shear rate as:

$$\dot{\gamma} = \frac{D\Omega}{2h} \quad (2.11)$$

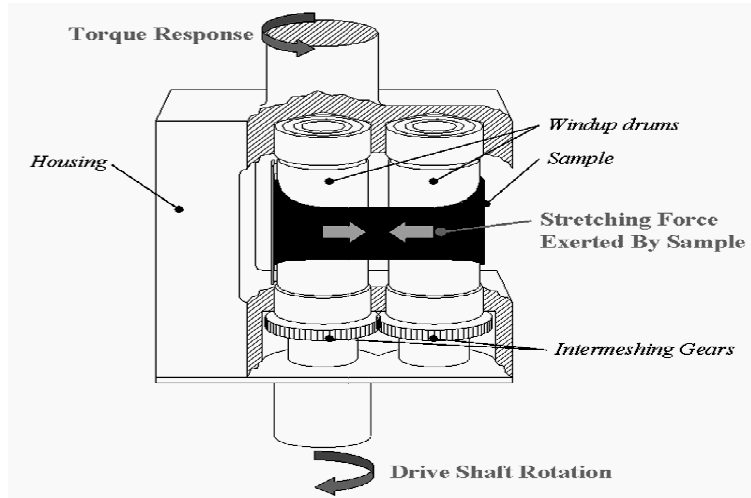


Fig.2.7: Schematic diagram of Sentmanat Extensional Rheometer.

Where  $\Omega$  is the motor rotation rate. The resulting Hencky strain rate for the SER is then given by:

$$\dot{\epsilon}_H = \frac{2\Omega R}{L_o} \quad (2.12)$$

Where  $R$  is the radius of the windup drum and  $L_o$  is the fixed, unsupported length of the specimen sample being stretched (equal to the centerline distance between the master and slave drums).

For the ARES software to apply a shear rate equal to the Hencky strain rate, the following equation must hold:

$$\frac{D\Omega}{2h} = \frac{(2R)\Omega}{L_o} = \frac{(4R)\Omega}{2L_o} \quad (2.13)$$

An uniaxial extension is applied to the sample. The torque measured by the FR Transducer can be then translated into an elongational force.

Thus, specifying  $D=4R=0.812$  mm and  $h=L_0=0.501$  mm will ensure that the specified extensional rate for the test will be equal to the Hencky strain rate. This is true as long as the dimensional ratio is constant ( $D/h = 1.62$ ).

### **2.2.1. Test Setup**

To perform extensional flow measurements, the windup drums must operate at a constant rate of rotation. This can be achieved by operating the ARES to perform step rate test using the steady motor and transient measurement type. Under this set-up, the data acquisition rates can be separated into four zones, which allow faster data sampling at shorter times (which is essential for high extensional deformation rate) and slower data sampling at longer times. During the test temperature control is achieved by controlling temperature of the oven. This is done by selecting the oven air PRT in the temperature control loop.

### **2.2.2. Data analysis**

The required data obtained from the ARES rheometer is the shear rate (equal to the Hencky strain rate), time and the corresponding torque. In many experiments below a Hencky strain rate of  $1\text{ s}^{-1}$ , there may be a small initial time offset visible in the data due to the slight “slack” due to sample loading and melt expansion. This slight deformation delay is highly exaggerated on a log-log plot, but is negligible on a linear plot. Therefore, a time offset must be incorporated for such experiments. The time offset varies from test to test, depending on the “slack” that exists in the sample, and thus it must be evaluated in each case. At the same time, it may be necessary to correct the collected torque data for any residual stress in the sample due to sample loading. Again, the torque offset varies from test to test, but at high

temperature measurements, it is rare that one needs to incorporate any torque offset.

Once the torque measurement data are available, the time dependent tensile force  $F_E(t)$  can be calculated from the torque as:

$$F_E(t) = \frac{T - T_{offset}}{2R} \quad (2.14)$$

where T is the torque and again R is the radius of the windup drum.

If there is no deviation between the nominal and actual strain rates, the instantaneous cross sectional area,  $A(t)$  of the stretched specimen changes exponentially with time  $t$  and for a constant Hencky strain rate it can be expressed as:

$$A(t) = A_o \exp[-\dot{\epsilon}_H t] \quad (2.15)$$

For polymer melts, the specimen exhibits a decrease in density upon melting which is manifested as a volumetric expansion of the specimen while loaded on the SER. To account for this dimensional expansion for the polymer melt, a density correction can be incorporated as follows:

$$A(t) = A_o \left( \frac{\rho_S}{\rho_M} \right)^{2/3} \exp[-\dot{\epsilon}_H t] \quad (2.16)$$

where  $\rho_S$  is the solid state density and  $\rho_M$  is the melt density of the polymer at the experimental temperature. Thus the tensile stress growth function,  $\eta_E^+(t)$  can be found using the following equation:

$$\eta_E^+(t) = \frac{F(t)}{\dot{\epsilon}_H A(t)} = \frac{(T - T_{offset})}{(2R)(\dot{\epsilon}_H) \left[ A_o (\rho_S / \rho_M)^{2/3} \exp(-\dot{\epsilon}_H [t - t_{offset}]) \right]} \quad (2.17)$$

In extension flow measurements, the tensile stress growth coefficient is plotted against time.

## **2.3. Differential Scanning Calorimetry**

Differential Scanning Calorimetry, DSC, is a thermo-analytical technique used quantitatively to describe the phase transitions occurring in a material. In DSC the difference between the amount of heat required to increase the temperature of the sample and that required to heat a reference material are measured as a function of temperature. Both sample and reference are maintained at nearly the same temperature throughout the experiment. Generally, the temperature program for a DSC analysis is designed so that the sample holder temperature increases linearly as a function of time. Alternatively, isothermal temperature tests can be also performed. Only a few milligrams of material are required to run the analysis.

### **2.3.1. Working Principle**

When a material undergoes a physical transformation such as a phase transition (crystallization, glass transition), more or less heat will be needed to flow to it with respect to the reference sample (typically, an empty sample pan) to maintain both at the same temperature. Whether more or less heat must flow to the sample depends on the direction of the process (exothermic or endothermic). For example, when a solid sample melts to a liquid it will require more heat flowing to the sample than to the reference to increase its temperature at the same rate. This is due to the absorption of heat by the sample as it undergoes the endothermic phase transition from solid to liquid. Likewise as the sample undergoes an exothermic process (such as crystallization) less heat is required to raise the sample temperature. By measuring the difference in heat flow between the sample and reference, DSC is able to measure the amount of heat absorbed or released during such transitions. DSC may also be used to observe more subtle phase changes,

## Chapter 2

---

such as glass transitions. A schematic diagram of DSC operations is shown in Fig.2.8.

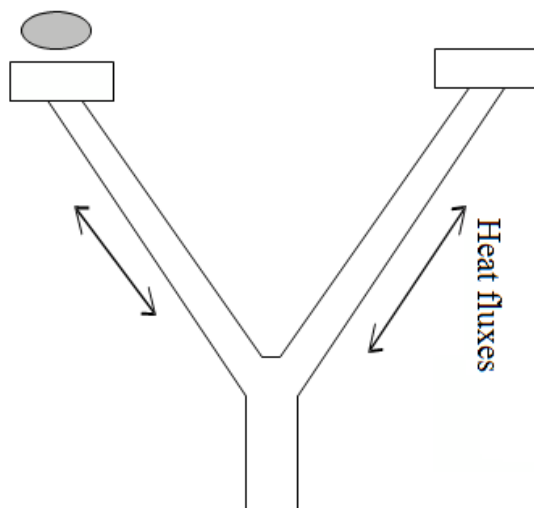


Fig.2.8: Diagram of operation DSC cell.

## Chapter 3

---

# Linear Viscoelasticity of Syndiotactic Polypropylenes

### 3.1. Introduction

Mechanical properties like high rigidity, high stress to break and viscoelastic properties like high deformability and ductility have made crystalline elastomers an attractive and promising class of innovative materials for applications in different areas [59,101]. Among crystalline polyolefins, syndiotactic polypropylene (sPP) has shown interesting and unexpected elastic properties [59]. In the case of sPP, the crystallization behavior is strictly related to the degree of tacticity of the polymer, that is to the local molecular architecture. In turn, a change in tacticity generates changes in the molecular weight between entanglements,  $M_e$ , of the polymer in the melt phase [69, 70]. Since  $M_e$  is directly related to the viscoelastic plateau modulus of the melt, it is expected that information on the degree of tacticity can be extracted from linear viscoelastic measurements in the melt state. Here, the basis for these relations, which were already presented in the Introduction chapter, is briefly revisited.

In their fundamental review paper of 1994, Fetters et al. [71] proposed a simple model to calculate the molecular weight between entanglements and to relate it to other molecular properties of the polymer chain to some macroscopic, measurable parameters. The starting point of the model is the distinction between the volume "occupied" by a chain and the volume "pervaded" by the same chain. The volume occupied by a chain is the actual volume filled by the chain. It can be written as:

$$V = \frac{M}{\rho N_A} \quad (3.1)$$

Where  $M$  is the molecular weight,  $\rho$  is the density and  $N_A$  is the Avogadro's number. The volume spanned by the chain is the portion of space spanned by the chain. It is chosen by Fetters et al. as:

$$V_{sp} = A \langle R_g^2 \rangle_0^{\frac{3}{2}} \quad (3.2)$$

In Eq. (3.2)  $A$  is a constant of order unity and  $R_g$  is the so-called radius of gyration, such that its mean square value is given by:

$$\langle R_g^2 \rangle_0 = \frac{\langle R^2 \rangle_0}{6} = \frac{C_\infty \frac{M}{m_0} l_0^2}{6} \quad (3.3)$$

In Eq. (3.3)  $\langle R^2 \rangle_0$  is the mean square end-to-end radius,  $C_\infty$  is the characteristic ratio,  $m_0$  is the molecular weight and  $l_0$  the length of a chain monomer. Based on Eq. (3.2) the pervaded volume can be written as:

$$V_{sp} = A \left( \frac{C_\infty M}{6m_0} \right)^{\frac{3}{2}} l_0^3 \quad (3.4)$$

We now call  $N$  the number of polymer chains that fill the pervaded volume. This will be given by the ratio of the two above defined volumes:

$$N = \frac{V_{sp}}{V} = AN_A \left( \frac{C_\infty}{6m_0} \right)^{\frac{3}{2}} l_0^3 M^{\frac{1}{2}} \quad (3.5)$$

From Eq.(3.5) the molecular weight between entanglements,  $M_e$ , can be defined as the chain molecular weight such that  $N=2$ . In fact, if  $M < M_e$  or  $N < 2$ , there is not a full second chain in the volume occupied by the test

chain, so there is no entanglement. Based on this definition,  $M_e$  can be written as:

$$M_e = \frac{1}{B^2 \left( \frac{\langle R^2 \rangle_0}{M} \right)^3 \rho^2 N_A^2} \quad (3.6)$$

In Eq. (3.6) the constant B is given by:

$$B = \frac{A}{12\sqrt{6}} \quad (3.7)$$

It must be noticed that  $M_e$  is a property of the polymer network. At the same time, however, it is completely defined by single chain parameters and by the polymer density. Another molecular quantity of interest is the so-called packing length [75], defined as:

$$p = \frac{M}{\rho N_A} \frac{1}{\langle R^2 \rangle_0} = \left( \frac{M_e B}{\rho N_A} \right)^{\frac{1}{3}} \quad (3.8)$$

Based on Eq. (3.1)  $p$  can be seen as follows. Take a chain spanning the volume  $V_{sp}$  and squeeze it to its real volume so that it occupies the volume of a disk-like cylinder whose radius is given (approximately) by  $\langle R^2 \rangle_0^{\frac{1}{2}}$ . Then  $p$  is the thickness of that disk. The packing length can be also seen as a measure of the lateral size of the polymer chain. By assuming that a chain is made of a sequence of freely-joined cylinders of diameter  $d$  and length  $b_k$ , then [148]:

$$p = \frac{\pi d^2}{4 b_k} \quad (3.9)$$

Larger values of  $p$  imply that chain segments are shorter and fatter so that within the spanned volume, there is less room left for other chains. As a

consequence, larger packing lengths determine a reduced tendency for the chain to become entangled. The expressions for the  $M_e$  and  $p$  derive from "geometrical" considerations about the space filling of the polymer melt. The connection between these quantities and the macroscopic rheological parameters is given by a suitable theory for chain dynamics. In particular, if the Doi-Edwards model is used, then the following expression for the plateau modulus applies:

$$G_N^0 = \frac{4}{5} \frac{\rho N_A kT}{M_e} \quad (3.10)$$

As a consequence, measurements of the plateau modulus can directly yield the value of the molecular weight between entanglements. Conversely, independent measurements of the ratio between the average chain size and

the polymer molecular weight,  $\frac{\langle R^2 \rangle}{M}$  (for example, by Small Angle Neutron

Scattering) can lead to predictions for the packing length. Furthermore, the second equality of Eq. (3.8) allows for a quantitative determination of the parameter  $A$  (from  $B$  through Eq. (3.7)) and therefore to  $M_e$  (through Eq. (3.6)) and to the plateau modulus (through Eq.(3.10)).

Following these lines Fetters et al. [71], analyzed 26 different polymers for which both SANS measurements of  $\frac{\langle R^2 \rangle}{M}$  and viscoelastic measurements of  $G_N^0$  were available. As already mentioned in Chapter 1, they found a "universal" correlation between the different parameters. In particular, at a temperature of 140°C, the fit of the data with a single value of  $A=1.518$  gave excellent quantitative agreement for all polymers. As a consequence the following quantitative relationships were established:

$$G_N^0 = 12.16 p^{-3} \quad (3.11)$$

$$M_e = 225.8 p^3 \rho \quad (3.12)$$

The numerical factor in Eq. (3.12) has units  $\text{cm}^3 \text{\AA}^{-3} \text{mol}^{-1}$  and that in Eq. (3.11)  $\text{MPa} \text{\AA}^3$ .

In the present chapter the viscoelasticity response of a series of syndiotactic polypropylenes of varying degrees of syndiotacticity has been investigated. Quantitative values of the plateau modulus have been determined and, by use of the quantitative relations reported above they have been translated into molecular information by determining the corresponding molecular weight between entanglements and packing length. The results have been compared with existing data on syndiotactic polypropylene and interpreted in terms of the effect that the degree of stereo-regularity has on the polymer melt organization and on the rheological response.

## 3.2. Experimental Section

### 3.2.1. Materials

Samples of sPP with different degrees of syndiotacticity were used for the viscoelastic study. They were provided by the Department of Chemistry of the University of Naples. All samples were provided in the form of thermally compressed films of about 0.5 mm thickness. The relevant properties of the polymers are reported in Table 3.1. Samples labeled sPP-9 and sPP-5 are commercial polymers (supplied by Montell Technology). The others come from laboratory synthesis using metallocene catalysts [44-50]. It can be noted from Table 3.1 that samples are characterized by varying degree of syndiotacticity (%rrrr), melting temperature ( $T_m$ ) and molecular

weight ( $M_w$ ). A detailed description of these properties and of their determination can be found in [152].

Table 3.1 shows that the sPPs have very different levels of stereo-regularity. Correspondingly, their melting temperature also changes over a considerable range.  $T_m$  decreases as tacticity decreases. An exception is sPP-18, where the stereo-regularity is so low that crystallization cannot be observed. This sample can be seen as equivalent to an atactic sPP. Notice also that the commercial samples sPP-5 and sPP-9 are characterized by higher values of polydispersity. The polydispersity values are only indicative and must be considered accurate with an approximation of  $\pm 5\%$ . As it will be shown later, the relation  $M_w \gg M_e$  is well obeyed for all sample, which therefore can be considered well entangled polymer melts.

Table.3.1: List of materials used and its properties.

Sample	(% rrrr)	( $T_m$ )	$M_w$ (Da)	$M_w/M_n$
sPP-3	93	149	213,000	2.4
sPP-5	91.5	145	766,000	4.5
sPP-11	70.6	100	297,000	2.4
sPP-12	60.1	77	241,000	2.4
sPP-15	46.9	48	885,700	2.4
sPP-18	26.5	N.A.	1,190,800	2.4

### 3.2.2. Methodology

All viscoelastic tests were performed on an ARES rotational rheometer (TA Instruments) equipped with 8 mm diameter parallel plate geometry. Dynamic frequency sweep tests were performed at different temperatures for all polymer samples after confirming the linearity by dynamic strain sweep tests. All experiments were performed under a nitrogen atmosphere in order to minimize sample degradation.

In the present work we performed experiments at different temperatures ranging from 50°C to 220°C. All experiments were performed at a different gap depending on the as provided sample thickness as provided. The gap thickness was always in the order of 0.5 mm. Variation of temperature during the experiment will cause thermal expansion or contraction of the rheometer tools, which in turn will vary the actual gap of the experiment. To avoid this problem and make the results error free, we determined the thermal expansion co-efficient of the parallel plates. This was done by measuring the zero gap position at different temperatures. The results of this test are plotted in Fig.3.1. From the slope of the linear regression a thermal expansion value of 0.58  $\mu\text{m}/^\circ\text{C}$  was found. This value was incorporated in the option available in the Orchestrator software in order to automatically adjust the gap during the temperature varying experiments.

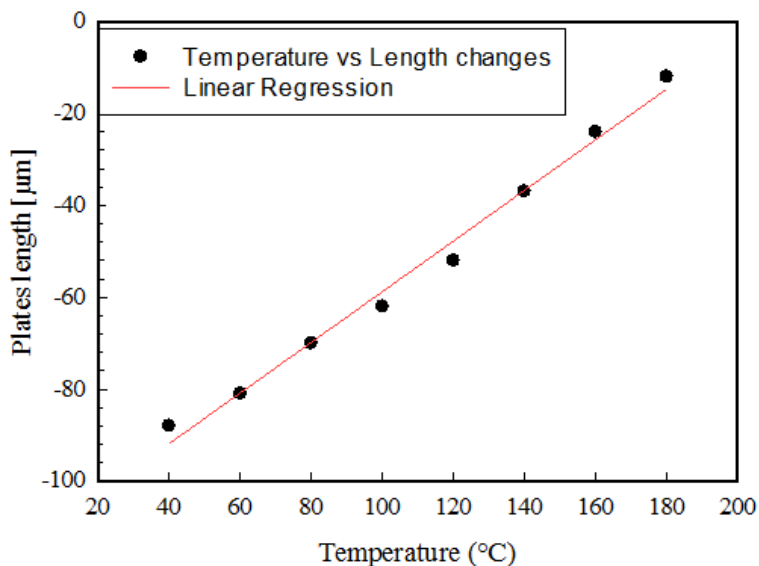


Fig.3.1: Plot between changes in length of plates vs Temperature.

### 3.3. Results and Discussion

A first test performed for all samples was a thermal stability test. All samples were put in the rheometer at 200°C and a constant frequency and constant strain isothermal annealing was allowed in order to clear the sample from any crystalline phase and to make sure about thermal stability. During the annealing the viscoelastic moduli were measured as a function of time. Two different behaviors were found in this type of experiments. For some samples, as is the case in Fig. 3.2 for sPP-9, moduli stayed essentially constant with time, indicating a fast melting and a good thermal stability. For other samples, such as sPP-3, the transient was longer. In this case, the time evolution of the moduli shows a continuous increase which eventually levels off at steady-state conditions after a relatively long time.

The time increase of the moduli is quite unexpected. If crystal melting were the only phenomenon involved, a decreasing in the moduli would have been found. An increase of the moduli could be attributed to a residual reactivity of the samples. This might be due to the presence of catalyst traces, or to chain crosslinks. Both phenomena would determine an increase in molecular weight and/or the formation of branched chains, thus resulting in an increase of the polymer viscoelasticity.

In order to assess the issue of thermal stability the time evolution moduli data were fitted by a simple exponential growth equation:

$$G(t) = G_0 + (G_\infty - G_0) \left[ 1 - \exp\left(-\frac{t}{\tau}\right) \right] \quad (3.13)$$

where  $G_0$  is the value at time zero,  $G_\infty$  is the long time value, and  $\tau$  is a characteristic time of the process. An example of the fit is shown in Fig.3.3

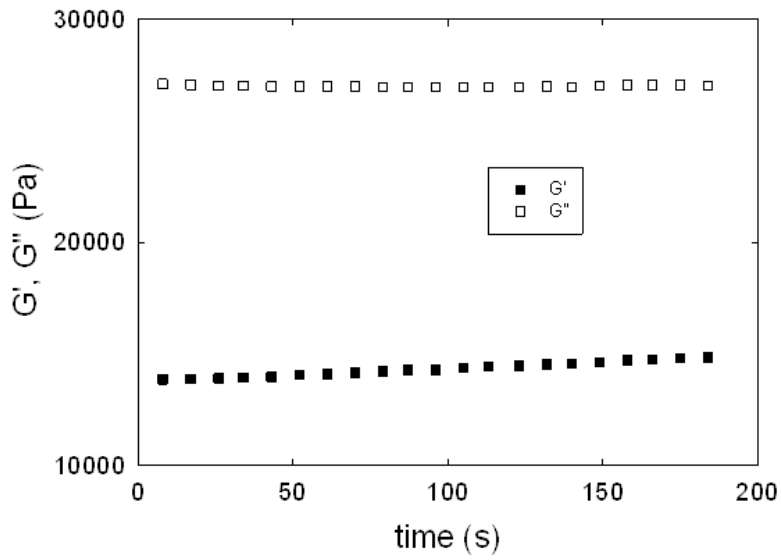


Fig. 3.2: Dynamic time sweep for sPP-9 at 200°C and 10 rad/s.

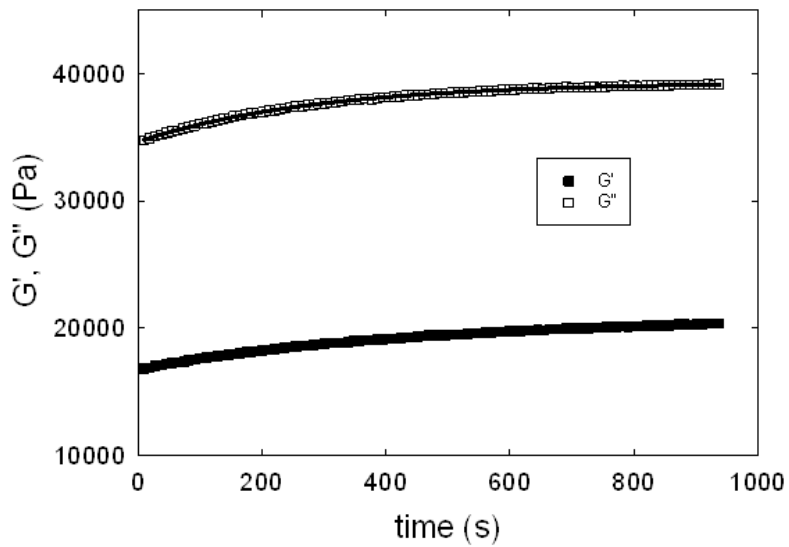


Fig.3.3: Dynamic time sweep for sPP-9 at 200°C and 10 rad/s. The thick line is the best fit of Eq. (3.13).

From time sweep experiments performed on all samples, a longest annealing time of 1000 s was found. For this reason all samples were annealed at 200°C for 20 minutes before any test was started.

After confirming the stability by the isothermal time sweep tests, linearity of all the samples was checked by strain sweep test. Linearity was obviously checked for any sample at all measuring temperatures. One example is shown in Fig.3.4 for sPP-9. In this case linearity is well obeyed in the strain range from 0.1 to 10%.

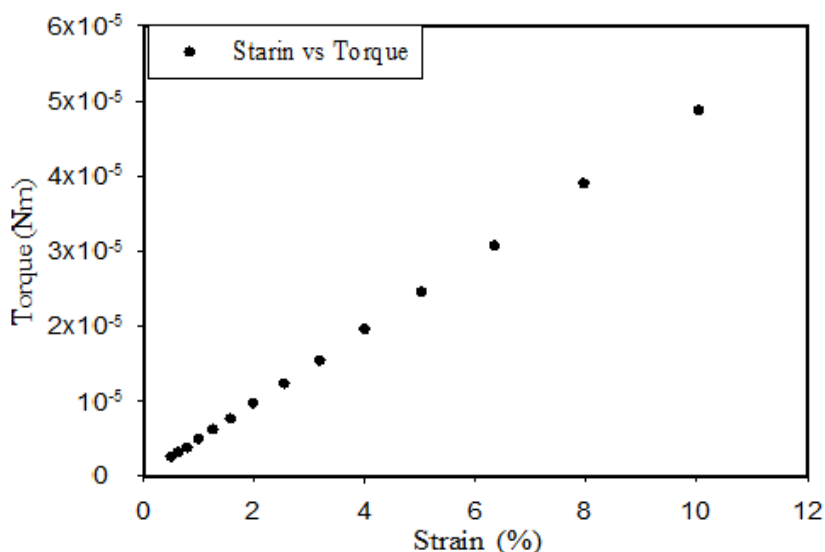


Fig.3.4: Dynamic strain sweep test of sPP-9 at 150°C.

Once the linearity limits had been established, the linear viscoelastic characterization was performed by frequency sweep tests. In a typical experiment after clearing the sample at 200°C, change of temperature during the experiment was done by a controlled constant rate heating or cooling using the temperature ramp option of the instrument.

After confirming linearity and stability of all the samples frequency sweep tests were performed at different temperatures to investigate the viscoelastic response as a function of frequency. Tests were performed at a given temperature in the 1÷100 rad/s or in the 0.1÷100 rad/s frequency range. One example of the frequency response for sPP-3 at 200°C is given in Fig.3.5.

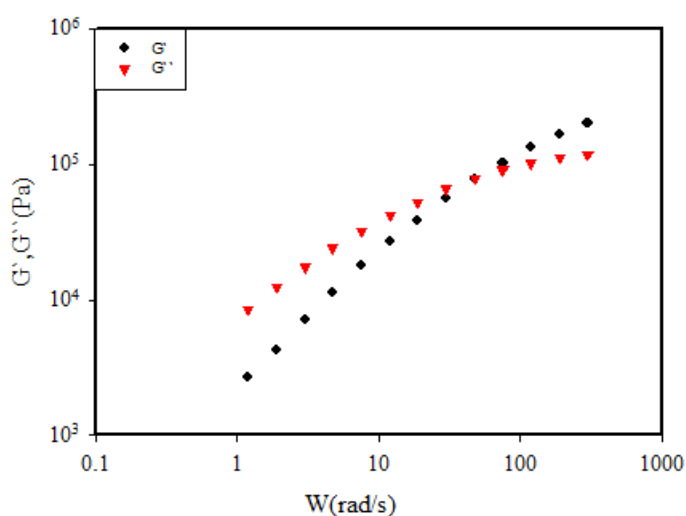


Fig.3.5: Dynamic frequency sweep test of sPP-3 at 200°C.

In order to obtain the widest frequency response, each sample was tested at different temperatures and the Time Temperature Superposition (TTS) principle was then applied to obtain master curves. TTS was applied by using a two dimensional minimization shifting method using the Orchestrator rheometer software. The highest temperature was always set at 200°C. For the lowest temperature, the crystallization behavior of the samples had to be taken into account. Samples with higher tacticity have also a higher melting temperature, which of course limits the value of the lowest temperature that can be reached in rheological experiments.

In order to better clarify this point, Fig. 3.6 shows the time evolution of the elastic modulus for sPP-5 at different temperatures. The sample was quickly cooled down from 200°C to the test temperature and the modulus evolution under isothermal conditions was monitored. After an initial increase, which corresponds to the cooling down from the higher temperature, the moduli show an initial plateau followed by a sharp upturn. The latter indicates the onset of crystallization. Fig. 3.6 shows that even at temperatures lower than the melting temperature, the sample still behaves as a molten liquid for some time. Such a time, which is called induction time can be used to perform a frequency sweep while the polymer is still in the melt state. Notice that even for a temperature of 125°C, the induction time is of the order of a few hundreds of seconds. This is a sufficient time to perform a frequency sweep from 1 to 100 rad/s.

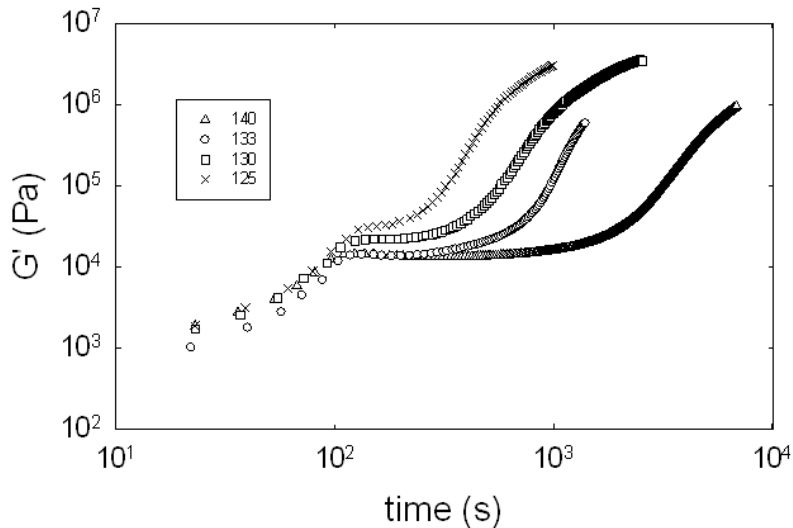


Fig.3.6: Isothermal time sweep for sPP-5 at different temperatures.

Based on the above observations a different temperature window for each sample was used to perform the frequency response measurements. The test

temperatures used for each sample are listed in Table.3.2. In all cases master curves were built at the reference temperature of 200°C.

Table.3.2: List of selected temperatures for time temperature superposition principle.

Sample	(%rrrr)	Test temperature (°C)			
sPP-3	93-94	200	175	155	135
sPP-5	91.5	200	170	140	125
sPP-11	70.6	200	170	140	80
sPP-12	60.1	200	160	120	70
sPP-15	46.9	200	140	60	30
sPP-18	26.5	200	100	60	30

In order to remove the possible error due to density variation caused by the changes in temperature, the density of all polymer samples was calculated at different temperatures by using equation of state of Simha-Somcynsky [112, 113].

$$\ln \frac{v}{v^*} = a_0 + a_1 \left( \frac{T}{T^*} \right)^{\frac{3}{2}} \quad (3.13)$$

where  $a_0 = -0.10346$ ,  $a_1 = 23,854$ , and while  $v^*$  and  $T^*$  are the specific volume and temperature respectively. Values of densities were inserted in the orchestrator software TTS spreadsheet after calculating them at different temperatures. The Orchestrator software TTS spreadsheet bar is shown in Fig.3.7 and Fig.3.8 before and after the shifting respectively.

	A Temp °C	B $a_T$	C $b_T$	D $\rho$ g/cm <sup>3</sup>	E $\chi^2$	F Vert_Shift	G Horz_Offset	H Vert_Offset
1	99.86	1.00000	1.00000	0.77160		1.00000	0.00000	0.00000
2	139.99	1.00000	1.00000	0.74840		1.00000	0.00000	0.00000
3	169.99	1.00000	1.00000	0.73070		1.00000	0.00000	0.00000
4	199.99	1.00000	1.00000	0.71290		1.00000	0.00000	0.00000
5								

Fig.3.7: Spread sheet before shifting.

	A Temp °C	B $a_T$	C $b_T$	D $\rho$ g/cm <sup>3</sup>	E $\chi^2$	F Vert_Shift	G Horz_Offset	H Vert_Offset
1	99.86	68.1172	1.00000	0.77160	0.01744	1.17195	0.00000	0.00000
2	139.99	10.1555	1.00000	0.74840	0.01986	1.09090	0.00000	0.00000
3	169.99	4.02874	1.00000	0.73070	0.03336	1.04168	0.00000	0.00000
4	199.99	1.00000	1.00000	0.71290		1.00000	0.00000	0.00000
5								

Fig.3.8: Spread sheet after shifting. The vertical shift factor calculated by the software after density correction is shown in column F.

In the following examples of the master curves obtained for the sPP samples are presented and discussed. Figure 3.9 shows the master curve for sPP-3. This is the polymer with the highest stereo-regularity and therefore, with the highest melting temperature. As a consequence the measurements could not be performed at temperatures sufficiently low to disclose the plateau region. In fact it must be reminded that based on the TTS principle, measurements at lower temperature allow to widen the frequency window towards higher frequencies.

Fig.3.9 indicates that  $G'$  is still far away from reaching the plateau region and that  $\tan\delta$  does not show a minimum, which means that the rigorous method for the determination of the plateau modulus (see Eq. (3.17)) cannot be used. Furthermore, the loss modulus is almost reaching a maximum,

which however cannot be well appreciated. This situation is better understood if the loss modulus is plotted as a function of frequency of a linear-log scale, as in Fig. 3.10. As a consequence, even the methods based on integration of the  $G''$  curve (Eq. (3.15)) cannot be used.

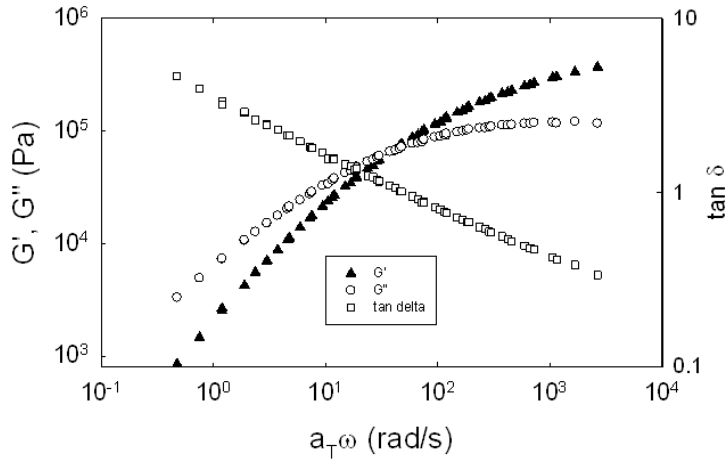


Fig.3.9: Master curve for sPP-3 at reference temperature of 200.

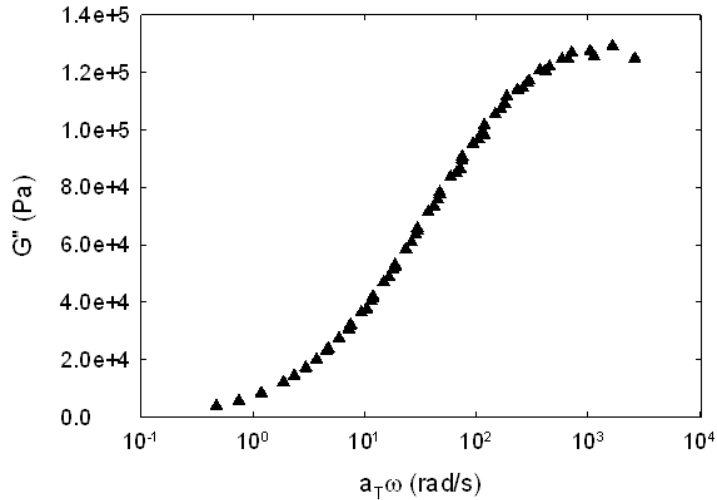


Fig.3.10: Master curve of the loss modulus for sPP-3 on a linear-log scale.

Based on the above considerations, in this case the method used to determine the plateau modulus is the cross-over method, whose equation is here reported again for clarity:

$$\text{Log}(G_N^0 / G_{cop}) = 0.38 + [2.63 * \log(M_w / M_n) / 1 + 2.45(M_w / M_n)] \quad (3.14)$$

It must be reminded that Eq. (3.14) is known to give acceptable results only for polymers with a polydispersity index less than three [90]. In this case, sample sPP-3 exhibits a  $M_w/M_n=2.4$ . This means that the resulting plateau modulus can be affected by a considerable error.

Figures 3.11 and 3.12 show the same results for sample sPP-5. The minimum in  $\tan\delta$  is not observed also in this case, However, the possibility to explore a wider range of temperatures, coupled to the higher molecular weight of sPP-5, makes it possible to observe a well-defined maximum in the loss modulus curve. This is made clearer in the linear-log plot of  $G''$  reported in Fig. 3.12. As a consequence, for sPP-5 the more reliable method based on the integration of the  $G''$  curve can now be used:

$$G_N^0 = (2/\pi) \int_{-\infty}^{\infty} G''(w) d \ln(w) \quad (3.15)$$

Following several authors (see, for example [86, 96, 97], the integral in Eq. (3.15) has been calculated by performing a linear extrapolation of the data set both on the left and right part of the frequency region.

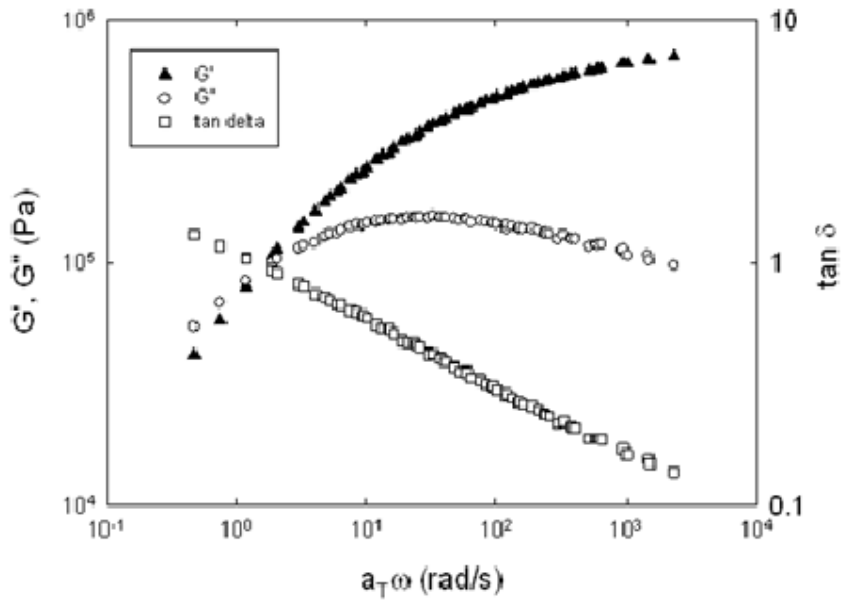


Fig. 3.11: Master curve for sPP-5.

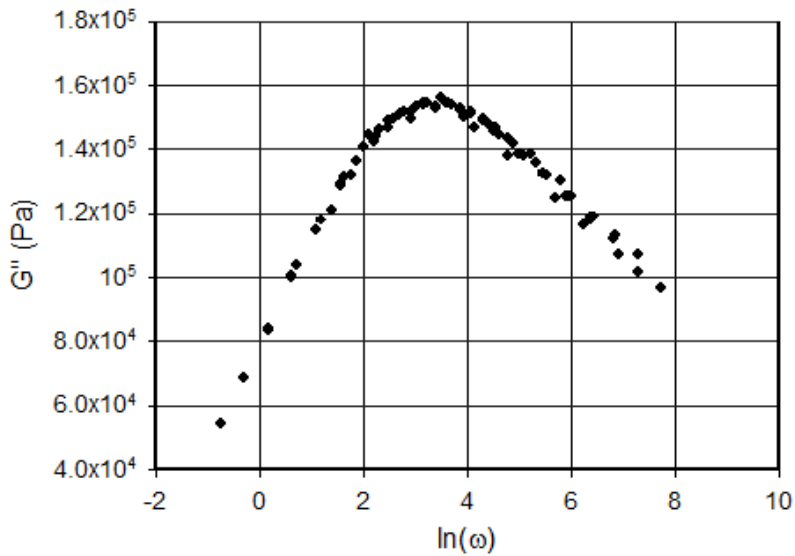


Fig. 3.12: Master curve of the loss modulus for sPP-5 on a linear-log scale.

Results similar to those reported for sample sPP-5 have been also obtained for samples sPP-9 and sPP-11 (not reported here).

In the case of the samples with the lowest syndiotacticity, that is, sPP-15 and sPP-18, the possibility to measure the viscoelastic response at low temperatures allows for the determination of the “complete” frequency response curve. This is shown in Fig. 3.13 for sample sPP-15. The minimum in  $\tan\delta$  is now clearly appreciated, which makes it possible to apply the theoretical model for a direct determination of the plateau modulus:

$$G_N^0 = (G')_{\tan\delta \rightarrow \min} \quad (3.16)$$

As said above, the same analysis could also be applied to sample sPP-18 (not shown here). The plateau moduli calculated from the experimental data are reported in Table 3.3. Notice that, in order to compare the data with those obtained in previous studies, the following expression for the plateau modulus has been used:

$$G_N^0 = \frac{\rho N_A kT}{M_e} \quad (3.17)$$

In Eq. (3.17), if compared with Eq. (1.36) of Chapter 1, the prefactor 4/5 has been omitted. Obviously, in view of a comparison between data, the numerical prefactor is non-influent.

It should be noticed that sample sPP-3 is the only sample for which the (less reliable) cross-over method has been used. For sample sPP-15 and sPP-18 the values obtained from integration of  $G''$  are in both cases slightly lower than those obtained by the (more reliable) minimum  $\tan\delta$  method. The good agreement between the values obtained by the two methods however, confirms the overall consistency of the experimental procedure. In the following discussion, the average values obtained from the two methods will be used for samples sPP-15 and sPP-18.

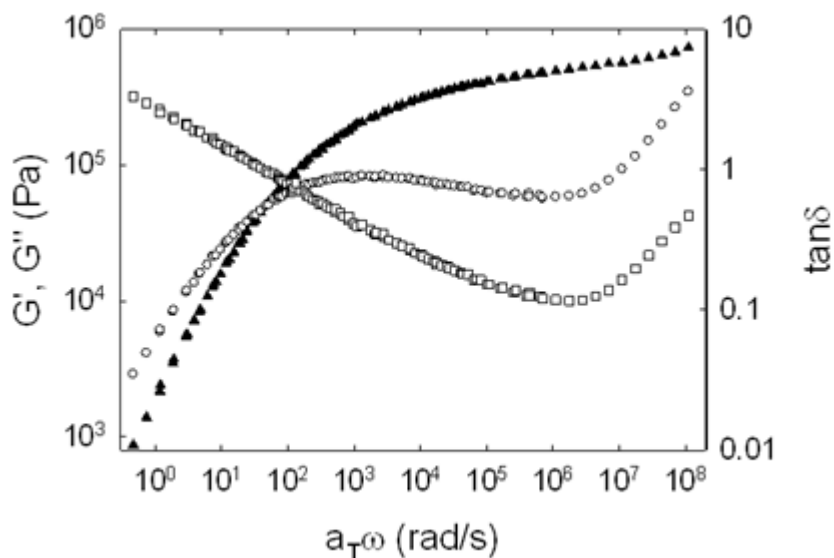


Fig. 3.13: Master curve for sPP-15 at reference temperature of 200.

Table.3.3: The plateau modulus of the different sPP samples.

Sample	Cross-over method	$G''$ integral Method	min $\tan\delta$ method
sPP-3	883,000	---	---
sPP-5	---	644,000	---
sPP-11	---	530,000	---
sPP-12	---	491,000	---
sPP-15	---	458,000	477,000
sPP-18	---	411,000	439,000

### 3.3.1. Discussion

The plateau modulus rheological data obtained in the previous section can now be used to determine the microscopic parameters characterizing the polymer chain, according to what has been already discussed in Chapter 1 and in Section 3.1 of the present chapter. In particular, predictions can be

made for the molecular weight between entanglements,  $M_e$ , and for the packing length,  $p$ .

The former is directly related to the plateau modulus by the following expression:

$$M_e = \frac{\rho N_A kT}{G_N^0} \quad (3.18)$$

A direct determination of the packing length would require (see Section 3.1) knowledge of the quantity  $\frac{\langle R^2 \rangle}{M}$ , which is not available. Use can be made, however, of the empirical equation (3.11), derived by Fetters et al. [71]. By considering the omission of the prefactor 4/5 in Eq. (3.17), the relation between packing length and plateau modulus is given by:

$$p = \left( \frac{15.2}{G_N^0} \right)^{\frac{1}{3}} \quad (3.19)$$

The results of the calculations are shown in Table 3.4, where sample tacticity is also added.

The results reported in Table 3.4 can be used in two different ways. First of all comparison can be made between the values obtained in this work and those already presented in the literature.

Rheological data on syndiotactic polypropylene are not very common in the literature. Eckstein et al. [86] measured the plateau moduli of three PP samples, namely a syndiotactic PP ( $\%rr=93\%$ ) and an isotactic PP ( $\%mm=98.7$ ) both characterized by a high stereo-regularity, and an atactic PP ( $\%rr=17.0$ ). Therefore, their sPP can be compared to our sPP-3 sample, whereas their aPP can be considered similar to our sPP-18. For the polymer investigated, Eckstein et al. found plateau moduli of 1.35 MPa for sPP, 0.427

MPa for iPP and 0.418MPa for aPP. Comparison with the data reported in Table 3.4 shows a good correspondence between the two different sets of data. In particular, while the plateau modulus measured by Eckstein et al. for sPP is somewhat larger than that measured in the present work for sample sPP-3, the values of their aPP and our sPP-18 sample compare very well.

Table.3.4: List of values of packing length and mean square end to end distance of all samples.

Sample	% rrrr	$G_N^0$ (Pa)	$M_e$ (Da)	$p$ (Å)
sPP-3	93	883,000	3,170	2.58
sPP-5	91.5	644,000	4,350	2.87
sPP-9	78	530,000	5,280	3.06
sPP-12	70.6	491,000	5,700	3.14
sPP-15	60.1	468,000	5,980	3.19
sPP-18	26.5	425,000	6,590	3.29

It should be pointed out that the plateau modulus of the sPP sample of Eckstein et al. has been obtained by the  $G''$  integral method, although in their case (as in the case of the sPP-3 reported in this work), the maximum in  $G''$  is very difficult to detect. The discrepancy might be then due to either different methods used (in our case we used the empirical cross-over method) or to the intrinsic uncertainty related to both calculations methods.

In a more recent work [153] Liu et al. measured the plateau modulus of three high syndiotactic ( $\%rrrr \cong 78$ ) sPP samples and compared their results with those of Eckstein et al. They come to the conclusion that the plateau modulus of highly stereo-regular sPP is of 0.87MPa, which is very close to the value for sample sPP-3 in this work. From the above comparisons, it can

be concluded that the plateau moduli measured in this work are consistent with the data already present in the literature.

Even less frequent in the literature are data on the packing length of sPP. To our knowledge, the only explicit reference to this parameter is given by Fetters et al. [107], who compared the molecular parameters of different olefin-based polymers. For a highly stereo-regular sPP, they report a packing length value of  $p=2.22 \text{ \AA}$ , which compares well with the value of  $p=2.55 \text{ \AA}$  reported in Table 3.4.

Of more relevance to this work is the internal comparison between the results reported in Table 3.4. From these data it is apparent the role of stereo-regularity on the molecular characteristics of syndiotactic polypropylene. The main message is that an increase in syndio-tacticity results in an increase of the plateau modulus and correspondingly in a decrease of both the molecular weight between entanglements and of the packing length. This result is made clearer in Figure 3.14, where both  $M_e$  and  $p$  are plotted as a function of the degree of syndiotacticity.

When plotted as a function of the degree of syndiotacticity,  $M_e$  is a decreasing linear function of the stereo-regularity. Exceptions are the data at the highest syndiotacticity. As said before, this may be related to the higher uncertainty in calculating the plateau modulus in that region. The fact that the data for high tacticity are quite consistent with those of Eckstein et al. and of Liu et al. may suggest that a highly stereo-regular syndiotactic chain represents a somewhat special case with respect to lower tacticity polymers.

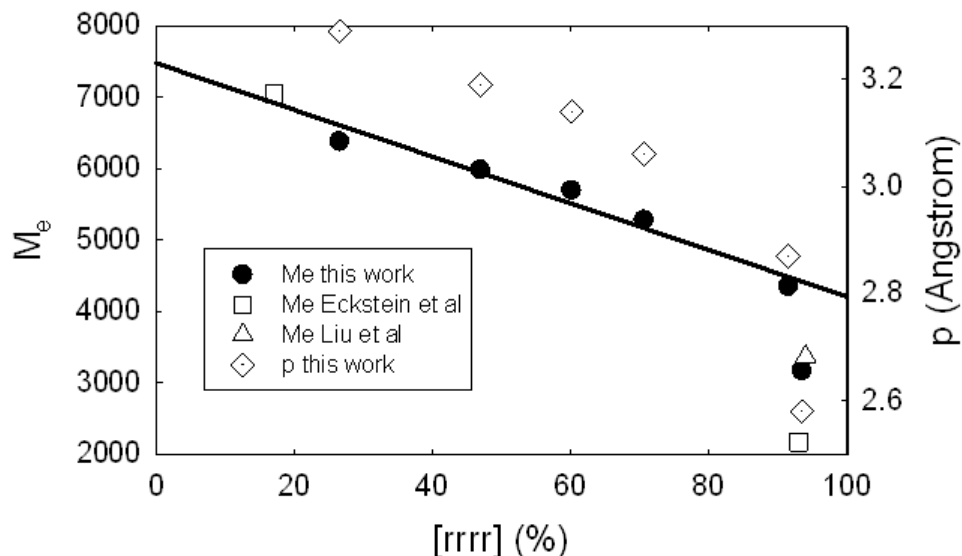


Fig. 3.14: The molecular weight between entanglements and the packing length as a function of the degree of tacticity. The straight line is drawn through the  $M_e$  data just to guide the eye.

In terms of interrelations between molecular architecture and microscopic properties, the data suggest the following scenario. For high degrees of syndiotacticity polymer chains "fill" the available space in a more efficient way than either lower syndiotacticity or atactic/isotactic chains. This is confirmed by the lower value of the packing length at high  $rrrr$  values, meaning that isotactic and atactic polymers are "bulkier" than the more syndiotactic ones. This might be explained by the alternate disposition of the side methyl group along the PP backbone. It is reasonable that such a disposition generates a better packing of the chain units even with respect to the isotactic arrangement, where the methyl group placed on the same side of the chain may form a closer sequence of side groups, giving raise to larger repulsion effects.

### **3.4. Concluding Remarks**

The linear viscoelastic measurements performed on sPPs of different stereoregularity show that the plateau modulus and therefore the molecular weight between entanglements significantly depend upon on the degree of syndiotacticity of the polymer chain. In particular it was shown that  $M_e$ , as well as the packing length decreases with increase in the degree of syndiotacticity.

It is also verified that viscoelasticity is sensitive to chain parameters and can be used to predict it.

The results demonstrate that viscoelasticity is a powerful tool determines the local details of the molecular architecture and chain parameters of the crystalline elastomers.

## Chapter 4

---

# Quiscent Crystallization of Syndiotactic Polypropylenes

### 4.1. Introduction

Crystallization of polymers is a process associated with the partial alignment of the molecular chains. These chains fold together and form ordered regions called lamella, which compose larger spheroidal structures named spherulites. From thermodynamic consideration alone, a crystal is at lower energy state than the liquid when the temperature is below the melting point, while at melting point a condition of equilibrium exists between the crystal and the liquid as both phases have the same value of free energy ( $G$ ) and  $\Delta G = 0$  [109]. For the isothermal process such as fusion at  $T_m$ ,  $\Delta G_f = 0$ .

$$\Delta G = \Delta H - T\Delta S \quad (4.1)$$

$$\text{At } T_m \quad \Delta H - T\Delta S = 0 \quad (4.2)$$

$$\Delta H = T\Delta S \quad (4.3)$$

$$T_m = \Delta H / \Delta S \quad (4.4)$$

Thus both the enthalpic and entropic effects will determine the equilibrium melting point temperature of any crystalline polymer.

During the last decades, the use of rheological techniques to examine polymer crystallization has got increasing importance. When cooled below thermodynamic melting temperature, crystalline polymers undergo crystallization. The early stages of this process are characterized by the gradual change in the mechanical response of the material from the liquid to the solid, which is due to the microstructure evolution of the system. This is

one of the great features of the rheological technique, which distinguishes it from the traditional DSC technique.

The main advantage of rheological technique, over traditional ones such as DSC, is that they can be more sensitive when crystallization kinetics are slow [12] and can provide information on the morphology of the crystallizing material [149]. On the other hand, the major drawback in the use of rheological techniques is that a universal correlation between viscoelastic properties and crystallinity is still missing. And also rheometry is unable to analyze the crystallization process when the crystallization kinetics are very fast. In this case DSC is the better candidate for the study of crystallization kinetics. To overcome these limitations, Kiewit et al. [150] have recently combined a rheometer and a DSC into a single instrument to compare the evolution of rheological properties to crystallinity as measured from heat flow integration. While this RheoDSC instrument was shown to provide reliable measurements, a systematic study on crystallizing systems is still missing.

Rheological functions can be used to calculate the evolution of relative crystallinity,  $x(t)$ , once a functional relation is assumed. Khanna [88], for example, suggested a linear relation between elastic modulus and crystallinity and used this idea to study the crystallization kinetics of different, nucleated and un-nucleated, polymers.

$$x(t) = (G' - G'_0) / (G'_\infty - G'_0) \quad (4.5)$$

where  $x(t)$  = Relative crystallinity,  $G'_0$  = Initial plateau value of elastic modulus,  $G'_\infty$  = Final plateau value of elastic modulus and  $G'$  = Elastic modulus at all points

Polymer crystallization is a complex phenomenon that affects the final properties of processed polymeric materials. The quality and quantity of

crystallization, i.e., the number, size, shape, and crystalline form of the crystallites depend upon on a number of different parameters like molecular weight, polydispersity and tacticity of the polymer system under consideration [151]. Among all tacticity is one of the important factors, which affects the crystallization process.

The aim of the present work is to study the quiescent crystallization behavior of a series of syndiotactic polypropylenes of different degrees of syndiotacticity by coupling rheological method to more conventional technique (Differential Scanning Calorimetry) and to relate the crystallization behavior to the syndiotacticity of the syndiotactic polypropylene chain.

## **4.2. Experimental Section**

### **4.2.1. Material**

Samples of sPP with different degrees of syndiotacticity were used for the crystallization study. The relevant properties of the polymers are reported in Table 4.1. The samples labelled sPP-8 and sPP-5 are commercial polymers (supplied by Montell Technology). The others come from laboratory synthesis using metallocene catalysts [44-50]. It can be noted from Table4.1 that samples are characterized by varying degrees of syndiotacticity (%rrrr), melting temperature ( $T_m$ ) and molecular weight distribution.

Table4.1: List of materials used and its properties.

Samples	Tacticity (%rrr)	Melting point ( $T_m$ )	Polydispersity
sPP-5	91.5	145	4.5
sPP-8	87	136	4.5
sPP-9	78.0	124	4.5
sPP-11	70.6	100	2.4
sPP-12	60.1	77	2.4

### 4.2.2. Methodology

Thermal behavior and overall crystallization kinetics of sPPs were examined by rheological and differential scanning calorimetric techniques. ARES rheometer (TA-Instrument) and differential scanning calorimeter (Shimadzu DSC60) equipped with an intra-cooler to permit operations of down to about  $-60^{\circ}\text{C}$  were used to investigate the thermal behavior and overall crystallization kinetics of a series of syndiotactic polypropylene samples.

Fundamental and basic operation principle of ARES rheometer has been explained in detail in the Chapter 2 of this report. Detail information about the ARES operation and hardware can also be found in the reference [102].

Both isothermal and non-isothermal crystallization behaviors of the syndiotactic polypropylene samples were explored by using rheological and differential scanning calorimetric techniques (DSC). In rheological experiments during crystallization ARES rheometer (strain controlled) equipped with 8 mm plates of parallel geometry were used. First of all discs of 8 mm diameter of sPPs were prepared for the crystallization experiments.

Procedure used for the non-isothermal crystallization analysis by rheological method has been mentioned below step by step.

1. First the sample was annealed at 200 °C in order to make it crystal free and melt completely. The annealing of sample was done by time sweep test.
2. After annealing linearity of all the samples was checked by the strain sweep test in the range of 0.1 to 10% of strain.
3. After confirming the linearity of the sample it was cooled from 200 °C to 50 °C by temperature ramp test at a cooling rate of 10°C/ min and constant frequency and deformation of 1 rad/s and 5% respectively.

After performing the non-isothermal crystallization, a second series of experiments were conducted on the syndiotactic polypropylene samples in order to monitor the isothermal crystallization of the sPPs using rheological technique. These experiments were conducted in order to determine quantitative temperature dependence of the crystallization kinetics. After annealing at 200 °C and confirming linearity by dynamic strain sweep test a temperature ramp test was conducted at a cooling rate of 40 °C/min and at a constant frequency and deformation of 1rad/s and 5% respectively. In order to explore the crystallization kinetics closer to the melting point cooling was done from 200 °C to different temperatures closer to the melting point of the samples.

Both isothermal and non-isothermal crystallization tests were also carried out using differential scanning calorimetric technique (DSC).

Non-isothermal crystallization tests were performed using DSC. Step by step procedure of the non-isothermal crystallization tests is mentioned below in detail.

1. Sample having weight of 4 mg was heated upto 200<sup>0</sup>C at a constant heating rate of 10<sup>0</sup>C/min. The sample was kept under this annealing

process for 5 minutes in order to make it crystal free or remove the thermal history.

2. Then the sample was cooled up to  $-30^{\circ}\text{C}$  by a cooling rate of  $-10^{\circ}\text{C}/\text{min}$ .
3. After this thermal treatment by DSC we are able to evaluate the glass transition temperature ( $T_g$ ), crystallization temperature ( $T_c$ ) and melting temperature ( $T_m$ ). The evaluations were made through the instrument software TA60.

Isothermal crystallization experiments with the instrument DSC were performed according to the following standard procedure:

The polymer samples (with a mass of about 4 mg) were melted for 5 minutes at  $200^{\circ}\text{C}$ , to eliminate previous thermal history. The samples were then cooled at the maximum cooling rate achieved by the tool, of approximately  $-15^{\circ}\text{C} / \text{min}$ . The crystallization was observed at different temperatures between  $T_c$  and  $T_m$ , the isotherm is maintained for a time sufficient to complete the crystallization. The crystallization was recorded during the heat flux ( $q$ ) and has been processed as a function of time ( $t$ ) which has been used to calculate the relative degree of crystallization  $\theta(t)$  according to the following relationship:

$$\theta(t) = \frac{\int_0^t \dot{q} dt}{\int_0^{\infty} \dot{q} dt} \quad (4.6)$$

The numerator of Eq.(4.6) represents the heat at time  $t$ , while the denominator is the total heat released during the process of crystallization.

## 4.3. Results and Discussion

### 4.3.1. Non-Isothermal crystallization

#### 4.3.1.1. Results

Non-isothermal crystallization behavior of the samples listed in the table.4.1 was investigated by rheological technique. Non-isothermal crystallization test of sPP-9 has been shown in Fig.4.1.

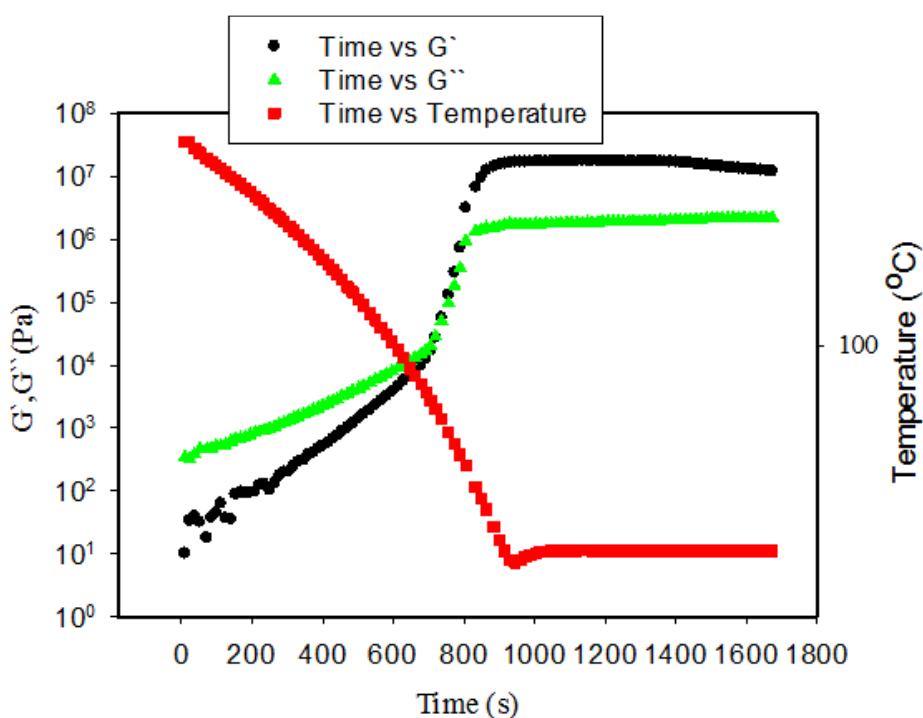


Fig.4.1: sPP-9 non-isothermal crystallization from 200  $^{\circ}\text{C}$  to 50  $^{\circ}\text{C}$  at a cooling rate of 10  $^{\circ}\text{C}$  / min and at a frequency and deformation of 1 rad/s and 5 % respectively.

Fig.4.1 depicts that both the moduli increase with the time from the start of the experiment. A sharp increase in both the moduli was found at a

temperature of 90 °C (below melting point), which shows that the material has started to crystallize. The intersection of both the moduli at this stage further verifies that the material is solidifying. Both the moduli were found to reach the plateau values at a set temperature, which is 50°C in this case.

Non-isothermal crystallization behavior was also examined by differential scanning calorimetric technique (DSC). DSC measures the heat flow as a function of temperature, which is directly related to the latent heat of crystallization. In DSC measurements temperature at the peak of the endothermic heat flow is the crystallization temperature of the polymer sample. DSC experimental observation has been shown graphically in the Figure.4.2 for sPP-5.

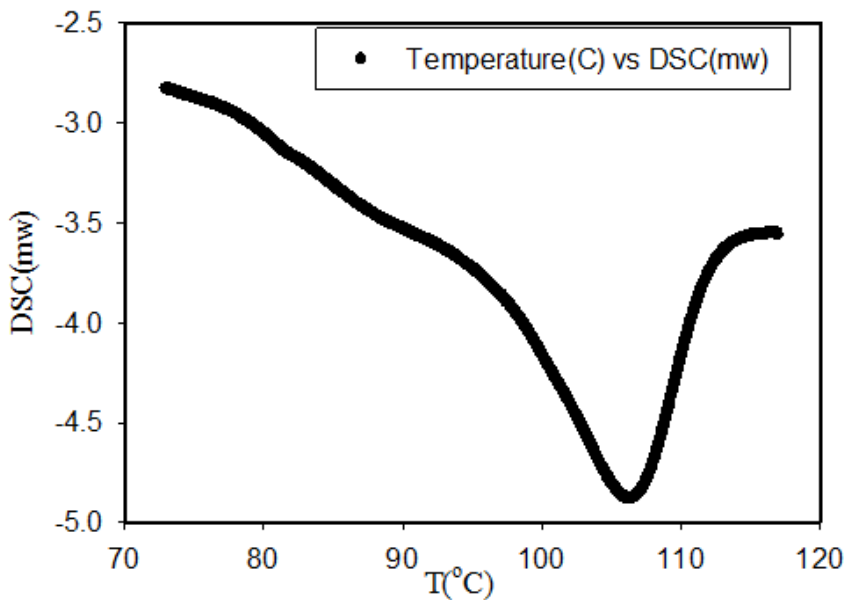


Figure 4.2: DSC non-isothermal crystallization test of sPP-5. (Cooling from 200°C to -30°C at a cooling rate of 10 °C/min).

### 4.3.1.2. Discussion

Peak temperatures (crystallization temperatures) were calculated from the non-isothermal crystallization tests conducted by using rheological and differential scanning calorimetric techniques. In order to obtain the crystallization temperature by rheological technique, complex modulus is plotted against the temperature as shown in Fig.4.3. First derivative of the complex modulus with respect to temperature was calculated. The plot of derivative resembles more with the DSC plot. The temperature peak of the first derivative resembles with the peak obtained by DSC measurement. A comparison of this plot with DSC has been shown in Fig.4.4.

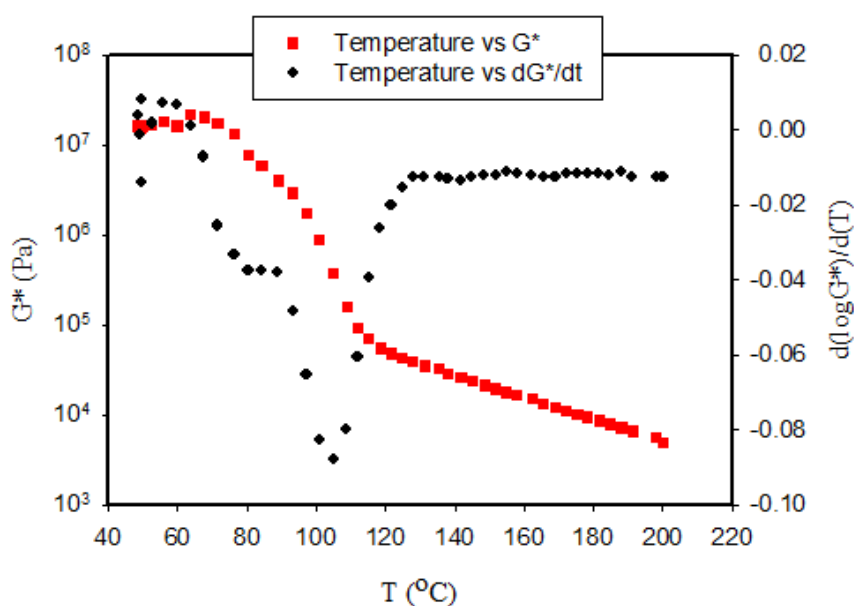


Fig.4.3: sPP-5 Complex modulus as a function of temperature with 1<sup>st</sup> order derivative during non-isothermal crystallization from 200 to 50 °C at a frequency of 01 rad/s and strain of 5%.

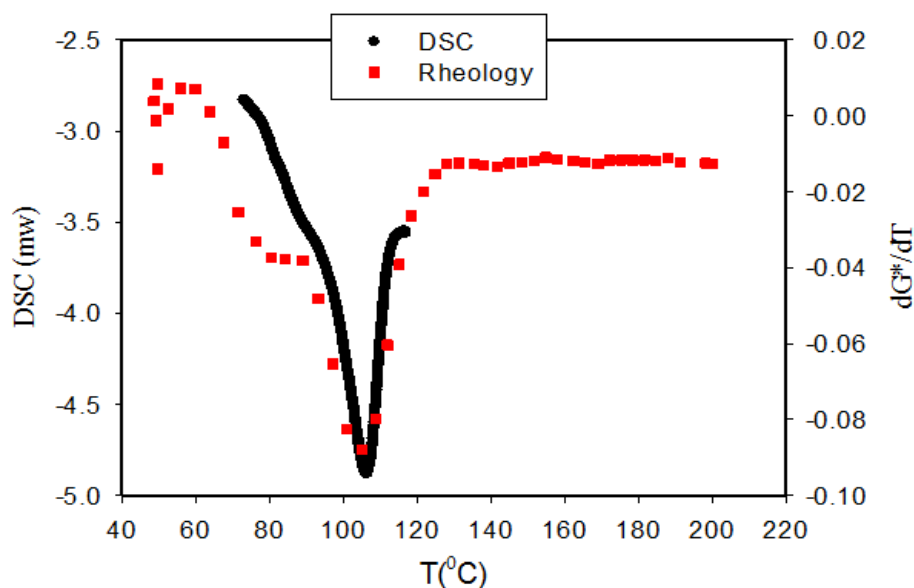


Fig.4.4: Comparison of non-isothermal tests of Rheology and DSC of sPP-5.

Peak temperatures (crystallization temperatures) were calculated for all other samples using the same procedure. Values of peak temperatures determined by both rheological and differential scanning calorimetric methods are listed in table.4.2 for all the samples.

Relationship between peak temperatures and syndiotacticity has been shown in Fig.4.5 for syndiotactic polypropylenes. It is clear from the Fig.4.5 that with the decrease in syndiotacticity, crystallization temperature (peak temperature) decreases, which may be due to the reason that decrease in syndiotacticity decreases the crystalline phase. In Fig.4.4 a comparison has been shown between peak temperatures determined by DSC and rheological techniques. The difference in the results of two equipments can be related to the difference in the sensitivity level of the two equipments. The difference can also be related to the high sensitivity of rheological technique at low crystallization kinetics, where differential scanning calorimetric technique (DSC) fails.

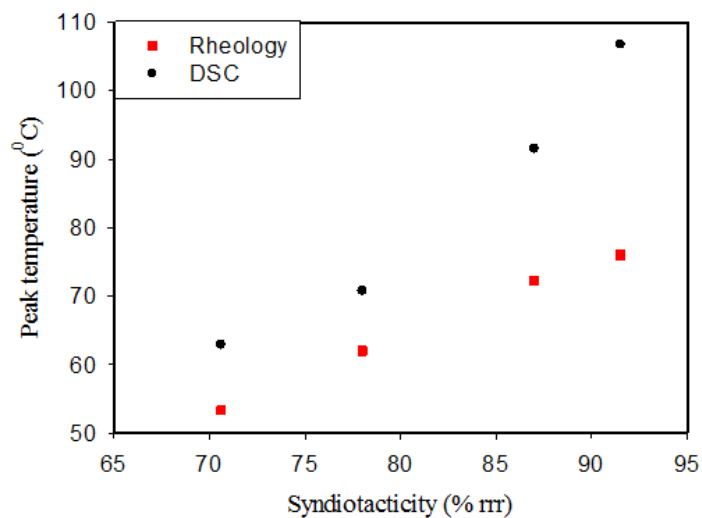


Fig.4.5: Crystallization temperature as a function of degree of syndiotacticity of polypropylenes.

Table 4.2: Peak temperatures of syndiotactic polypropylenes by Rheological and DSC techniques.

Polymer samples	Tacticity(% rrr)	Peak Temperature (°C) (Rheological Technique)	Peak Temperature (°C) (DSC Technique)
sPP-5	91.5	76.3	106.75
sPP-8	87.0	72.3	91.53
sPP-9	78.0	62.0	70.82
sPP-11	70.6	53.3	62.9

### 4.3.2. Isothermal crystallization

#### 4.3.2.1. Results

Isothermal crystallization tests of all the samples at different temperatures close to the melting point was conducted at a cooling rate of 40°C/min by using rheological technique. Different temperatures at which isothermal crystallization tests were conducted for all the samples are listed in table.4.3. Isothermal crystallization of sPP-5 has been shown in the Fig.4.6.

Table.4.3: List of final temperatures of isothermal crystallization for all the samples (Rheological Technique).

Polymer samples	T <sub>m</sub> (°C)	Final temperature (°C)			
sPP-5	145	125	130	133	140
sPP-8	136	120	125	130	--
sPP-9	124	100	105	110	--
sPP-11	100	70	75	80	--
sPP-12	77	50	40	35	25

Isothermal crystallization test of the sPPs were also carried out by the differential scanning calorimetric technique (DSC). As already explained in the methodology section of this chapter, the sample is heated upto 200°C by a constant heating rate of 10°C/min and then cooled by the maximum possible cooling rate of -15°C/min of the DSC. Calorimetric data collected under isothermal crystallization are reported in Fig. 4.7 in terms of heat flux versus time. Data show negative (exothermic) peaks that progressively

## Chapter 4

flatten out as the crystallization temperature increases. The overall heat released during crystallization does not change significantly with crystallization temperature.

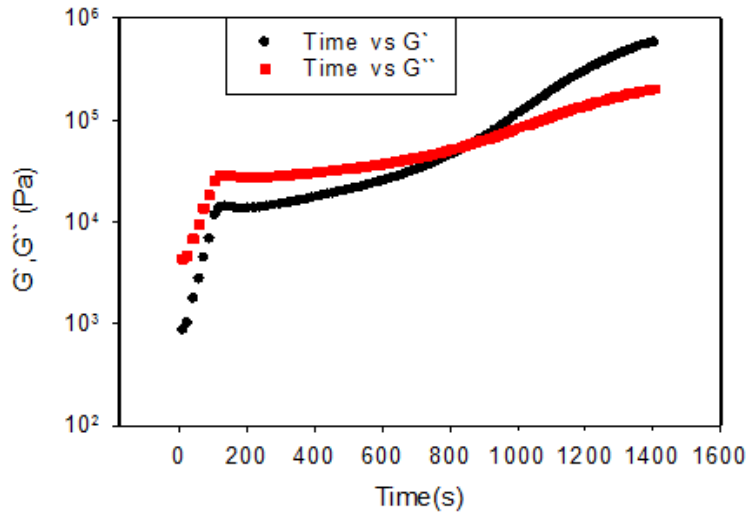


Fig.4.6: Isothermal crystallization of sPP-5 at 133°C at a constant cooling rate of 40°C/min.

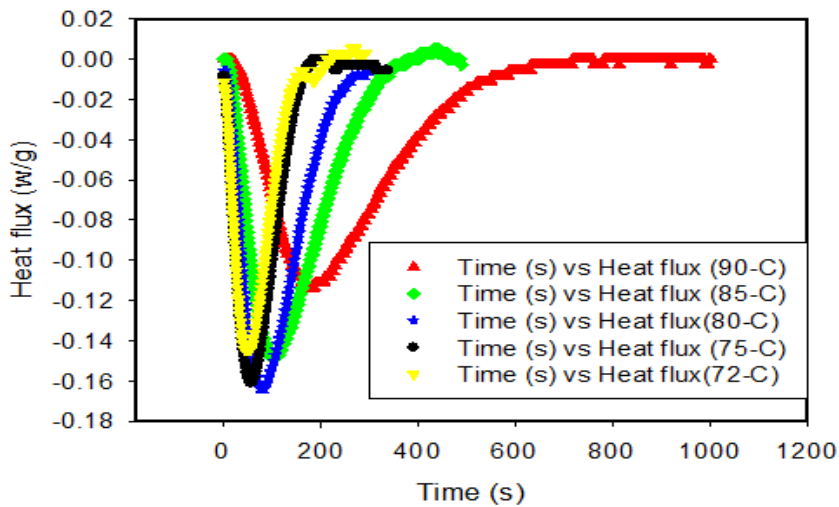


Fig.4.7: Heat flux as a function of time at different temperatures for sPP-9.

#### 4.3.2.2. Discussion

Fig.4.6 depicts that both the moduli are nearly constant at the beginning of the crystallization test. This phase consists of short time, which shows that crystallization has not started yet. The time during this phase is called induction time, which can be defined as the time required for reaching to the steady state of nucleation. Both induction time and nucleation rate have nearly an inverse relationship. In case of higher crystallization rate, the induction time becomes shorter. It was also found that lowering the final temperature during cooling from 200<sup>0</sup>C decreases the period of induction time and as a consequence increases rate of crystallization. This concept has been explained graphically in Fig.4.8 for sPP-9, which shows the isothermal crystallization at three different temperatures. Lowering the temperature near the crystallization temperature during the isothermal crystallization process increased the rate of crystallization and as a consequence decreased the induction time. The induction time at 100<sup>0</sup>C is much shorter than the induction time at 110<sup>0</sup>C during the isothermal crystallization process.

The 2<sup>nd</sup> part of the plot (Fig.4.6) starts with a sharp increase in both the moduli and ends after the cross over, which in general gives us two main information. Part of the region before cross over indicates start of crystallization, while part after the cross over shows the maximum point of crystallization. The rapid increase in the  $G'$  and reaching to its maximum value during that part shows the rapid increase in the rate of crystallization and its maximum value.

The characteristic time required for the crystallization to reach its maximum value during that part is called time of maximum crystallization rate denoted by  $t^*$ . This characteristic time is determined by calculating the first derivative of the  $G'$  with respect to the time.

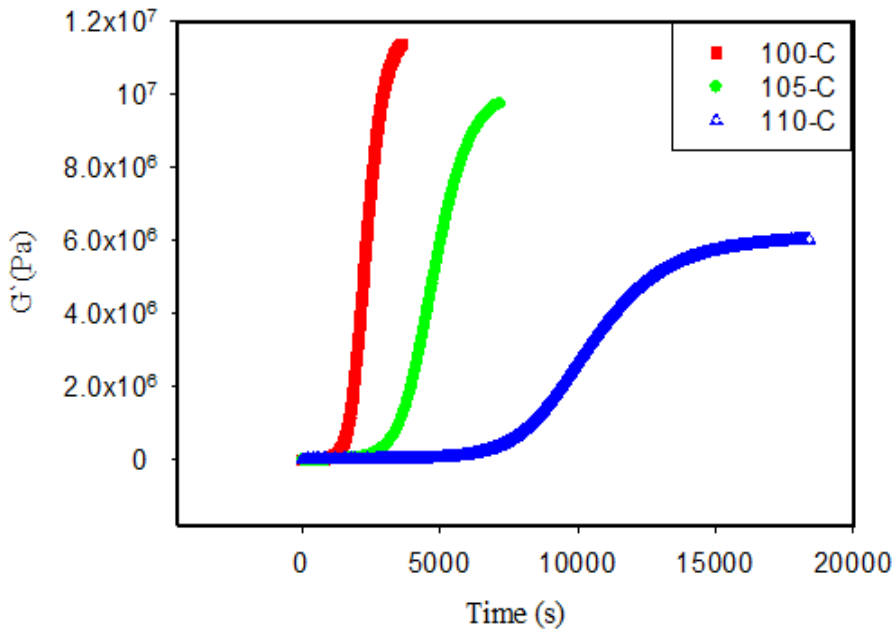


Fig.4.8. sPP-9 isothermal crystallization curves at different temperatures.

The time corresponding to the maximum point of the derivative, which corresponds to the inflection point of the function  $\log G'$  represents the time of maximum crystallization rate. This characteristic time was found to decrease with lowering the temperature near the crystallization temperature, which indicates that crystallization kinetics becomes faster by lowering the temperature near the crystallization temperature. With this again one can easily see the analogy with the calorimetric measurements. In fact the maximum value of the derivative of the  $\log G'$  versus time corresponds to the maximum flow in the DSC.

The third and last part of the isothermal crystallization plot (Fig.4.6) consists of plateau values of both the moduli. This part is relatively longer. Plateau values of  $G'$  at both the ends can be used to calculate the half crystallization by applying the correlation developed by Khanna [88]. Half

crystallization time is the time in which the degree of crystallization  $\alpha(t)$  is equal to 0.5 i.e when half of the crystalline phase is formed.

The characteristic times (induction time, maximum and half crystallization time) have been plotted against  $1/T$  for all the samples as shown in Fig.4.9 to Fig.4.13.

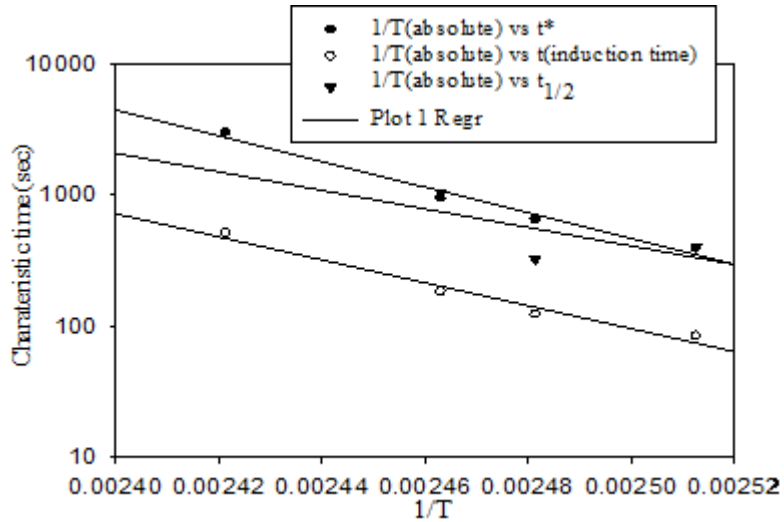


Fig.4.9: sPP-5 characteristic times as a function of reciprocal of absolute temperature.

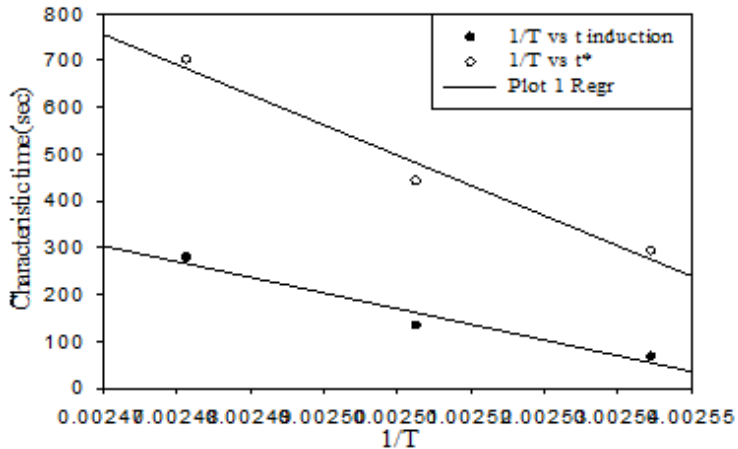


Fig. 4.10: sPP-8 characteristic times as a function of reciprocal of absolute temperature.

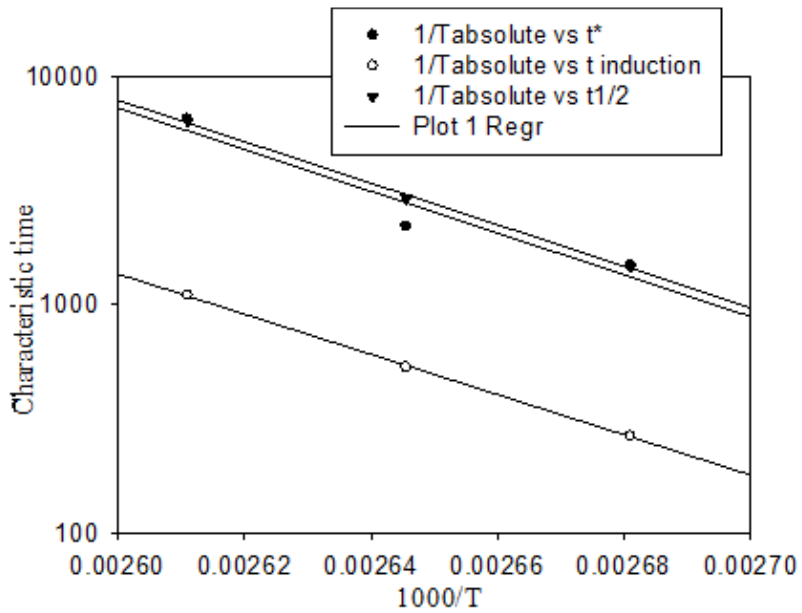


Fig.4.11: sPP-9 characteristic times as a function of reciprocal of absolute temperature.

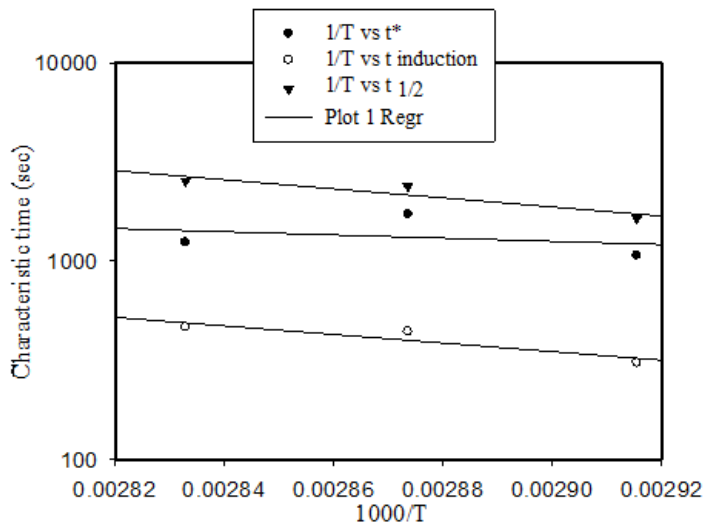


Fig.4.12: sPP-11 characteristic times as a function of reciprocal of absolute temperature.

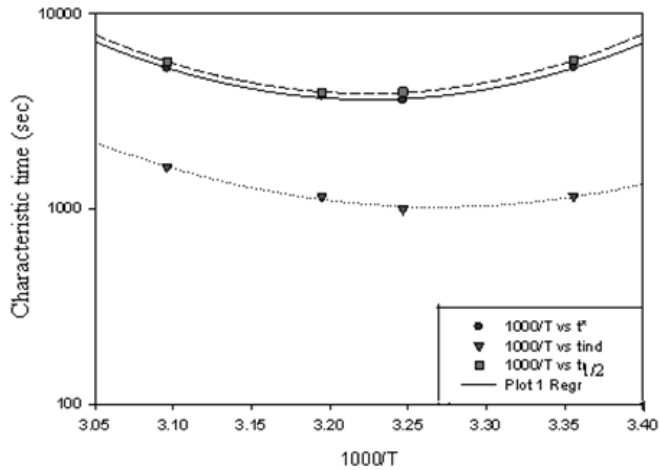


Fig.4.13: sPP-12 characteristic times as a function of reciprocal of absolute temperature.

Characteristic times are different by definition but as the crystallization process depends on the chemistry of the material. The slopes of the characteristic times as a function of  $1/T$  are the same. It is known that the crystallization rate and therefore the inverse of its characteristic time has a dependency on temperature. In Fig.4.13, the minimum point (the point where the crystallization characteristic times are low) is the point showing maximum crystallization rate. sPP-12 is a low syndiotactic sample, where the crystallization kinetics are slow and differential scanning calorimetric technique (DSC) is failed to analyze its crystallization behavior.

Activation energy was calculated from the slope of Arrhenius fit to the plot between  $\log(t)$  as a function of  $1/T$ . Slope of the Arrhenius plot corresponds to the  $-E_a/R$ , where  $R$  is the universal gas constant. Mathematical expression of Arrhenius equation is given as Eq.(4.7). Activation energy of all the samples is listed in the table.4.4.

$$r \propto \frac{1}{t_{car}} \propto \exp\left(-\frac{E_a}{RT}\right) \quad (4.7)$$

Thermodynamic crystallization temperature can be calculated from the characteristic crystallization times. Thermodynamic crystallization temperature can be calculated by linear regression of the plot between  $1/T$  vs  $1/t^*$  and limit  $1/t^*$  tends to zero. This plot has been shown for sPP-5 in the Fig.4.14.

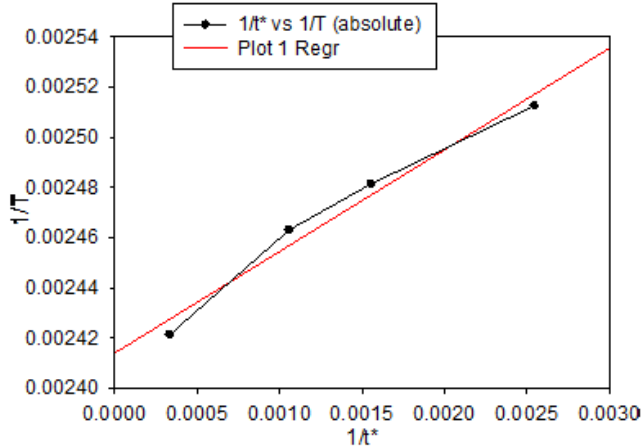


Fig.4.14: sPP- 5 plot of  $1/T$  as a function of  $1/t^*$  for the calculation of the thermodynamic crystallization temperature.

Thermodynamic crystallization temperature ( $T_m$ ) calculated for all the samples from the plot between  $1/T$  vs  $1/t^*$  and limit  $1/t^*$  tends to zero are listed in table.4.4.

Isothermal crystallization kinetics of calorimetric data obtained were analyzed using Avrami equation [98,109].

$$\theta(t) = 1 - \exp(k * t^n) \quad (4.8)$$

Where  $\theta(t)$  =Relative crystallinity, Where  $n$ =Avrami constant that depends on the mechanism of nucleation and crystal growth,  $t$ =The real time of crystallization,  $k$  = Rate constant of crystallization which involves both nucleation and speed of crystal growth.

Table.4.4: List of thermodynamic crystallization temperature and activation energy.

Samples	(%rrr)	(T <sub>m</sub> ) (Rheology)	(T <sub>m</sub> ) (DSC)	E <sub>a</sub> (kJ/mol) (Rheology)	E <sub>a</sub> (kJ/mol) (DSC)
sPP-5	91.5	141	145.1	81.26	126.40
sPP-8	87	132	139.2	49.87	-
sPP-9	78.0	113	112.91	76.00	75
sPP-11	70.6	94	100.0	18.95	-
sPP-12	60.1	-	77	9.45	-

The model properly interpolates the data of crystallization for values up to 90%. At higher values of  $\theta(t)$ , the curves deviate from linearity, this thing is attributed to secondary crystallization. According to Eq (4.8), the Avrami exponent was obtained as the slope of a linear regression and  $\ln(k)$  as the intercept when  $\ln(-\ln(1-\theta(t)))$  is plotted against  $\log(t)$  (not shown here). The kinetic parameters are listed in Table 4.5. Lower values of  $n$  (less than 3) suggest homogeneous nucleation, while higher values of  $n$  suggest heterogeneous growth of crystals.

If  $\theta(t)=0.5$ , then the relationship between half time of crystallization and crystallization kinetics constant ( $k$ ) can be written as:

$$t_{1/2} = \left(\frac{\ln 2}{k}\right)^{1/n} \quad (4.9)$$

If  $t_{1/2}$  is evaluated from the experimental data, the value of  $k$  can be calculated theoretically using the equation (4.9).

## Chapter 4

It is clear from the table.4.5 that Avrami constant ( $n$ ) and half crystallization time ( $t_{1/2}$ ) vary with the temperature ( $T_{\text{cry}}$ ). This results show that the mechanism of growth of crystals varies with the temperature ( $T_{\text{cry}}$ ) in particular when the closer we get to the temperature of melting, the crystals tend to grow with heterogeneous mechanisms. It is also clear from the table.4.5 that increase in temperature ( $T_{\text{cry}}$ ) increases the half crystallization time ( $t_{1/2}$ ). It means that increase in temperature ( $T_{\text{cry}}$ ) decreases the nucleation rate. In the other words increase in temperature ( $T_{\text{cry}}$ ) reduces the speed of crystallization kinetics. Half crystallization time is the time in which half of the crystallization is completed. These results are reported in the Fig.4.15.

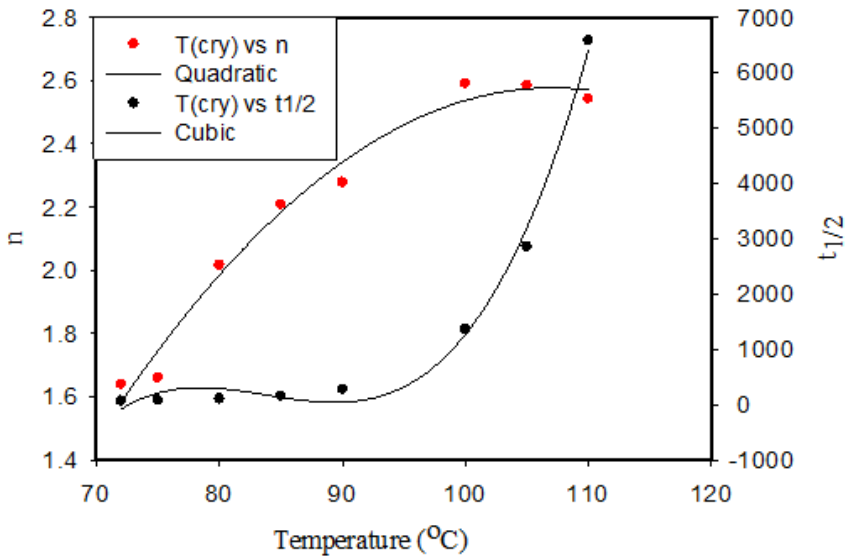


Fig.4.15: Avrami parameters ( $n$  and  $t_{1/2}$ ) as a function of temperature ( $T_{\text{cry}}$ ). The lines through the Avrami exponent and half crystallization time is for the guidance of the eye.

Table.4.5: List of Avrami exponent (n) and crystallization rate constant (k).

Polymer sample	T (°C)	n	K	t <sub>1/2</sub>
sPP-9	72	1.6398	6.906*10 <sup>-4</sup>	67.7
	75	1.6599	4.937*10 <sup>-4</sup>	78.7
	80	2.0157	5.883*10 <sup>-5</sup>	104.7
	85	2.2077	1.027*10 <sup>-5</sup>	154.0
	90	2.2773	1.915*10 <sup>-6</sup>	276.0
	100	2.5913	5.292*10 <sup>-9</sup>	1356.7
	105	2.5844	8.140*10 <sup>-10</sup>	2853.7
sPP-5	110	2.5425	1.360*10 <sup>-10</sup>	6575.8
	100	1.2291	3.400*10 <sup>-3</sup>	75.7
	110	1.9048	3.274*10 <sup>-5</sup>	186.6
	125	2.3186	3.357*10 <sup>-7</sup>	529.1
	130	2.2542	7.409*10 <sup>-8</sup>	1237.3
	140	2.5008	1.146*10 <sup>-9</sup>	3247.4

The Avrami parameters can be used to calculate the activation energy of the crystallization isotherm. The constant k can be approximated by an equation of Arrhenius form:

$$k^{1/n} = k_0 \exp \left( -\frac{E_a}{RT_c} \right) \quad (4.10)$$

Where  $K_0$  is the pre-exponential factor independent of temperature,  $E_a$  is the activation energy,  $R$  is the universal gas constant and  $T_c$  is the crystallization temperature.

After the linearization of Eq.(4.10) we have :

$$\frac{1}{n} \ln(k) = \ln(k_0) - \frac{E_a}{R} * \frac{1}{T_c} \quad (4.11)$$

$E_a$  can be obtained from the slope of the linear regression of the plot between  $\frac{1}{n} \ln(k)$  and  $1/T$  as shown in Fig.4.16 for sPP-9. Values of  $E_a$  are listed in the table 4.4.

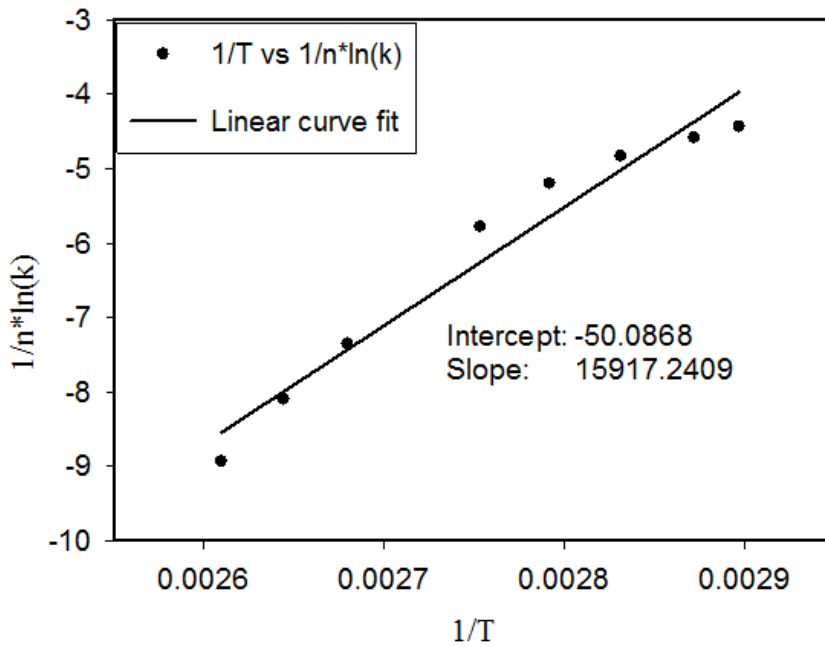


Fig.4.16: Linear regression of the plot between  $\frac{1}{n} \ln(k)$  and  $1/T$  for sPP-9.

Activation energy of crystallization is found sensitive to the syndiotacticity of the syndiotactic polypropylenes. It is found to increase with the increase in the degree of syndiotacticity. Comparison of activation energy calculated by both rheological and differential scanning calorimetric techniques and its relationship with the degree of syndiotacticity is reported in the Fig.4.17.

Thermodynamic crystallization temperatures calculated for all the samples from the DSC peak during the isothermal crystallization process are listed in the table 4.4. Comparison between thermodynamic crystallization temperatures calculated by both the rheological and differential scanning calorimetric techniques and its relationship with the degrees of syndiotacticity of sPPs is reported in the Fig.4.18. Thermodynamic

crystallization temperatures of sPPs determined by two different techniques are in good reasonable agreement.

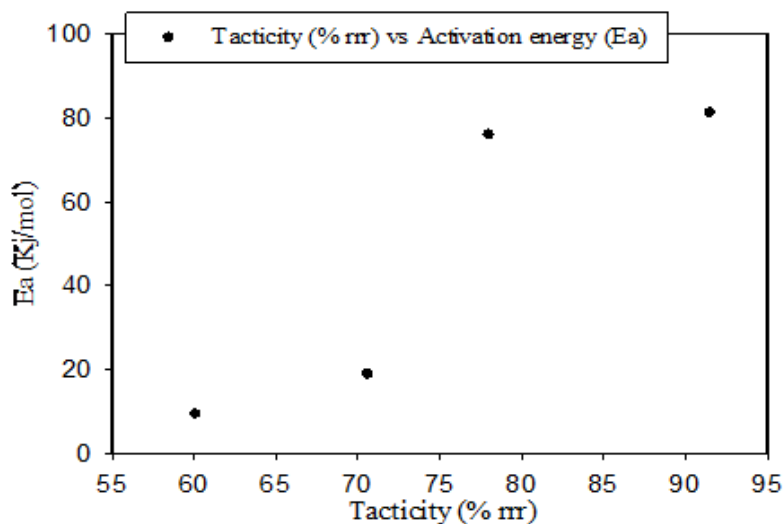


Fig.4.17: Activation energy of crystallization as a function of tacticity.

Thermodynamic crystallization temperature (melting temperature) is found to increase with increase in the degrees of syndiotacticity of syndiotactic polypropylenes. Which can be related to the fact that sPP with the higher degree of syndiotacticity has larger crystalline mass compare to the sPP with low degree of syndiotacticity.

Relative crystallinity can be calculated from the isothermal crystallization data of differential scanning calorimetry (DSC). Successive integration and normalization of thermograms obtained during the isothermal crystallization experiments of the sPPs allow us to calculate the evolution of the relative crystallinity as a function of time,  $x(t)$ , as reported in Fig. 4.19.

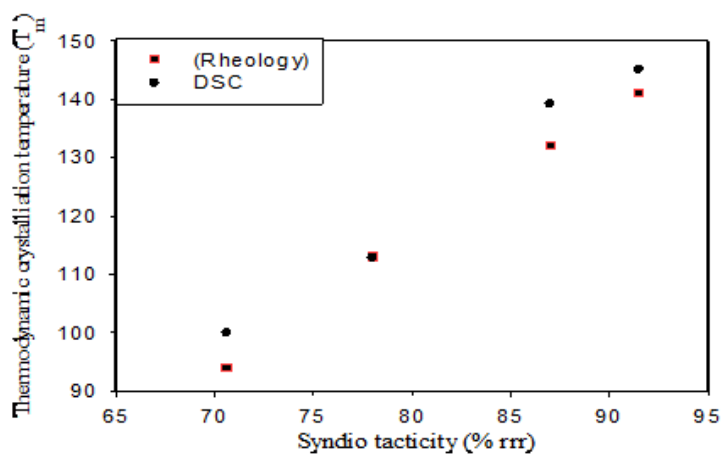


Fig.4.18: Relationship between thermodynamic crystallization temperature and degree of syndiotacticity.

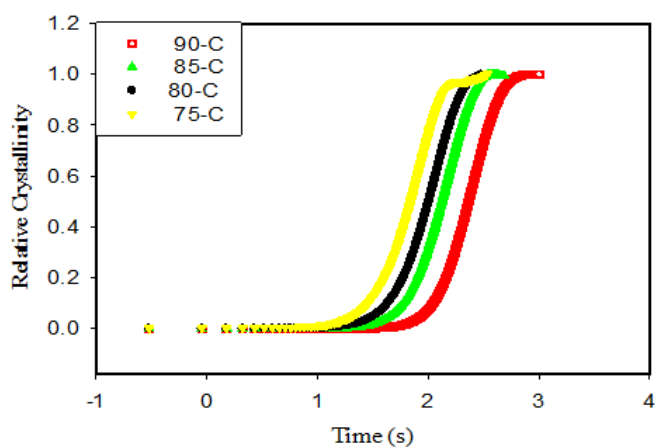


Fig.4.19: Relative crystallinity as a function of time at different temperatures for sPP-9.

## 4.4. Concluding remarks

The crystallization measurements performed on sPPs of different degrees of syndiotacticity show that the crystallization temperature and activation energy of crystallization significantly depend upon on the degree of syndiotacticity of the polymer chain. In particular activation energy was found to increase with increasing the degree of syndiotacticity. More over peak temperature (crystallization temperature) in case of non-isothermal

crystallization was found sensitive to the degree of syndiotacticity of the polymer chain. The difference in both thermodynamic crystallization temperatures and peak crystallization temperatures determined by rheological and differential scanning calorimetric techniques can be related to the difference in sensitivity level of the two equipments. Rheological technique was found more sensitive and accurate for the samples having low syndiotacticity as compare to differential scanning calorimetric technique (DSC).

In general it is concluded that crystallization measurements by rheological technique is an accurate and easy method at low crystallization kinetics as compare to the differential scanning calorimetric (DSC) technique.

## **Chapter 5**

---

# **Linear Viscoelasticity of Isotactic, Atactic and Syndiotactic Poly-1Butenes**

### **5.1. Introduction**

The ability to predict the polymer properties like molecular weight, polydispersity and molecular architecture from the knowledge of rheology is one of the big achievements of polymer rheology. In Chapter 3 we have already shown some relations between the viscoelastic response and the molecular architecture of syndiotactic Polypropylene (sPP). Following the same lines, in the present chapter we present a similar analysis for another polyolefin, namely, Poly-1Butene. The importance of determining the rheology of stereo-regular Poly-1Butenes is somewhat twofold. On the one hand, unlike sPP, whose rheology has been the subject of different studies in the literature, little or nothing is known about the linear viscoelastic response of syndiotactic poly-1Butene. On the other hand, having a second, well characterized syndiotactic polyolefin opens the way to a possible confirmation of the role that stereo-regularity plays in determining the rheological viscoelastic behavior in the melt state.

In order to achieve the above objectives, as it was the case in Chapter 3, frequency sweep tests at different temperatures were conducted after confirming the linearity by strain sweep tests. Master curves were obtained by applying the Time Temperature Superposition principle using the Orchestrator software. The plateau modulus was determined for all samples by the best suitable method for the given shape of the viscoelastic curves.

The entanglement molecular weight, as well as the packing length of the different PB samples were calculated by using the correlation between plateau modulus and entanglement molecular weight (reptation theory) [70], and the models proposed by Fetters et al. [71].

## 5.2. Experimental Section

### 5.2.1. Material

Three different samples of syndiotactic (sPB), atactic (aPB) and isotactic (iPB) Poly-1Butene were used for the viscoelastic study. The relevant properties of the polymers are reported in Table.5.1. The structure of the poly-1Butene repeating unit is reported in Fig.5.1.

It can be noted from Table.5.1 that the syndio- and iso- samples are characterized by high degree of tacticity. Stereo-regularity data for the atactic PB are not available. The sPB shows a very low value of the melting temperature, which is also related to slow crystallization kinetics. Like Polypropylene, iPB melts at a much higher temperature, and displays a much faster kinetics.

Table 5.1: List of materials with some properties.

Sample	$T_m$ (°C)	% (rrrr)	% (mmmm)	$M_w$
sPB	39.2	96		115.000
aPB				339.000
iPB	134		99	430.000

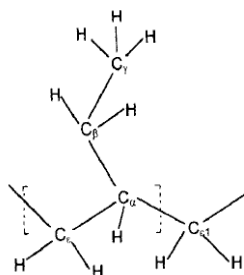


Fig. 5.1: Structure of the poly-1Butene repeating unit.

## 5.2.2. Methodology

All viscoelastic measurements were performed using the ARES rheometer (TA Instruments) equipped with the 8 mm diameter parallel plate geometry and commanded by the TA Orchestrator. Experiments were performed under a nitrogen atmosphere (instead of air) in order to minimize thermal degradation. All experiments were performed at a different gap depending on the as provided sample thickness as provided. The gap thickness was always in the order of 0.5 mm. Upon changes in temperature, the gap was always adjusted to account for thermal expansion of the rheometer tool.

### 5.2.2.1. Dynamic strain sweep test

Dynamic strain sweep tests were performed at different temperatures and a constant frequency of 10 rad/s for each sample in order to determine the linearity limit. The strain was varied from 0.1 to 10 %.

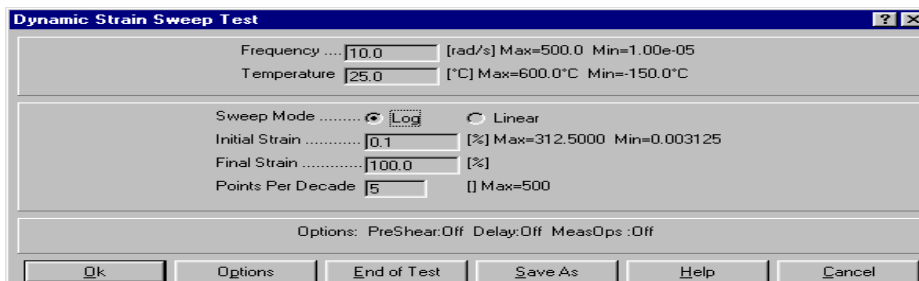


Fig.5.2: Dynamic strain sweep test set-up screen.

All samples were found to be linear in this range at all temperatures investigated. Therefore a strain within this range was selected for all the subsequent tests. As a way of an example, the dynamic strain sweep test of sPB at 100°C is shown in Fig.5.3.

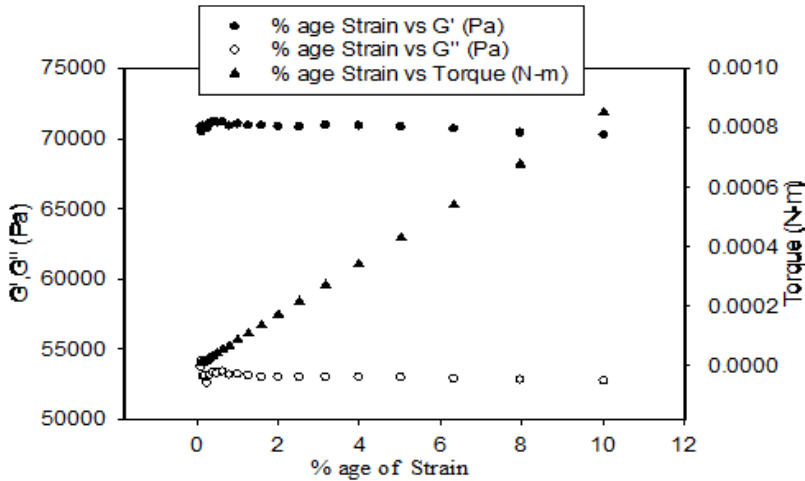


Fig.5.3: Dynamic strain sweep test of sPB at 100°C.

### 5.2.2.2. Dynamic time sweep test

A time sweep test takes successive measurements at constant temperature, frequency and strain at selected time intervals. The time required to make a measurement is frequency dependent. At frequencies less than 2 rad/sec, it is equal to the time required to complete approximately 1.5 cycles of oscillation. At high frequency the limit is approximately 2 seconds per measurement.

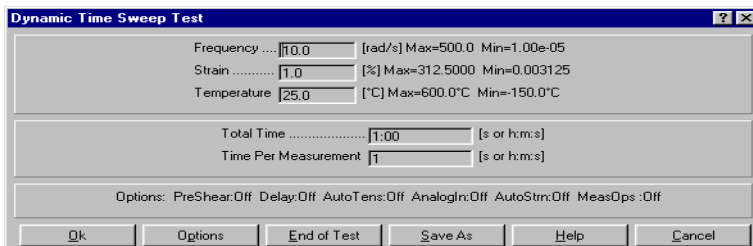


Fig.5.4: Dynamic time sweep test set-up screen.

We performed the time sweep test for each sample at an annealing temperature of 150°C prior to all other experiments. The purpose of this constant frequency and constant strain isothermal annealing is to clear the sample from crystallinity and check for its thermal stability. Experimental observations of the time sweep test of sPB are shown in Fig.5.5. Both elastic and viscous moduli become constant almost immediately after the beginning of the test and remain stable for a time of 300 seconds. After confirming the stability by time sweep test and linearity by strain sweep test frequency sweep tests were performed for all the samples.

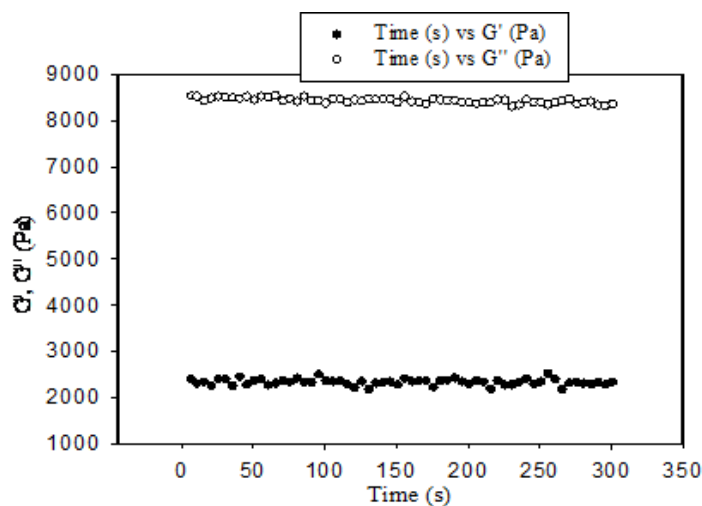


Fig.5.5: Dynamic time sweep test of sPB at 150°C.

### 5.2.2.3. Dynamic Frequency Sweep Test

The frequency sweep test takes successive measurements at selectable frequencies while holding the temperature and strain constant. The time it takes to complete the test is highly dependent on the lower end of frequency selected. Lower values of the lower end of the frequency window can significantly increase the test time. Dynamic frequency sweep tests were

## Chapter 5

conducted at different temperatures in the frequency range of 0.1 to 100 rad/sec at a constant strain of 3%.

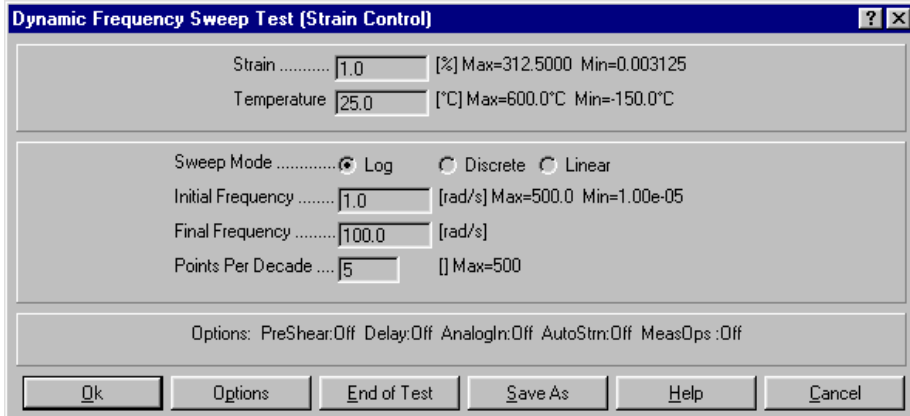


Fig.5.6: Dynamic frequency sweep test set-up screen.

As it was the case for PP, even for PB the temperature window for the experiments was accurately considered. The temperature dependence of the crystallization kinetics of the different samples determined the minimum test temperature that could be reached. Change of temperature from one experiment to the next one was performed by a controlled constant rate heating or cooling test using the temperature ramp option of the instrument. List of temperatures at which frequency sweep tests were performed is reported in table 5.2.

Table.5.2: List of selected temperatures for time temperature superposition principle.

Sample	Temperature (°C)							
	150	130	100	80	60	40	30	10
sPB	150	130	100	80	60	40	30	10
aPB	150	120	90	60	40	30		
iPB	150	130	110	100	80			

### 5.3. Results and Discussion

After confirming linearity and stability by strain sweep test and time sweep test respectively, frequency sweep tests were performed at different temperatures to examine the viscoelastic response as a function of frequency. In the following, the main experimental results are summarized by means of the master curves for the three PBs at the reference temperature of 25°C.

The master curve for frequency response of sPB is shown in Fig.5.7. Those for aPB and iPB are shown in Fig 5.8 and 5.9.

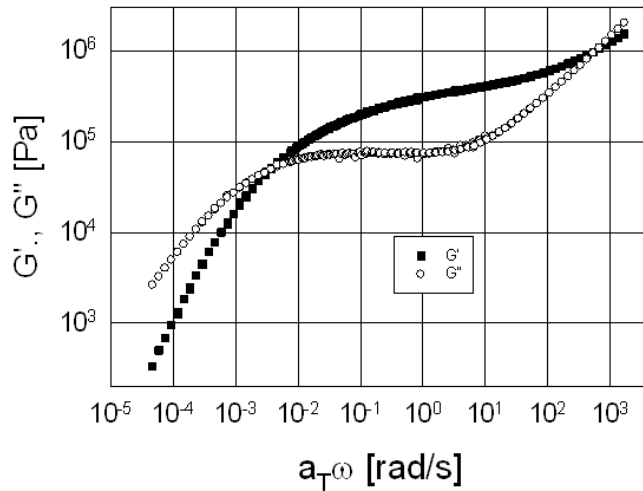


Fig.5.7: sPB frequency response master curve at 25°C.

The temperature range afforded for the sPB is wide enough to allow for a fully viscoelastic characterization of the system. The terminal region, as well as the plateau and the glassy region can be all observed. In particular, the presence of a minimum in the ratio between loss modulus and elastic modulus ( $\tan\delta$ ) allows calculating the plateau modulus with high accuracy by using the criterion of  $\min(\tan\delta)$ .

The same holds true for the atactic sample, as shown in Fig.5.8. In this case, the glassy region is less extended, but the plateau modulus is well determined by the min ( $\tan\delta$ ) rule.

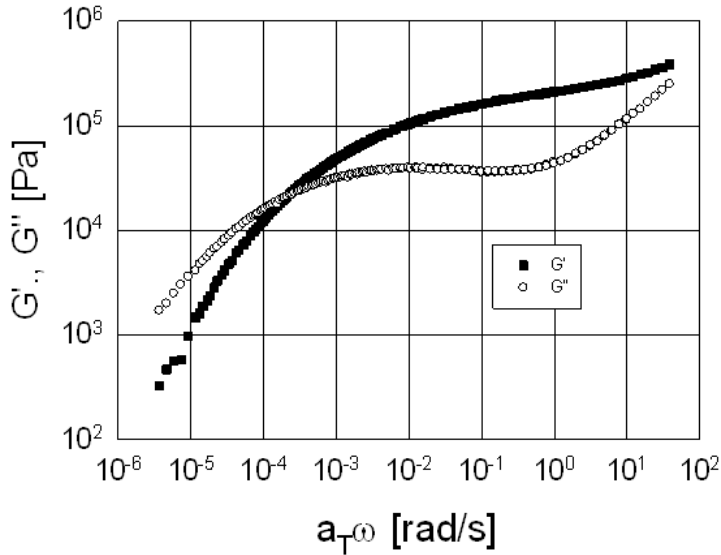


Fig.5.8: aPB frequency response master curve at 25°C.

The situation is different in the case of the isotactic PB, shown in Fig.5.9. Here, as it usually happens, the melting temperature of the isotactic polymer is much higher than that of the syndiotactic counterpart, which makes it impossible to reveal the intermediate plateau region. In this case, the best way to determine the plateau modulus is by using the empirical cross-over modulus relationship:

$$\text{Log}\left(G_N^0 / G_{cop}\right) = 0.38 + [2.63 * \log(M_w / M_n) / 1 + 2.45(M_w / M_n)] \quad (5.1)$$

In Eq. (5.1)  $G_{cop}$  is the value of the modulus at the cross-over point, and  $M_w/M_n$  is the polydispersity index which, in this case, is equal to 2.

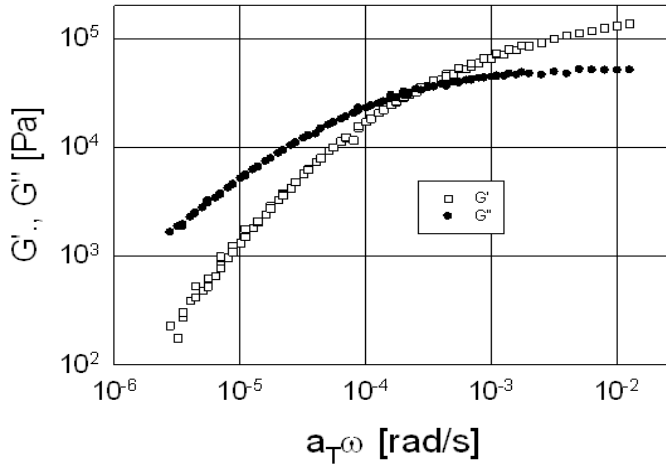


Fig.5.9: iPB frequency response master curve at 25°C.

The data in Figs.5.7-5.9 confirm the thermo-rheological simplicity of the three polymer samples. The double (horizontal and vertical shift) allows in fact obtaining excellent master curves for the linear viscoelasticity. The determination of the horizontal shift factor has also allowed estimating the parameters of semiempirical equation of Williams, Landel and Ferry (WLF) for Poly-1Butene.

The WLF equation is based on the assumption that above the glass transition temperature, the fractional free volume increases linearly with temperature. This leads to the following expression:

$$\log a_T = -c_1(T-T_0)/[c_2 + (T-T_0)] \quad (5.2)$$

where  $C_1$  and  $C_2$  are the WLF parameters and  $T_0$  the reference temperature.

Figure 5.11 shows the shift factor as a function of the temperature for all samples and temperatures investigated. It is clear that all data can be well fitted by a single WLF curve, which is reported as a solid line in Fig. 5.10. The WLF parameters obtained by the nonlinear regression of the data with Eq. (5.2) are (at  $T_0=298$  K)  $C_1=9.05$  and  $C_2=123$  K.

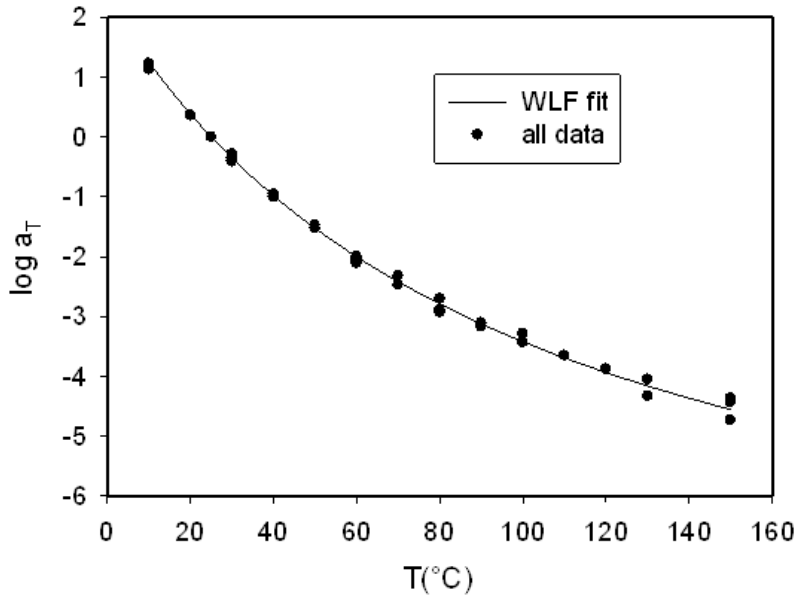


Fig.5.10: The horizontal shift factor as a function of temperature for all PBs investigated. The reference temperature is 25°C. The solid line is the best fit of the WLF equation.

Once the plateau modulus is determined from the linear viscoelasticity plots, the molecular weight between entanglements can be directly calculated as:

$$M_e = \frac{\rho N_A kT}{G_N^0} \quad (5.3)$$

Furthermore, as done also in Chapter 3 for Polypropylene, the packing length was also calculated. In this case, the empirical relation used was that proposed by Fetters et al. [71] at the reference temperature of 25°C (the same temperature used in the present work):

$$p = \left( \frac{13.2}{G_N^0} \right)^{\frac{1}{3}} \quad (5.3)$$

In order to use Eq. (5.3), the density of Poly-1Butene at 25°C was necessary. This information was not available, and the density of PB was

approximated to that of PIB (Poly-iso-butene) that, at 25°C, has a density of 0.918 g/cm<sup>3</sup>. The values of plateau modulus, of molecular weight between entanglements and of the packing length for the three polymer samples are summarized in table 5.4.

Table 5.3: Plateau modulus, entanglement molecular weight and packing length for the three PB samples.

Sample	$G_N^0$ (Pa)	$M_e$ (Da)	$p$ (Å)
sPB	353,000	6,440	3.34
aPB	195,000	11,700	4.08
iPB	226,000	10,100	3.88

Table 5.3 confirms what had been already observed in Chapter 3 for Polypropylene, that is, the syndiotactic molecular architecture fills the space of the polymer melt in a more efficient way if compared to both iso- and atactic polymer structure. This is confirmed by the lower value of  $M_e$ , and even more clearly by the low value of the packing length.

## 5.4. Concluding Remarks

The viscoelastic properties of high molecular weight isotactic, syndiotactic and atactic poly-1Butene prepared by metallocene catalysis were examined. The influence of stereo-regularity on activation energy of flow, plateau modulus and entanglement molecular weight was investigated. The WLF equation parameters and therefore the activation energies were found to be essentially independent upon the type of stereo-regularity of PB chains. A single set of WLF parameters was able to fit quantitatively well the shift factors of the three samples examined here.

Moving to the determination of the plateau modulus, both sPB and aPB samples enabled the measurement of both elastic and viscous modulus over a range necessary to obtain a significant onset of the plateau zone. The plateau modulus of both the syndio and atactic PBs were determined successfully by theoretically rigorous  $\min(\tan\delta)$  method. In the case of isotactic PB the plateau regime was not available and the plateau modulus was determined by the empirical cross-over modulus method.

It was confirmed that the plateau modulus of syndio-PB was significantly larger than that of the chemically equivalent but stereo-regularly different aPB and iPB samples. This fact confirms what had been already observed in chapter 3 for Polypropylene and gives more strength to the hypothesis that the syndiotactic conformational arrangement is a more efficient space filling architecture in the melt state.

## Chapter 6

---

# Influence of extensional flows on the crystallization of syndiotactic Poly-1butene

## 6.1. Introduction

It is well known from the existing literature that crystallization of polymer melts can be enhanced by the application of flow or deformation. Both shear and extensional flow produce molecular orientation, which enhance the rate of crystallization process. In this chapter, we investigate the effect of extensional flows on the crystallization kinetics of syndiotactic poly-1Butene.

## 6.2. Experimental Section

### 6.2.1. Material

The material investigated here is the same sPB that has been used in the previous chapter for the linear viscoelasticity characterization. Its main physical properties are summarized in Table.6.1.

Table.6.1: Properties of the syndiotactic poly-1Butene.

Sample	$T_m$ (°C)	% (rrrr)	$M_w$
sPB	39.2	96	115.000

Table 6.1 shows that, in spite of the high degree of tacticity, sPB has a very low melting temperature, which is also the symptom of slow

crystallization kinetics. For this reason, sPB is a good candidate to explore the effect of flow and deformation on the crystallization process.

### **6.2.2. Methodology**

All experiments shown in this chapter has been performed on samples that received the same thermo-mechanical history. In particular, samples were compression-molded in a Carver hydraulic press at the temperature of 70°C. This temperature is well above the melting point, thus guaranteeing complete melting of the crystallites.

Quiescent crystallization was studied in two different ways. On the one hand, calorimetric measurements were performed on a DSC apparatus (Shimadzu, A60). On the other hand, small amplitude oscillatory time sweep experiments were performed in the ARES rheometer at a frequency of 10 rad/s.

The stretch-induced crystallization experiments were performed by the Sentmanat Extensional Rheometer (SER) attached to the ARES rheometer. The Sentmanat Extensional Rheometer (SER) consists of two small cylinders arranged in parallel. The sample is positioned between the cylinders at the middle height using two clips. When attached to a rotational rheometer, such as the, one cylinder is connected to the force transducer and the other to the motor. The outer cylinder rotates around the inner one, while rotating on its own axis. By this way the sample is stretched uniaxially. Different extensional rates in the range of 0.001 to  $7s^{-1}$  at a constant Hencky strain of 3 were applied at two different temperatures, namely, 40°C (slightly above the melting temperature) and 25°C (well below the melting temperature). The temperature is regulated by a forced convection chamber.

Stretch rheological experiments were also complemented by Small Angle X-Ray Scattering (SAXS) experiments performed at the Department of

Chemistry of the University of Naples. Details of the SAXS apparatus and of the experimental methods can be found elsewhere [147].

### 6.3. Results and Discussions

The extremely slow quiescent crystallization of sPB is demonstrated in Figures 6.1 and 6.2. Fig.6.1 shows the time evolution of the viscoelastic moduli for a sample that has been prepared by the above described procedure. Time zero roughly corresponds to the time of compression molding at 70°C. Only few minutes run from the actual preparation to the start of the rheological experiment.

Fig.6.1 clearly shows the signature of the crystallization process, as indicated by the sharp upturn of the moduli. It must be noted that the time at which the upturn is first detected corresponds to the so-called "induction time", that is, the time necessary for crystals to grow (in number and size) to a sufficient extent so has to affect significantly the rheological response of the sample. For this reason, the calculated induction time  $t_{\text{ind},0} \cong 22$  hr, must be considered as a rheological induction time.

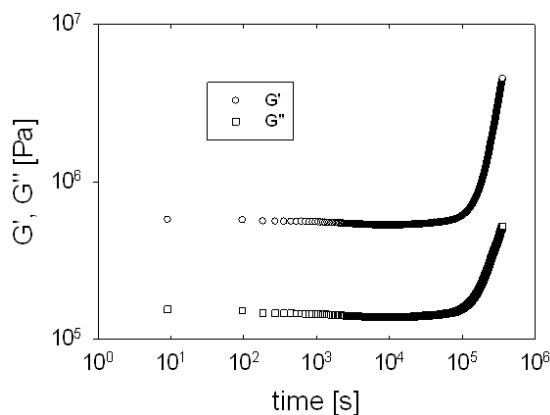


Fig.6.1: Oscillatory time sweep of sPB at 25°C.

The slow kinetics of the sPB quiescent crystallization is confirmed also by calorimetric measurements. Fig. 6.2 shows the raw heat flux from a DSC experiment for two sPB sample. In the first case, the sample has been heated at a rate of  $10^{\circ}\text{C}/\text{min}$  immediately after compression molding at  $70^{\circ}\text{C}$ . In the second case, the same heating cycle has been applied to a sample which had been prepared one week before and had been kept at room temperature.

From Fig.6.2 it is clear that after one week enough crystalline phases have been built up to produce a significant endotherm peak in the calorimetric measurement. The data reported in Figs 6.1 and 6.2 clearly indicate that quiescent crystallization of sPB at room temperature is a slow process and that a rheological induction time of about one day can be clearly estimated.

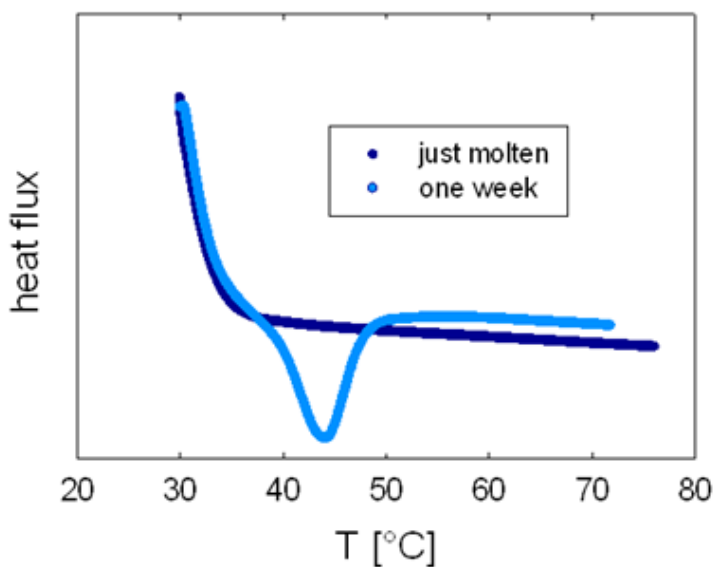


Fig.6.2: DSC of sPB immediately after sample preparation and after one week at room temperature. The heating rate is  $10^{\circ}\text{C}/\text{min}$ .

After probing the quiescent crystallization kinetics, extensional experiments were performed in order to investigate the effect of flow on the

crystallization process. Fig.6.3 shows the results of different extensional tests performed at the temperature of 40°C. Notice that such a temperature is slightly above the nominal melting temperature for sPB crystallization (see Table 6.1). In this case, no crystallization is expected.

The data in Fig.6.3 are presented in terms of an extensional viscosity growth function as a function of time. The extensional viscosity growth function is defined as:

$$\eta_e = \frac{M}{2R\dot{\epsilon}_H A_T \exp(-\dot{\epsilon}_H t)} \quad (6.1)$$

where  $M$  = Torque (g cm),  $R$  = Drum radius,  $\dot{\epsilon}_H$  = Extension rate ( $s^{-1}$ ), and  $A_T$  = Cross-sectional area at temperature  $T$  [ $mm^2$ ].

On the same plot the linear viscoelasticity line, as obtained from the frequency response measurements is also plotted. The data in Fig.6.3 are typical of the extensional response of a polymer melt. At the initial times, for any given stretching rate, the extensional viscosity follows the linear viscoelastic behavior. At the lowest stretching rate (red curve) the LV line is followed almost to steady-state conditions, although the total strain reached in the SER device is still too small to confirm that a steady-state, linear extensional flow is actually attained. For higher stretching rates the limitedness in the applied strain becomes more crucial, and the curve stop well before any steady-condition can be detected.

Although the data in Fig.6.3 cannot be used to extract a quantitative information on the extensional viscosity, they are extremely relevant when read in terms of crystallization. It is indeed apparent from Fig.6.3 that no crystallization takes place at 40°C under the applied stretching conditions. Notice that a more than one hundred-fold change in stretching rate is applied

to sample without any apparent sign of qualitative change in its extensional response.

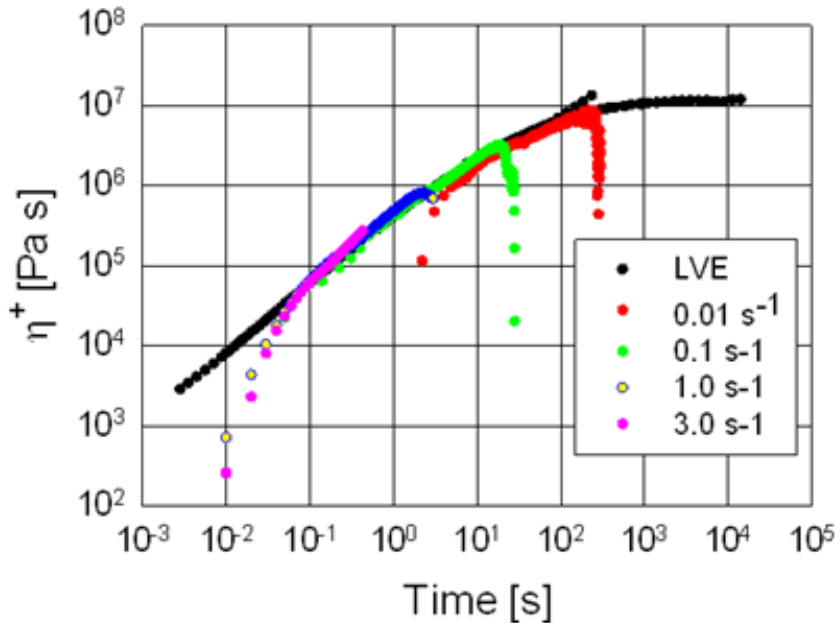


Fig.6.3: Extensional viscosity growth function for sPB at 40°C. The linear viscoelasticity line is also reported for reference.

The situation depicted in Fig.6.3 is drastically changed when the extensional flow is applied at the temperature of 25°C. A summary of all experiments conducted on sPB at this temperature is reported in Fig.6.4, along with the LV line at the same temperature.

For the lowest stretching rate ( $10^{-3} \text{ s}^{-1}$ ) the extensional responses closely match the linear viscoelastic behavior, at least until sample breakup. Breakup is in all cases indicated by the sudden down turn in the extensional curve. Since the cross-over relaxation time of sPB at 25°C is about 270 s, the corresponding Weissenberg number results to be  $We=0.27$ .

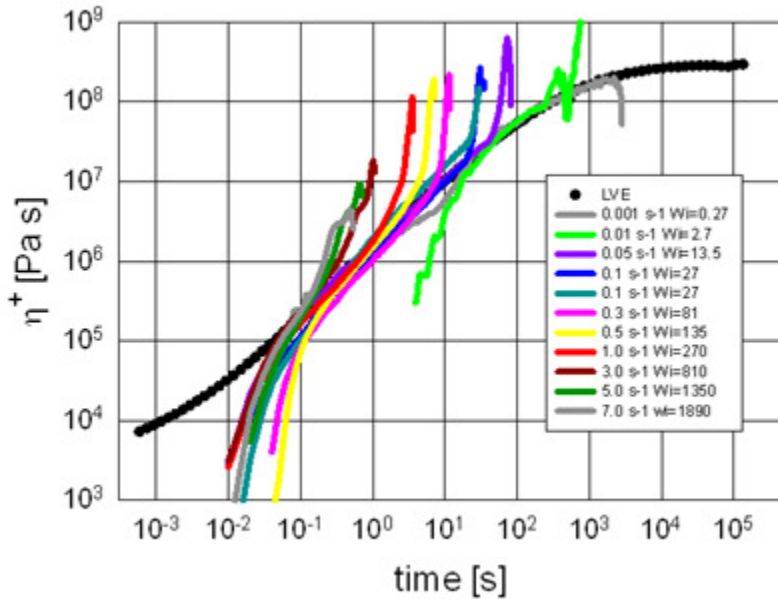


Fig.6.4: Extensional viscosity growth function for sPB at 25°C. The linear viscoelasticity line is also reported for reference. The legend also shows the Weissenberg number (based on the cross-over relaxation time) corresponding to each applied stretching rate.

This value is significantly less than unity, indicating that no or little orientation of the polymer chains takes place during extension at this stretching rate.

Starting from the next higher stretching rate (in this case  $0.01 \text{ s}^{-1}$ ) the Weissenberg number becomes larger than unity. At the same time the extensional curve displays a qualitatively different response. After an initial, smooth raise, where the LV line is substantially followed, a sudden upturn in viscosity is observed. The viscosity increases by orders of magnitude in a very short time, and the sample reaches a breakdown point in a short time after the sudden upturn.

The behavior observed for the stretching rate of  $0.01 \text{ s}^{-1}$  is repeated at all higher rates. The pattern is the same, but the time where the upturn occurs is a strong decreasing function of the stretching rate. We found a good quantitative reproducibility of this behavior. One example of reproducibility is given in Fig. 6.4 for the stretching rate of  $0.1 \text{ s}^{-1}$ . We assume that the observed upturn in extensional viscosity under constant extension rate is the signature of stretch-induced crystallization. To support these hypothesis two different considerations can be done.

The first consideration is that the upturn is not observed at the temperature of  $40^\circ\text{C}$  (see Figure 6.3). In extensional flow of amorphous polymer melts the upturn in viscosity is usually referred to as the "strain hardening" phenomenon. This effect, which is known to occur with particular relevance in branched polymer systems, is related to the flow-induced stretch of the polymer coil, which in turn determines a sudden increase in the elastic stress component. As a consequence, the elongational viscosity increases and typically becomes larger (even much larger) than the value reached at vanishing stretching rates. One example of the strain hardening effect is given in Figure 6.5, where the extensional viscosity growth curve of a Low Density Polyethylene (LDPE) is plotted as a function of time for different values of the stretching rate. In this case, the positive, strong of the viscosity curve from the LV curve is a signature of strain hardening. If the results of Figure 6.5 are compared with those of the sPB used in this work, it becomes clear that a mere change in  $15^\circ\text{C}$  temperature, from  $25^\circ\text{C}$  to  $40^\circ\text{C}$ , would produce a relatively small change in the relaxation time. As a consequence, if strain hardening would be responsible for the observed upturn in the viscosity at  $25^\circ\text{C}$ , the same strain hardening would occur also at  $40^\circ\text{C}$ . This is not being the case, as it is apparent from

Figure 6.3, the possibility that the upturn observed at 25°C were due to strain hardening can be safely ruled out. When comparing Figures 6.4 and 6.5, it must be noted that the upturn occurring in sPB under extensional flow is much sharper than that typically observed for strain hardening melts. Such a sharp change in the rheological behavior of the system suggests that a much more abrupt and catastrophic change in the polymer microstructure is taking place, such as is the case in crystallization.

A second, more direct proof that the observed behavior is indeed due to flow-induced crystallization is given by Small Angle X-Ray Scattering (SAXS) measurements. SAXS experiments were performed at the Department of Chemistry of the University of Naples on the same sPB sample used in this work. Measurements were taken at 25°C on a unstretched sample and on a stretched film. The stretching rate was not controlled, but a total of two Hencky deformation units were applied. The results are summarized in Fig.6.6.

Fig. 6.6 unequivocally shows that crystallization indeed takes place in sPB as a consequence of stretching. It should be noted, incidentally, that the equatorial intensity profiles highlight the presence of both form I and form II crystalline structures. Having established that the extensional flow is able to induce a fast crystallization of the sPB polymer, we now analyze the quantitative dependence of the crystallization process upon the flow characteristics.

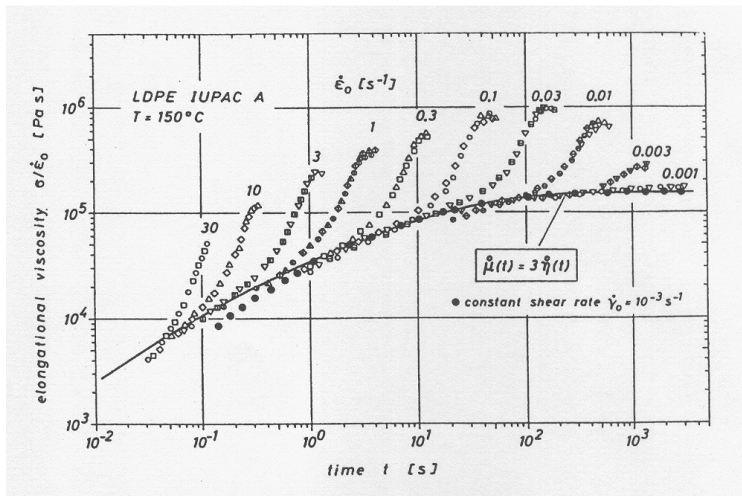


Figure 6.5: The extensional viscosity growth function for a Low Density branched Polyethylene (LDPE) at 150°C for different values of the stretching rate (HDPE).

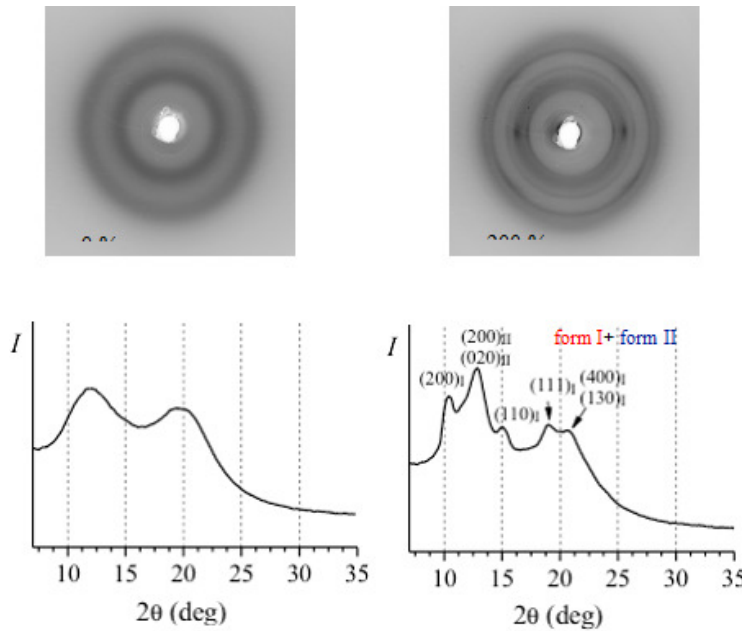


Figure 6.6: SAXS of sPB before (left) and after (right) a sudden stretch at 25°C. The total Hencky deformation is 2. Top: SAXS image. Bottom: Equatorial intensity profiles.

Figure 6.7 shows the crystallization rate enhancement as a function of the applied stretching rate. In particular, the induction time for crystallization is

determined as the time where the abrupt upturn in the extensional viscosity is monitored. Such an induction time is made dimensionless by taking the ratio with the quiescent induction time previously determined by small amplitude oscillatory shear experiments (see Fig.6.1). On the other hand, the stretching rate is made dimensionless by defining the Weissenberg number for this flow:

$$Wi = \dot{\epsilon}\tau \quad (6.2)$$

that is, the product of the stretching rate times the polymer relaxation time.

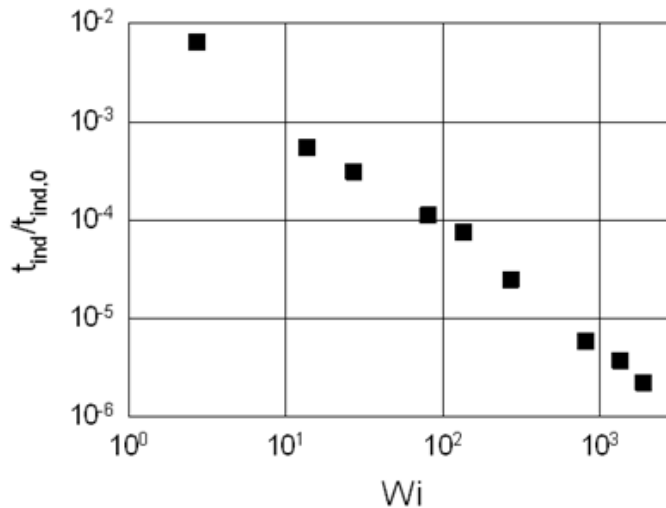


Figure 6.7: Dimensionless induction time as a function of the Weissenberg number for sPB 25°C.

The dimensionless induction time is a strong function of the Weissenberg number. The roughly inverse proportionality between the dimensionless induction time and the Weissenberg number suggests indeed the crystallization process is actually controlled by the applied stretch, rather than the applied stretching rate. This is checked in Fig.6.8, where the strain at the crystallization onset is plotted as a function of the stretching rate.

The data in Fig. 6.8 shows that the strain necessary for the extensional-induced crystallization is a function of the stretching rates. At higher stretching rates the strain necessary to determine crystallization is smaller. At the same time, however, it must be stressed that the strain variation is relatively small. A change in strain of less of a factor of five is in fact observed over a three orders of magnitude change in stretching rate. This confirms that the extensional induced crystallization of sPB is a stretch-dominated process, rather than a stretching rate-dominated one.

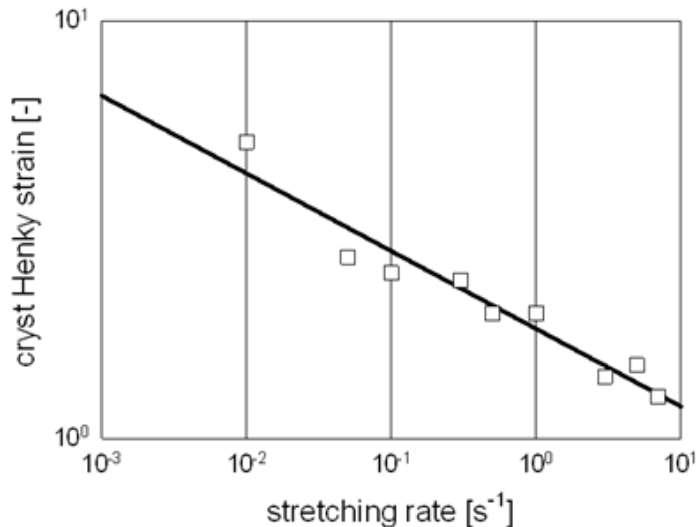


Figure 6.8: The Hencky strain at the onset of crystallization as a function of the stretching rate for sPB 25°C.

The total applied work extensional can also have a role in flow-induced crystallization. Figure 6.9 shows the total specific work at stress at the onset of crystallization as a function of stretching rate. The applied work at crystallization is calculated just as the product of the applied stress times the total strain. It does not correspond to the cumulative work applied to the system, which would be difficult to compute in this stress-varying transient process. In any event, unlike strain, the extensional work necessary to

crystallize the polymer is a slightly increasing function of the stretching rate. The weak dependence of the work done for crystallization upon the stretching rate indicates that a roughly constant amount of work is necessary to determine the polymer crystallization.

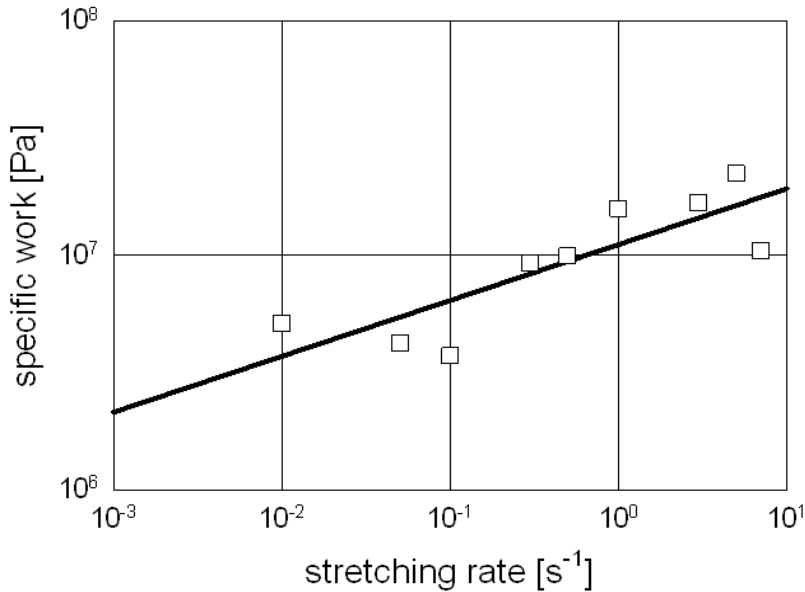


Figure 6.9: The specific work at the onset of crystallization as a function of the stretching rate for sPB 25°C.

## 6.4. Conclusion

The Sentmanat Extensional Rheometer (SER) was used to investigate the effect of uniaxial flow on the crystallization of syndiotactic poly-1Butene. Prior to stretching, isotactic poly-1Butene samples were heated to a temperature well above the melt temperature to erase their thermal and mechanical histories.

The crystallization kinetics of sPB was found to be strongly affected by the application of extensional flow in a wide range of stretching rates (0.001s<sup>-1</sup> to 7s<sup>-1</sup>).

The experimental data seem to suggest that the extension enhanced crystallization process is controlled more by the applied deformation (stretch) than by the deformation rate (stretching rate).

In the present research work relationships between rheological parameters and molecular structure of syndiotactic polypropylenes (sPP) and poly-1Butenes of different stereoregularity are explored by performing oscillatory shear experiments using ARES rheometer. Crystallization behavior of a series of syndiotactic polypropylenes of different degrees of syndiotacticity is investigated by performing both isothermal and non-isothermal crystallization tests using rheological and differential scanning calorimetric (DSC) techniques. The aim is to clarify the effect of degree of syndiotacticity on the crystallization behavior of the syndiotactic polypropylene. The effect of extensional flow on the crystallization kinetics of sPB is examined both in the melt and crystal phase by applying different extensional rates using sentmanat extensional rheometer (SER).

Rheological parameters, plateau modulus and entanglement molecular weight are found very sensitive to the degree of syndiotacticity of syndiotactic polypropylene (sPP). Plateau modulus is found to increase with increase in the degree of syndiotacticity and consequently entanglement molecular weight is found to decrease with increase in the degree of syndiotacticity of syndiotactic polypropylene (sPP). The same situation was found for PBs. Rheological parameters, plateau modulus and therefore entanglement molecular weight are found dependent on stereoregularity. It is concluded that the sensitivity of rheological parameters to stereoregularity is true for both the sPP and PBs.

Crystallization behavior is found very sensitive to the degree of syndiotacticity of sPP. Both activation energy and peak temperature determined by non-isothermal crystallization are found to increase with increase in the degree of syndiotacticity. Thermodynamic crystallization temperature determined by isothermal crystallization is also found to increase with increase in the degree of syndiotacticity of sPP. The difference in the crystallization measurements made by the rheological and differential scanning calorimetric techniques can be related to the difference in sensitivity to temperature of the two equipments. Rheological technique is found more sensitive and accurate for the samples having low syndiotacticity as compare to differential scanning calorimetric technique (DSC). Because at low syndiotacticity, the samples have small crystalline material and consequently have low crystallization kinetics. In general it is concluded that crystallization measurements by rheological technique is an accurate and easy method at low crystallization kinetics as compare to the differential scanning calorimetric (DSC) technique.

The crystallization process is investigated under the action of extensional flow by using sentmant extensional rheometer (SER). The crystallization kinetics of syndiotactic poly-1Butene is found very strongly affected by the application of extensional flow in the crystal form. Nucleation rate and therefore crystallization kinetics are found to increase with increase in the extensional rate.

The present research work can be further extended by studying the effect of syndiotacticity on rheological and crystallization behavior of the crystalline elastomer co-polymers. The effect of extensional flow on the crystallization behavior of poly-1Butenes and polypropylenes of different stereoregularity can be explored and influence of stereoregularity on the

## Chapter 7

---

crystallization process can be investigated. The results of this research work are expected to be useful for the assessment of alternatives, actual synthesis and applications of poly-olefins in polymer and processing industries.

---

## References

- [1] A.B.Samsuri, "*Degradation of natural rubber and synthetic elastomers*", in "*Shreir's Corrosion*", Elsevier (2010) pp.2407-2438.
- [2] H.Barnes, J.F.Hutton, K.Walters, "*An introduction to rheology*", Elsevier 1989.
- [3] W. McKeen, "*The effect of temperature and other factors on plastics and elastomers*", 2nd edition, William Andrew Inc. 2008.
- [4] J.Li, H.Li, C.Wu, Y.Ke, D.Wang, Q.Li, L.Zhang, Y.Hu., "*Morphologies, crystallinity and dynamic mechanical characterizations of polypropylene/polystyrene blends compatibilized with PP-g-PS copolymer: Effect of the side chain length*", Eur. Polym. J. (2009), 45 2619-2628.
- [5] K.W. JR., "*Crystallinity of cellulose and its significance for the fiber properties*", Txt. Res. J. (1950), 20, 363-372.
- [6] W.Kaminsky., "*New polyolefins by metallocene catalysts*", Pure & Appl. Chem. (1998), 70, 1229-1233.
- [7] F.Auriemma, O.R.Ballwesteros, C.D.Rosa., "*Origin of the elastic behavior of syndiotactic polypropylene*", Macromolecules. ( 2001), 34, 4485-4491.
- [8] F.Auriemma, C.De Rosa., "*New concepts in thermoplastic elastomers: the case of syndiotactic polypropylene, an unconventional elastomer with high crystallinity and large modulus*", J. Am. Chem.Soc. (2003), 125, 13143-7.

## REFERENCES

---

- [9] V.De La Torre, J.A.Rodriguez Fris, M.D.Failla, L.M.Quinzani., “*Effect of melt annealing on the phase structure and rheological behavior of propylene-ethylene copolymers*”, *Poly.Eng.Sci.* (2007), 47, 912-921.
- [10] J.Wang, Z.Yea, H.Fan, B.G.Li, S.Zhu., “*Dynamic mechanical and rheological properties of metallocene-catalyzed long-chain-branched ethylene/propylene copolymers*”, *Polymer.* (2004), 45, 5497-5504.
- [11] A.Eckstein,C.Friedrich, A.Lobbrecht, R.Spitz, R.Mulhaup., “*Comparison of the viscoelastic Properties of Syndiotactic and Isotactic Polypropylenes*”, *Acta Polym.* (1997), 48,41-46.
- [12] S.Acierno, R.Pasquino, N.Grizzuti., “*Rheological techniques for the determination of the crystallization kinetics of a polypropylene–EPR copolymer*”, *J.Therm.Anal.Calorim.* (2009), 98, 639-644.
- [13] J.M.Dealy,R.G.Larson, “*Structure and rheology of molten polymers*”, Hanser publisher, 2006.
- [14] R.J. Young, P.A.Lovell, “*Introduction to polymers*”, Chapman & Hall, 1987.
- [15] O.G.Lewi,R.M.J.R.King, “*Free radical polymerization kinetics of immobilized chains bulk polymerization of acrylonitrile*”, “*Advances in chemistry*” ACS (1969)pp. 25-45.
- [16] D.J.Metz. “*Radiation-induced ionic Anionic free radical polymers of  $\alpha$ -olefins polymerization*”, “*Advances in chemistry*”, ACS(1969) pp.202 -218.
- [17] M.Szwarc, “*Mechanism of propagation of ionic polymerizations*”, “*Advances in chemistry*”, ACS(1969) pp.236-249.
- [18] J.Jezl, N.S.Chu, I.H.M.Khelghatian, “*Anionic Free radical polymers of  $\alpha$ -olefins*”, “*Advances in chemistry*”, ACS(1969) pp.268-286.

## REFERENCES

---

- [19] V.Jaacks, "*Cationic copolymerization of trioxane and 1,3-dioxolane*", "Advances in chemistry", ACS(1969)pp.371-386.
- [20] P.Cossee., "*Ziegler-Natta catalysis I. Mechanism of polymerization of  $\alpha$ -olefins with Ziegler-Natta catalysts*", J.Catal. (1964), 3, 80-88.
- [21] V.A.Kormer, B.D.Babitskiy and M.I.Lobach, "*Stereospecific polymerization of 1,3-butadiene initiated by the transition metal  $\pi$ -complexes*", "Advances in chemistry", ACS(1969)pp.306-316.
- [22] P.Cossee., "*On the reaction mechanism of the ethylene polymerization with heterogeneous ziegler-natta catalysts*", Tetrahedron Lett. (1960), 38,12-16.
- [23] A.Zambelli, C.Tosi., "*Stereochemistry of propylene polymerization*", Adv.Polym.Sci. (1974), 15, 31-60.
- [24] G.Natta, I.Pasquon, A.Zambelli., "*Stereospecific catalysts for the head-to-tail polymerization of propylene to a crystalline syndiotactic polymer*", J.Am.Chem.Soc. (1962), 84,1488-90.
- [25] A. Zambelli, G.Natta, I.Pasquon., "*Polymerization of propylene to a syndiotactic polymer*", J Polym Sci. (1963), 4, 411-26.
- [26] Y.Do, S.Suzuki, K.Soga., "*A perfect initiator for living coordination polymerization of propene: tris(2-methyl-1,3-butanedionato) vanadium/diethylaluminium chloride system*", Makromol. Chem. Rapid. Commun. (1985), 6,639-42.
- [27] A.Zambelli, G.Natta, I.Pasquon, R.Signorini., "*Polymerization of propylene to syndiotactic polymer. II. Behavior of the catalytic system vanadium(IV) chloride-chlorodiethylaluminum*", J Polym. Sci. Polym.Symp. (1967), C16, 2485-99.
- [28] A.Zambelli, I.Pasquon, R.Signorini, G.Natta., "*Polymerization of propylene to syndiotactic polymer. III. Behavior of the catalyst*

## REFERENCES

---

- system vanadium tetrachloride-diethylaluminum chloride in the presence of Lewis bases*", Makromol Chem. (1968), 112, 160-82.
- [29] G.Natta, A.Zambelli, G.Lanzi, I.Pasquon, E.R.Mognaschi, A.L.Segre., "*Polymerization of propylene to syndiotactic polymer part I: Valence of active vanadium in the catalytic systems*", Makromol.Chem. (1965), 81,161-72.
- [30] M.Y.D.Reardon,S.Gambarotta,Y.G.Zahalka,H.L.C.Hyder., "*Vanadium-catalyzed ethylene-propylene copolymerization: the question of the metal oxidation state in ziegler-natta polymerization promoted by (b-diketonate)<sub>3</sub>V*", Organomet. Chem. (1999), 18, 2773-81.
- [31] D.Y.M.Takada, T.Keii., "*Stereochemical structure and molecular weight distribution of polypropylenes prepared with vanadium-based catalyst systems*", Makromol.Chem.(1979), 180, 57-64.
- [32] A. Zambelli, M.G.Giongo, G.Natta., "*Polymerization of propylene to syndiotactic polymer. IV. Addition to the double bond*", Makromol.Chem. (1968), 112,183-96.
- [33] P.Locatelli, M.C.Sacchi, E.Rigamonti, A.Zambelli., "*Syndiotactic polymerization of propene: regiospecificity of the initiation step*", Macromolecules. (1984), 17,123-5.
- [34] A.Zambelli, C.Tosi, C.Sacchi., "*Polymerization of propylene to syndiotactic polymer. VI. Monomer insertion*", Macromolecules. (1972), 5, 649-54.
- [35] A.Zambelli, C.Wolfsgruber, G.Zannoni, F.A.Bovey., "*Polymerization of propylene to syndiotactic polymer. VIII. Steric control forces*", Macromolecules. (1974), 7, 750-2.

## REFERENCES

---

- [36] A.Zambelli, P.Ammendola., “*Stereospecific polymerization of  $\alpha$ -olefins: end groups, polymer structure and reaction mechanism*”, Prog.Polym.Sci. (1991), 16,203-18.
- [37] A.Zambelli, I.Sessa, F.Grisi , R.Fusco, P.Accomazzi., “*Syndiotactic polymerization of propylene: single-site vanadium catalysts in comparison with zirconium and nickel*”, Macromol.Rapid.Commun., 22 (2001) 297-310.
- [38] Y.Doi, T.Koyama, K.Soga, T.Asakura., “*Stereochemistry in living co-ordination polymerization of propene initiated by vanadium-based catalytic systems*”, Makromol. Chem. (1984), 185,1827-33.
- [39] Y.Doi, S.Ueki, T.Keii., “*Living coordination polymerization of propene initiated by the soluble  $V(acac)_3-Al(C_2H_5)_2Cl$  system*”, Macromolecules. (1979), 12, 814-819.
- [40] Y.Doi, S.Ueki, T.Keii., “*Preparation of living polypropylenes by a soluble vanadium-based Ziegler catalyst*”, Makromol. Chem. (1979),180, 1359-61.
- [41] J.A.Ewen., “*Mechanism of stereochemical control in propylene polymerizations with soluble group 4B metallocene/methylalumoxane catalysts*”,J.Am.Chem.Soc.(1984),106 ,6355-6364.
- [42] W.Kaminsky,K.Kulper,H.H.Brintzinger,F.R.W.Wild.,“*Polymerization of propene and butene with a chiral zirconocene and methylaluminoxane as co-catalyst*”, Angew.Chem. (1985), 97, 507-508.
- [43] H.Sinn, W.Kaminsky, W.J.Vollmer, R.Woldt., “*Living polymers with Ziegler catalysts of high productivity*”, Angew.Chem. Int.Ed.Engl. (1980), 92,396-402.

## REFERENCES

---

- [44] J.A.Ewen, R.L.Jones, A.Razavi, J.D.Ferrara, "Syndiospecific propylene polymerizations with Group IVB metallocenes", *J. Am. Chem. Soc.* (1988), 110, 6255-6256.
- [45] A.Razavi, J.L.Atwood., "Synthesis and characterization of the catalytic isotactic-specific metallocene complex ( $h_5-C_5H_3C_4H_9-CMe_2-h_5-C_{13}H_8$ )ZrCl<sub>2</sub>: Mechanistic aspects of the formation of isotactic polypropylene, the stereoregulative effect of the distal substituent and the relevance of C<sub>2</sub> symmetry", *J. Organomet. Chem.* (1996), 520, 115-20.
- [46] K.Mislow, M.Raban., "Stereoisomeric relations of groups in molecules", *Top Stereochem.* (1967), 1, 1-38.
- [47] LA.Castonguay, A.K.Rappe, Z.Natta., "A theoretical study of the isotactic polymerization of propylene", *J. Am. Chem. Soc.* (1992), 114, 5832-42.
- [48] Z.Yu, J.C.W.Chien., "ansa-Zirconocenium catalysis of syndiospecific polymerization of propylene: theory and experiment", *J. Polym. Sci. Part A Polym. Chem.* (1995), 33, 1085-1094.
- [49] JA.Ewen, M.J.Elder, R.L.Jones, L.Haspelagh, J.L.Atwood, S.G.Bott., "Metallocene/ polypropylene structural relationships: implications on polymerization and stereochemical control mechanisms", *Macromol. Symp.* (1991), 1, 253-295.
- [50] G.Balbontin, D.Dainelli, M.Galimberti, G.Paganetto., "Thermal behaviour of highly stereoregular syndiotactic polypropene from homogeneous catalysts", *Macromol. Chem.* (1992), 193, 693-703.
- [51] J.A.Ewen, L.Haspeslagh, J.L.Atwood, H. Zhang., "Crystal structures and stereospecific propylene polymerizations with chiral hafnium metallocene catalysts", *J. Am. Chem. Soc.* (1987), 109, 6544-6545.

## REFERENCES

---

- [52] A.Razavi, L. Peters, L. Nafpliotis., “*Geometric flexibility, ligand and transition metal electronic effects on stereoselective polymerization of propylene in homogeneous catalysis*”, J. Mol. Catal. A: Chem. (1997), 115, 129-154.
- [53] A.L.McKnight, RM.Waymouth., “*ChemInform Abstract: Group 4 ansa-cyclopentadienyl- amido catalysts for olefin polymerization*”, Chem.Rev. (1999), 30, 2587-298.
- [54] M.Brookhart,LK.Johnson,CM.Killian,S.Mecking,J.Tempel., “*Palladium(II)-and nickel(II)-catalyzed olefin polymerization*”, Polym.Prepr.(1996), 37, 254-255.
- [55] C.Pellecchia, A.Zambelli., “*Syndiotactic-specific polymerization of propene with a Ni-based catalyst*”, Macromol.Rapid.Commun. (1996), 17,333-338.
- [56] D.J.Arriola, E.Carnahan, P.D.Hustad, R.Kuhlman,T.T.Wenzel., “*Catalytic production of olefin block co-polymers via chain shuttling polymerization*”, Science. (2006), 312,714-719.
- [57] V.C.Gibson., “*Shuttling polyolefines to a new materials dimension*”, Science. (2006), 312, 703-704.
- [58] C.D.Rosa,C.F.Auriemma,D.Capua,L.Resconi,S.Guidotti,I.Camurati ,Nifantev,I.E.Laishevtsev., “*Structure-property correlations in polypropylene from metallocene catalysts: stereodeficient, regioregular isotactic polypropylene*”,J.Am.Chem. Soc. (2004), 126,17040-17049.
- [59] C.D.Rosa,F.Auriemma., “*Structural-mechanical phase diagram of isotactic polypropylene*”, J.Am.Chem.Soc. (2006), 128,11024-11025.
- [60] E.B.Gowd, K.Tashiro, C.Ramesh., “*Structural phase transitions of syndiotactic polystyrene*”, Prog.Polym.Sci. (2009), 34, 280-315.

## REFERENCES

---

- [61] T.T.Wang., “*Morphology and mechanical properties of crystalline polymers. I. Transcryst- -alline polyethylene*”, J.Appl.Phys.(1973), 44, 2218-2224.
- [62] G.S. Rajan, Y.T.Vu, J.E. Mark, C.L.Myers., “*Thermal and mechanical properties of polypropylene in the thermoplastic elastomeric state*”, Eur. Polym. J. (2004), 40, 63-71.
- [63] H.Uehara, Y.Yamazaki, T.Kanamoto., “*Tensile properties of highly syndiotactic polypropylene*”, Polymer. (1996), 37, 57-64.
- [64] C.D. Aniello, P.Rizzo, G.Guerra., “*Polymorphism and mechanical properties of syndiotactic polystyrene films*”, Polymer. (2005), 46, 11435-11441.
- [65] C.D. Rosa, F.Auriemma, M.Paolillo, L.Resconi, I.Camurati., “*Crystallization behavior and mechanical properties of regiodefective, highly stereoregular isotactic polypropylene: Effect of regiodefects versus stereodeflects and influence of the molecular mass*”, Macromolecules. (2005), 38, 9143-9154.
- [66] R.O.Ebewele, “*Polymer science and technology*”, CRC Press.2000.
- [67] F.Auriemma, O.R.Ballesteros, C.D.Rosa., “*Origin of the elastic behavior of syndiotactic polypropylene*”, Macromolecules. (2001), 34, 4485-4491.
- [68] F.Auriemma, C.D.Rosa, M.Corradi., “*Stereoblock Polypropylene as a prototype example of elasticity via a flip-flop reorientation of crystals in a compliant matrix*”, Adv. Mater. (2007), 19, 871-874.
- [69] J. D.Ferry, “*Viscoelastic properties of polymers*”, 3rd edition, John Wiley and Sons, 1980.
- [70] M.Doï, S. F.Edwards, “*The Theory of Polymer Dynamics*”, Oxford University Press, 1988.

## REFERENCES

---

- [71] L.J.Fetters,D.J.Lohse,D.Richter, T. A.Witten, A.Zirkel., “*Connection between polymer molecular weight, density, chain dimensions, and Melt viscoelastic properties*”, *Macromolecules*. (1994), 27, 4639-4647.
- [72] L.J.Fetters,D.J.Lohse,R.H.Colby., “*In physical properties of polymers handbook*”, AIP Press 1996.
- [73] L.J.Fetters,D.J.Lohse,W.W.Graessley., “*Chain dimensions and entanglement spacings in dense macromolecular systems*”, *J. Polym. Sci.,PartB:Polym. Phys. Ed.* (1999), 37,1023-1033.
- [74] Y.H.Lin., “*Number of entanglement strands per cubed tube diameter, a fundamental aspect of topological universality in polymer viscoelasticity*”, *Macromolecules*. (1987), 20, 3080-3083.
- [75] T.A.Witten,S.T.Milner,Z.G.Wang, “*In multiphase macromolecular systems*”, Springer 1989.
- [76] P. R.Sundararajan. *In physical properties of polymers handbook*. Mark, J. E. Ed.; AIP Press: Woodbury, NY, 1996;p 197.
- [77] G. Krause, “*In The stereo rubbers*”, John Wiley and Sons. 1977.
- [78] D.S.Pearson, L.J.Fetters,W.W.Graessley, G.V.Strate, E.V.Meerwall., *Macromolecules*. (1994), 27,711-719.
- [79] A.T.Boothroyd, A.R.Rennie, C.B.Boothroyd., “*Direct measurement of the temperature dependence of the unperturbed dimensions of a polymer*”, *Eur. Phys.Lett.* (1991), 15, 715-719.
- [80] G.D.Smith, D.Y.Yoon, R.L.Jaffe, R.H.Colby, R.Krishnamoorti, L.J.Fetters., “*Conformations and structures of poly(oxyethylene) melts from molecular dynamics simulations and small-angle neutron scattering experiments*”, *Macromolecules*. (1996), 29,3462-3469.

## REFERENCES

---

- [81] J.M.Carella, W.W.Graessley, L.J.Fetters., “*Effect of chain microstructure on the viscoelastic properties of linear polymer melts: Polybutadienes and hydrogenated polybutadienes*”, *Macromolecules*. (1984), 17, 2775-4647.
- [82] R. H. Colby, L.J.Fetters, W. W.Graessley., “*The melt viscosity-molecular weight relationship for linear polymers*”, *Macromolecules*. (1987), 20, 2226-2237.
- [83] J.Ren, A.S.Silva, R.Krishnamoorti., “*Linear Viscoelasticity of Disordered polystyrene-polyisoprene block co-polymer based layered-silicate nanocomposites*”, *Macromolecules*. (2000), 33, 3739-3746.
- [84] J. T.Gotro and W. W.Graessley., “*Model hydrocarbon polymers: rheological properties of linear polyisoprenes and hydrogenated polyisoprenes*”, *Macromolecules*.(1984), 17, 2767-2775.
- [85] M.J.Struglinski, W.W.Graessley. “*Effects of polydispersity on the linear viscoelastic properties of entangled polymers. Experimental observations for binary mixtures of linear polybutadiene*”, *Macromolecules*. (1985), 18, 2630-2643.
- [86] A.Eckstein, J. Suhm, C. Friedrich, R.D. Maier, J. Sassmannshausen, M. Bochmann, R. Mlhaupt., “*Determination of plateau moduli and entanglement molecular weights of isotactic, syndiotactic, and atactic polypropylenes synthesized with metallocene catalysts*”, *Macromolecules*. (1998), 31, 1335-1340.
- [87] B. Wunderlich, “*Thermal Analysis*”, Academic Press, 1990.
- [88] Y.P.Khanna., “*Rheological mechanism and overview of nucleated crystallization kinetics*”, *Macromolecules*. (1993), 26, 3639-3643.

## REFERENCES

---

- [89] V.R.Raju, H.Rachapudy, W. W.Graessley., “*Properties of amorphous and crystallizable hydrocarbon polymers.IV.Melt rheology of linear and star branched hydrogenated polybutadiene*”, J. Polym. Sci. Part A-2. (1979), 17, 1223-1235.
- [90] S.Wu., “*Chain structure and entanglement*”, J.Polym.Sci., Part B: Polym.Phys. (1989), 27,723-741.
- [91] M.V.Gurp, J.Palmen., “*Time temperature superposition for polymeric blends*”, J. Rheol. Bull. (1998), 67,5-8.
- [92] P.G.de Gennes., “*Reptation of a polymer chain in the presence of fixed obstacles*”, J. Chem. Phys. (1971), 55,572-579.
- [93] S.T.Milner, T.C.B.McLeish., “*Parameter-free theory for stress relaxation in star polymer melts*”, Macromolecules. (1997), 30, 2159-2166.
- [94] A.E.Likhtman,T.C.B.McLeish., “*Quantitative theory for linear dynamics of linear entangled polymers*”, Macromolecules. (2002), 35, 6332-6343.
- [95] G.Marrucci., “*Relaxation by reptation and tube enlargement: a model for polydisperse polymers*”, J. Polym. Sci. Polym. Phys. Ed. (1985), 23,159-177.
- [96] A.Leygue, C.Bailly R.Keunings., “*A differential formulation of thermal constraint release for entangled linear polymers*”, J.Non-Newton. Fluid. (2005), 128, 23-28.
- [97] A.Leygue, C.Bailly, R.Keunings., “*A differential tube-based model for predicting the linear viscoelastic moduli of polydisperse entangled linear polymers*”, J.Non-Newton. Fluid. (2006), 133, 28-34.
- [98] M.Avarmi., “*Kinetics of phase change. I general theory*”, J. Chem. Phys. (1939),7,1103.

## REFERENCES

---

- [99] L. J. Fetters, J.H. Lee, R.T. Mathers, P.D. Hustad, G.W.Coates, L.A. Archer, S.P. Rucker, and D.J. Lohse., “*Influence of syndiotactic propylene units on the rheological parameters of poly(ethylene-propylene)co-polymers*”, *Macromolecules*. (2005), 38,10061-10066.
- [100] S.Wu,R.Beckerbauer. “*Chain entanglement in homopolymer, copolymers and terpolymers of methylmetacrylates,styrene and N-phnylmaleimide*”, *Polymer*. (1992), 33,509-515.
- [101] G.Bhoje, T.Kohiji, C.Ramesh. “*Structural phase transition of syndiotactic Polystyrene*”, *Prog. Polym.Sci.* (2009), 34,280-315.
- [102] ARES Rheometer. Rheometric series manual. (2003), TA instruments, New Castle, DE19720.
- [103] A.Palekar, A.Starobin, A.Reikher., “*Die-casting end-of-fill and drop forge viscometer flow transients examined with a coupled-motion numerical model*”,68th WFC-World Foundry Congress. 2008, pp. 87-91.
- [104] R. H. Colby, L. J. Fetters, W. W. Graessley., “*The melt viscosity-molecular weight relationship for linear polymers*”, *Macromolecules*. (1987), 20, 2226-2237.
- [105] L.J.Fetters,D.J.Lohse, D.Richter, T.A.Witten, A.Zirkel., “*Connection between polymer molecular weight,density,chain dimensions and melt viscoelastic properties*”, *Macromolecules*. (1994), 27, 4639-4647.
- [106] L. J.Fetters, D. J.Lohse, G.Franco, C. A. Brant, P. D.Richter., *Macromolecules*. (2003), 36,10096.
- [107] Y.H.Lin., “*Number of entanglement strands per cubed tube diameter, a fundamental aspect of topological universality in polymer viscoelasticity*”, *Macromolecules*. (1987),20, 3080-3083.

## REFERENCES

---

- [108] M.Avarmi., "*Kinetics of phase change. II transformation-time relations for random distribution of nuclei*", J.Chem. Phys. (1940), 8,212.
- [109] L.Mandelkern, "*Crystallization of polymers*", McGraw-Hill.1964.
- [110] Y.Long. R.A. Shanks, Z.H.Stachurski., "*Kinetics of polymer crystallization*", Prog. Polym. Sci. (1995), 20,651-701.
- [111] E.Rojo, M.Fernandez, M.E.Munoz,A.Santamaria. "*Relation between PVT measurements and linear viscosity in isotactic and syndiotactic polypropylenes*", Polymer. (2006), 47,7853-7858.
- [112] R.Simha, T.Somcynsky., "*On the statistical thermodynamics of spherical and chain molecule fluids*", Macromolecules. (1969), 2, 342-350.
- [113] H. Janeschitz-Kriegl, E.Ratajski, M.Stadlbauer., "*Flow as an effective promotor of nucleation in polymer melts: a quantitative evaluation*", Rheol Acta. (2003), 42,355-364.
- [114] R.H.Somani,L.Yang,B.S.Hsiao., "*Shear-induced molecular orientation and crystallization in isotactic polypropylene: Effects of the deformation rate and strain*", Macromolecules. (2005, 38,1244-1255.
- [115] A.Keller., "*Organization of the macromolecules in the condensed Phase*", Faraday. Discuss. (1979), 68,145.
- [116] E.Schulz and B.Wunderlich., "*Crystal nucleation, growth, annealing*", Cryst.Res. Technol. (1977), 12, K12-K12.
- [117] G.Brandeis, C.Jaupart., "*The kinetics of nucleation and crystal growth and scaling laws for magmatic crystallization*", Contrib.Minral.Petr. (1987), 96, 24-34.

## REFERENCES

---

- [118] J.I. Lauritzen, J.D. Hoffman, “*Theory of formation of polymer crystals with folded chains in dilute solutions*”, J. Res. Natl. Inst. Stand. Technol. (1960), 64, 73-102.
- [119] S.Acierno, N.Grizzuti, “*Flow-induced crystallization of polymer: theory and experiments*”, Int. J.Mater.Form. (2008), 1, 583-586.
- [120] S.Acierno, N.Grizzuti, H.H.Winter., “*Effects of molecular weight on the isothermal crystallization of poly(1-butene)*”, Macromolecules. (2002), 35, 5043-5048.
- [121] C.Duplay, B.Monasse, J.M.Haudin, J.L.Costa. “*Shear-induced crystallization of polypropylene: influence of molecular weight*”, J. Mat. Sci. (2000), 35, 6093-6103.
- [122] F.Jay, B.Monasse, J.M.Haudin., “*Shear-induced crystallization of polypropylenes: effect of molecular weight*”, J. Mat. Sci. (1999), 34, 2089-2102.
- [123] S.Vleeshouwers, H.E.H.Meijer., “*A rheological study of shear induced crystallization*”, Rheol. Acta. (1996), 35, 391-399.
- [124] R.H.Somani, L.Yang, B.S.Hsiao., “*Shear-Induced molecular orientation and crystallization in isotactic polypropylene: Effects of the deformation rate and strain*”, Macromolecules. (2005), 38, 1244-1255.
- [125] Y.Fengyuan, H. Zhang, R.Liao, H.Zheng, W.Yu, C.Zhou., “*Flow induced crystallization of long chain branched polypropylenes under weak shear flow*”, Eur. Polym. J. (2009), 45, 2110-2118.
- [126] S.Wu., “*Dynamic rheology and molecular weight distribution of insoluble polymers: tetrafluoroethylene-hexafluoropropylene copolymers*”, Macromolecules. (1985), 18, 2023-2030.

## REFERENCES

---

- [127] M.I.Kolte, H.K.Rasmussen and O.Hassager. “*Transient filament stretching rheometry ii: Numerical simulation*”, *Rheol. Acta.* (1997), 36, 285-302.
- [128] C.Duplay, B.Monasse, J.H.Haudin, J.L.Costa., “*Shear-induced crystallization of polypropylene: influence of molecular structure*”, *Polym. Int.* (1999), 48, 320-326.
- [129] C.Duplay, B.Monasse, J.H.Haudin, J.L.Costa., “*Shear-induced crystallization of polypropylene: Influence of Molecular Weight*, *J.Mater. Sci.* 35(2000)6093-6103.
- [130] J.M.Haudin, C.Duplay, B.Monasse, J.L.Costa. “*Shear-induced Crystallization of Polypropylene. Growth Enhancement and Rheology in the Crystallization Phase*”, *Macromol. Symp.* (2002), 185, 119-133.
- [131] L.Bove, M.R.Nobile., “*Shear flow effects on polymer melts crystallization: kinetics features*”, *Macromol. Symp.* (2002a), 180, 169-180.
- [132] L.Bove, M.R.Nobile., “*Shear-induced crystallization of isotactic poly(1-butene)*”, *Macromol. Symp.* (2002b), 185, 135-147.
- [133] S.Acierno, B.Palomba, H. H.Winter, N.Grizzuti., “*Effect of Molecular Weight on the Flow-induced Crystallization of isotactic Poly(1-Butene)*”, *Rheol. Acta.* (2003), 42, 243-250.
- [134] M.I.Kolte, H.K.Rasmussen, O.Hassager., “*Transient filament stretching rheometry ii: Numerical simulation*”, *Rheol. Acta.* (1997), 36, 285-302.
- [135] C.Hadinata, D.Boos, C.Gabriel, E.Wassner, M.Rullmann, N.Kao, M.Lau-n, “*Elongation-induced crystallization of a high molecular weight isotactic poly-1Butene melt compared to shear-induced crystallization*”, *J.Rheol.* (2007), 51, 195-215.

## REFERENCES

---

- [136] R.H.Somani,L.Yang,B.S.Hsiao., “*Shear-induced molecular orientation and crystallization in Isotactic Polypropylene: Effects of the Deformation Rate and Strain*”,*Macromolecules*. (2005),38,1244-1255.
- [137] Y.Long,R.Shanks,Z.H.Stachursili., “*Kinetics of polymer crystallization*”, *Prog. Polym. Sci.* (1995), 20, 651-701.
- [138] S.Acierno,N.Grizzuti.,“*Flow-induced crystallization of polymer theory and experiments*”, *Int J Mater Form.* (2008), 1,583-586.
- [139] A.Keller, H.W.H.Kolnaar, “*Flow-induced orientation and structure formation*”, Wiley-VCH. 1997.
- [140] H.Janeschitz-Kriegl, E.Ratajski, M.Stadlbauer.,“*Flow as an effective promotor of nucleation in polymer melts: a quantitative evaluation*”, *Rheol Acta.* (2003), 42, 355-364.
- [141] C.Hadinata, D.Boos, C.Gabriel, E.Wassner, M.Rullmann, N.Kao, M.Laun.,“*Elongation-induced crystallization of a high molecular weight isotactic polybutene-1 melt compared to shear-induced crystallization*”, *J Rheol.* (2007), 51, 195-215.
- [142] M.Sentmanat,O.Delgadilloazquez,S.G.Hatzikiriakos.,“*Crystallization of an ethylene-based butene plastomer: the effect of uniaxial extension*”, *Rheol Acta.* (2010), 49, 931-939.
- [143] M.Chellamuthu,D.Arora,H.H.Winter,J.P.Rothstein.,“*Extensional flow induced crystallization of isotactic poly-1butene using a filament stretching rheometer*”,*J.Rheol*(2011), 5,901.
- [144] S.Acierno, B.Palomba, H.H.Winter, N.Grizzuti.,“*Effect of molecular weight on the flow-induced crystallization of isotactic poly(1-butene)*”, *Rheol Acta.* (2003),42,243-250.

## REFERENCES

---

- [145] R.Paukkeri,A.Lehtinen.,“*Thermal behaviour of polypropylene fractions: 1.Influence of tacticity and molecular weight on crystallization and melting behaviour*”, Polymer.(1993),34, 4075-4082.
- [146] C.D.Rosa,F.Auriemma,O.R.Ballesteros.,“*Influence of the stereoregularity on the crystallization of the trans planar mesomorphic form of syndiotactic polypropylene*”, Polymer.(2001)9729-9734.
- [147] C.D.Rosa,F.Auriemma,O.R.Ballesteros, F.Esposito, D.Laguzza,R.D. Girolamo,L.Resconi.,“*Crystallization properties and polymorphic behavior of Isotactic Poly(1-butene) from metallocene catalysts:The Crystallization of Form I from the Melt*”,Macromolecules. (2009), 42,8286-8297.
- [148] R.G. Larson, “*The structure and rheology of complex fluids*”, Oxford University Press 1999.
- [149] K.Boutahar, C.Carrot, J.Guillet.,“*Crystallization of polyolefins from rheological measurements-relation between the transformed fraction and the dynamic moduli*”, Macromolecules. (1998), 31, 1921-9.
- [150] S.Kiewiet,V.Jassens,H.E.Miltner,V.G.Assche,V.P.Puyvelde,V.B. Mele.,“*RheoDSC.A hyphenated technique for simultaneous measurement of calorimetric and rheological evolutions*”, Rev Sci.Instrum. (2008),79,1-7.
- [151] M.Gahleitner,K.Bernreitner,W.Neilb,C.Paulik,E.Ratajski.,“*Influence of Molecular Structure on Crystallization Behaviour and Mechanical Properties of Polypropylene*”, Polym.Test. (1995),14,173-187.
- [152] C. De Rosa, F. Auriemma, O. Ruiz de Ballesteros, “*The Role of Crystals in the Elasticity of Semicrystalline Thermoplastic Elastomers*”, Chem. Mater. (2006), 18, 3523-3530.

## REFERENCES

---

- [153] C. Liu, J. Yu, J. He, W. Liu, C. Sun, Z. Jing, *Macromolecules*, (2004), 37, 9279-9282.